Gluon and ghost propagator studies in lattice QCD at finite temperature

D I S S E R T A T I O N

zur Erlangung des akademischen Grades

doctor rerum naturalium

(Dr. rer. nat.)
im Fach Physik

eingereicht an der
Mathematisch-Naturwissenschaftlichen Fakultät I
Humboldt-Universität zu Berlin

von

Herrn Magister Rafik Aouane

Präsident der Humboldt-Universität zu Berlin:
Prof. Dr. Jan-Hendrik Olbertz

Dekan der Mathematisch-Naturwissenschaftlichen Fakultät I:
Prof. Stefan Hecht PhD

Gutachter:
1. Prof. Dr. Michael Müller-Preußker
2. Prof. Dr. Christian Fischer
3. Dr. Ernst-Michael Ilgenfritz

eingereicht am: 19. Dezember 2012
Tag der mündlichen Prüfung: 29. April 2013

Ich widme diese Arbeit
meiner Familie und meinen Freunden

Abstract

Gluon and ghost propagators in quantum chromodynamics (*QCD*) computed in the infrared momentum region play an important role to understand quark and gluon confinement. They are the subject of intensive research thanks to non-perturbative methods based on DYSON-SCHWINGER (DS) and functional renormalization group (FRG) equations. Moreover, their temperature behavior might also help to explore the chiral and deconfinement phase transition or crossover within *QCD* at non-zero temperature.

Our prime tool is the lattice discretized *QCD* (*LQCD*) providing a unique ab-initio non-perturbative approach to deal with the computation of various observables of the hadronic world. We investigate the temperature dependence of LANDAU gauge gluon and ghost propagators in pure gluodynamics and in full *QCD*. The aim is to provide a data set in terms of fitting formulae which can be used as input for DS (or FRG) equations. We concentrate on the momentum range $[0.4, 3.0]$ GeV. The latter covers the region around $O(1)$ GeV which is especially sensitive to the way how to truncate the system of those equations. Regarding the gluon propagator, we compute its longitudinal (D_L) as well its transversal (D_T) components.

For pure gluodynamics in a fixed-scale approach we show D_L to react stronger than D_T, when crossing the first order deconfinement phase transition. At the same time the ghost propagator G looks nearly insensitive to the temperature. Since the longitudinal component turns out to be most sensitive with respect to the critical behavior we propose some combinations of it playing the role of an indicator for the transition. Major attention is paid to the extraction of the continuum limit as well as to systematic effects, as there are the choice of the right POLYAKOV loop sector, finite size and GRIBOV copy effects. Fortunately, finite-size and GRIBOV copy effects are found to be weak in the momentum range considered and at temperatures close to the deconfinement phase transition.

In a second step we deal with full ($N_f = 2$) *LQCD* with the twisted mass fermion discretization. We employ gauge field configurations provided by the *tmfT* collaboration for temperatures in the crossover region and for three fixed pion mass values in the range $[300, 500]$ MeV. The gluon and ghost propagators in the momentum interval $[0.4, 3.0]$ GeV show a smooth temperature dependence. We provide fit formulae and extract D_L^{-1} at zero momentum being proportional to the electric screening mass squared.

Finally, within $SU(3)$ pure gauge theory (at $T = 0$) we compute the LANDAU gauge gluon propagator according to different gauge fixing criteria. Our goal is to understand the influence of gauge copies with minimal (non-trivial) eigenvalues of the FADDEEV-POPOV operator (FP). Therefore, we compare the gluon propagator according to two different criteria, namely gauge copies with maximal gauge functional values versus those with minimal FP eigenvalues. Such a study should clarify how the GRIBOV copy problem influences the behavior of the gluon and ghost propagators in the infrared limit. By tending to smaller FP eigenvalues the ghost propagator is expected to become more infrared singular. The main aim is then to see whether the gluon propagator becomes infrared suppressed and therefore whether *LQCD* may describe a larger manifold of the so-called decoupling solutions as well as the scaling solution of DS equations. In an exploratory study we restricted ourselves to small lattice sizes, for which the influence of those copies at smallest accessible momenta turned out to be small.

Zusammenfassung

Die im infraroten Impulsbereich der Quantenchromodynamik (*QCD*) berechneten Gluon- und Ghost-Propagatoren spielen eine große Rolle für das sogenannte Confinement der Quarks und Gluonen. Sie sind Gegenstand intensiver Foschungen dank nicht-perturbativer Methoden basierend auf DYSON-SCHWINGER- (DS) und funktionalen Renormierungsgruppen-Gleichungen (FRG). Darüberhinaus sollte es deren Verhalten bei endlichen Temperaturen erlauben, den chiralen und Deconfinement-Phasenübergang bzw. das Crossover in der *QCD* besser aufzuklären.

Unser Zugang beruht auf der gitter-diskretisierten *QCD* (*LQCD*), die es als ab-initio-Methode gestattet, verschiedenste störungstheoretisch nicht zugängliche *QCD*-Observablen der hadronischen Welt zu berechnen. Wir untersuchen das Temperaturverhalten der Gluon- und Ghost-Propagatoren in der LANDAU-Eichung für die reine Gluodynamik und die volle *QCD*. Ziel ist es, Datensätze in Form von Fit-Formeln zu liefern, welche als Input für die DS- (oder FRG-) Gleichungen verwendet werden können. Wir konzentrieren uns auf den Impulsbereich von $[0.4, 3.0]$ GeV. Dieses Intervall deckt den Bereich um $O(1)$ GeV mit ab, welcher für den auf verschiedene Weise vorzunehmenden Abbruch des Gleichungssystems sensitiv ist. Für den Gluon-Propagator berechnen wir deren longitudinale (D_L) sowie transversale (D_T) Komponenten.

Für die reine Gluodynamik bei fixierter kleiner Gitter-Einheit zeigt sich, dass D_L im Vergleich zu D_T stärker bei Überschreiten des Phasenübergangs erster Ordnung variiert. Andererseits reagiert der Ghost-Propagator nahezu unempfindlich auf die Temperaturänderung. Da sich die longitudinale Komponente als empfindlich gegenüber dem kritischen Verhalten erweist, schlagen wir einige Kombinationen der Komponenten vor, die die Rolle von Indikatoren für den Phasenübergang spielen können. Große Aufmerksamkeit schenken wir der Extraktion des Kontinuumslimes und den systematischen Effekten, wie der Wahl des richtigen POLYAKOV-Loop-Sektors, dem Einfluss des endlichen Volumens und der GRIBOV-Kopien. Es erweist sich, dass die Effekte endlichen Volumens und von GRIBOV-Kopien relativ schwach in unserem Impulsbereich sowie für Temperaturen in der Nähe des Deconfinement-Phasenübergangs sind.

In einem zweiten Abschnitt beschäftigen wir uns mit der vollen ($N_f = 2$) *LQCD* unter Verwendung der sogenannten twisted mass-Fermiondiskretisierung. Von der *tmfT*-Kollaboration wurden uns dafür Eichfeldkonfigurationen für Temperaturen im Crossover-Bereich sowie jeweils für drei fixierte Pion-Massenwerte im Intervall $[300, 500]$ MeV bereitgestellt. Die Gluon- und Ghost-Propagatoren zeigen im Intervall $[0.4, 3.0]$ GeV eine vergleichsweise schwache Temperaturabhängigkeit. Für die Impulsabhängigkeit lassen sich in diesem Intervall relativ gute Fits erhalten. D_L^{-1} bei verschwindendem Impuls, das proportional zum Quadrat der elektrischen Abschirmmasse ist, wird als Funktion der Temperatur dargestellt.

Schließlich berechnen wir innerhalb der reinen $SU(3)$-Eichtheorie (bei $T = 0$) den LANDAU Gluon-Propagator unter Verwendung verschiedener Eichfixierungskriterien. Unser Ziel ist es, den Einfluss von Eich-Kopien mit minimalen (nicht-trivialen) Eigenwerten des FADDEEV-POPOV-Operators (FP) zu verstehen. Eine solche Studie soll klären, wie GRIBOV-Kopien das Verhalten der Gluon- und Ghost-Propagatoren im infraroten Bereich prinzipiell beeinflussen. Durch kleinere FP-Eigenwerte wird der Ghost-Propagator singulärer. Das Hauptziel ist es zu sehen, ob der Gluon-Propagator im Infraroten unterdrückt wird,

und ob somit die *LQCD* eine größere Mannigfaltigkeit der sogenannten decoupling- und scaling-Lösungen der DS- Gleichungen zu beschreiben gestattet. In einer explorativen Studie beschränken wir uns auf kleine Gittergrößen, für die sich der Einfluss solcher Kopien bei den von uns erreichbaren kleinen Impulsen als noch relativ gering erwies.

CONTENTS

CHAPTER 1

General introduction

It is nowadays commonly believed that quantum chromodynamics (*QCD*) is the true theory describing the hadronic world. The elementary degrees of freedom of *QCD* are quarks and gluons. The quarks are fermions carrying a spin of $\frac{1}{2}$ while gluons are the gauge bosons mediating the strong interaction. The physical gauge group considered throughout this thesis is the physical color symmetry group, namely $SU(3)$. This non-abelian gauge group introduces extra features to *QCD* which do not exist in the abelian $U(1)$ theory as quantum electrodynamics *QED*. As an example, the gluons are interacting with themselves as well as with quarks. In fact, *QCD* becomes an asymptotically free theory at large momenta. Such typical aspect of *QCD* is often named as *asymptotic freedom*. This refers actually to the property of the quarks and gluons to behave nearly as a free particles system at small distances and/or high energies exchange. Hence, perturbation theory computing physical observables expanded in powers of the small coupling is of avail at this high energy scale. Indeed, perturbative results were confronted to experiments and proven to be valid in deep inelastic scattering [1, 2, 3].

Another essential aspect to be mentioned is the complexity to describe *QCD* in terms of elementary degrees of freedom, namely quarks and gluons. Consequently, quarks and gluons, and generally colored states, are not observed in nature as asymptotic states. This is described in a dynamical view by asserting that color-charged particles experience a linear potential if pulled apart, e. g. the quark-anti-quark constituents of a meson, such that only color singlets can form asymptotic states. This peculiar phenomenon is generally known as *confinement*. In addition, it rises specifically in the infrared region of momenta, i. e. at low momenta, where exactly *QCD* perturbative theory breaks down. Still, strong investigation efforts were dedicated to look for isolated quarks even if the answer remained negative. Hence, such imposing experimental fact motivated and supported the hypothesis of confinement such that only bound states as hadrons and also glueballs might be in principle observed.

Besides experiments *QCD* as a theory exhibits also a rich phase structures due to several symmetry properties. That is, different degree of freedom according to different phases of the theory should exist. For example, in the confining phase, at low temperature and low chemical

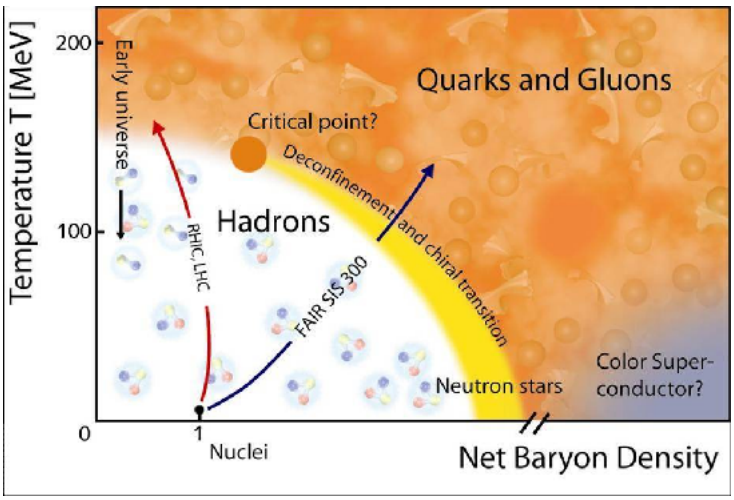

FIGURE 1.1: The expected *QCD* phase diagram in the $T-\mu_B$ plane, where T and μ_B refer to the temperature and the baryon chemical potential respectively. Different regimes of energies and densities are subjects of different experiments projects covering different phase diagram regions. In our present work we focus exclusively on the case $\mu_B = 0$ where lattice *QCD* is highly effective.

potential, hadrons are the degrees of freedom of interest. Therein chiral symmetry is spontaneously broken whereas the color center group symmetry is not. This latter group is nothing but $Z(3)$ supposed to be the underlying symmetry for confinement. On the other hand, at energy densities large compared to the natural scale ($\Lambda_{QCD} \sim 200\,\mathrm{MeV/fm^3}$) the situation is completely different, and one should expect a strong increase in the degrees of freedom of the theory. This means that gluons and quarks should in principle behave as a (nearly) free particle system. This latter state of matter is well described through the theoretical framework of *QCD*. Quantitatively speaking, at higher energies regime the average distance r between quarks and gluons becomes $r \ll \Lambda_{QCD}^{-1} \sim 1\,\mathrm{fm} \sim$ size of a hadrons exactly where *QCD* predicts a weak interaction, a phenomena, as already said, known as *asymptotic freedom* [4, 5, 6]. In other words, this is a consequence of the decrease of the coupling with the decrease of the distance between quarks and gluons, or equivalently with the increase of the momenta/energy exchange. Such free state of matter might be reached by increasing the temperature and/or densities. However, just before reaching this state matter should undergo a transition between a purely confined system of bound states to a plasma consisting of confined quarks and gluons. This latter state of matter is called in the literature the *quark-gluon plasma*, abbreviated as (*GPA*).

GPA studies are the concern of extensive experiments using heavy ions collisions at different scales of energies probing matter structures at extreme conditions. First experiments with moderate center mass energy per nucleon $\frac{\sqrt{s}}{A}$ of 2 GeV to 18 GeV were performed at the Alter-

nating Gradient Synchrotron (AGS) in Brookhaven and in the Super Proton Synchrotron (SPS) at CERN. More interesting results were also collected thanks to the Relativistic Heavy Ion Collider (RHIC), with $\frac{\sqrt{s}}{A} = 200\,\text{GeV}$. This race for higher energies goes on with the promising Large Hadron Collider (LHC) at CERN reaching $\frac{\sqrt{s}}{A} = 5.5\,\text{TeV}$ and with the heavy-ion detector ALICE. These multitude projects with their corresponding different phase diagram regions of interest are presented in Fig. 1.1. As a matter of fact, the main goal of the experimental efforts go into the direction of reaching high energy regimes as well as checking the reliability of many experimental models determining signatures of the *QGP*. In this thesis, we focus exclusively on the case $\mu_B = 0$ (zero baryon chemical potential) using lattice *QCD* (*LQCD*) as our prime tool. In a nutshell, the most problematic aspect of *LQCD* with finite chemical potential is the presence of the so-called "sign problem". This latter traces back to the fact that the fermion determinant becomes complex, and no standard *LQCD* computation might be possible.

One of the most interesting applications of *QCD* under extreme conditions is the study of the thermodynamics of the universe. It seems that during the evolution of the early universe a quark-hadron transition took place. Therefore a *QGP* formation seemingly happened shortly (around $\sim 10^{-5}$ sec) after the Big Bang. The early universe exposed a very hot state of matter (temperatures up to $\gtrsim 10^{12}$K) and looked quite different from actual observed universe. In fact, it was likely dominated by a total pressure of *QCD* degrees of freedom for temperatures larger than the transition temperature T_c. Further consequences of this are the actual rate expansion of the universe, and other physical phenomena as gravitational waves and dark matter. Other cases of matter under extreme conditions are the compact stellar objects whose the neutron stars are good examples. Since these stars expose high density regime $10^{16} - 10^{17}\, g/cm^3$ a production of *QGP* within these objects is very likely expected. Therefore, a proper understanding of basic thermodynamic quantities as the pressure among others as function of the temperature is essential for a proper understanding of our universe.

As said before, highly non trivial phenomena as confinement or chiral symmetry restoration are out of the reach of perturbation theory. As a result, perturbation theory which might be applied only at high temperatures (T) (or high densities μ_B), where essential non-perturbative effects has faded away, is of no avail. Thereby, one needs to consider non-perturbative methods to tackle such phenomena. However, successful predictions of perturbation theory (PT) suggests that the effective coupling must decrease with the increase of T and/or μ_B as

$$g(T) \sim \frac{1}{(11N_c - 2N_f)\log(T^2/\Lambda^2_{QCD})},$$

where, N_c and N_f are the number of colors and flavors respectively and Λ_{QCD} is the *QCD* scale. In fact, PT is successfully describing the hadronic matter in this regime. Nevertheless, it encounters serious problems at the stage of moderate temperatures around T_c. For example, in the case of zero temperature ($T = 0$) for a massless renormalizable theory the renormalization scale Λ is the only scale of the theory. Computing the self-energy correction(s) $\Pi(p)$ to the relevant propagator(s) of such theory -dimensional arguments and LORENTZ invariance taken into account-

will provide a behavior like $\Pi(p) = g^2 p^2 f(\frac{p^2}{\Lambda^2})$, where f is a dimensionless function. One points out that this correction is small compared to the scale introduced by external momentum p for small g, and no divergence happens when resumming in the propagator. At finite T ($T > 0$) the situation is fundamentally different. There, the temperature is introduced as a new scale, and it follows effects on the integrals for soft modes ($p < T$) which are dominated by momenta $k \sim T$. Note that within this scheme the self-corrections reads $\Pi \sim g^2 \cdot T^2$. Indeed, this means that these corrections become as large as the inverse propagator itself for soft modes $\sim gT$, and this is in fact this point which makes the PT framework break down [7]. For an overview of such non-perturbative problems we refer to [8] for example.

In order to overcome non-perturbative problems many strategies have been developed and proposed on the market. One might first talk briefly about the *Hard Thermal Loop* (HTL) resummation methods. Those latter provide a way out by improving the infrared behavior of the theory thanks to a consistent resummation of all loops dominated by hard thermal fluctuations [9, 10, 11, 12]. In general, these effects manifest themselves in gauge theories through the appearance of a thermally generated mass. It is worth to note, that a virtue of this scheme HTL is being manifestly gauge invariant and a consistent picture of *QCD* can be reproduced. One other strategy is the use of the so-called chiral perturbation theory (χPT) [13] which applies at low temperatures and low chemical potential. This method accounts for the smallness of the up and down quarks masses and for the broken chiral symmetry in a systematic way. The drawback, however, is the non predictability as the hadron resonances start to influence the properties of strong interacting matter. In general, such models base their study on phenomenology ingredients similar to that of *QCD* as there are WILSON lines or bound states.

Apart from the aforementioned methods Lattice *QCD* (*LQCD*) provides an ab-initio method to handle physical problems along the whole axis of energies/temperatures. For a comprehensive account of *LQCD* we refer to excellent standard books [14, 15, 16, 17]. In addition, simulations of *LQCD* with the help of Monte Carlo (*MC*) techniques provide a vast amount of data, and brings insights into the structure of the *QCD* phase diagram. In fact, Fig. 1.1 shows different regions of the phase diagram with different energy regimes. Actually, it is the crossover region close to the temperature axis which is explored by the experiments at *RHIC* and *LHC* at *CERN*. Note also the conjectured existence of a superconducting phase transition, in principle, reached by heavy ion collision depending on low temperature regime. Such superconducting behavior has been studied thanks to models yielding temperatures on the order of 50 MeV.

In order to study phase transitions within *LQCD* one needs to construct order parameters on the lattice in order to detect the passage from the confined to the deconfined regime. To illustrate, in pure gauge theory *LQCD*, when neglecting the fermion loops, the POLYAKOV loop plays the role of an order parameter for both $SU(2)$ and $SU(3)$ gauge groups [18, 19]. This is based on the fact that the center group $Z(3)$ (for $SU(3)$) is spontaneously broken crossing the phase transition temperature $T = T_c$. Hence, in the broken phase region a reduced number of flips are observed between different sectors of the POLYAKOV loop, and the transition expected in the pure gauge sector is of first order. In contrast, the situation dealing with full *QCD* is more

involved, and different observables might help. The chiral condensate is a good example of such order parameters whereas the POLYAKOV loop is not an exact order parameter. This chiral condensate signals the restoration of the chiral symmetry above the phase transition.

The observables of interest in this thesis are mainly the gluon and ghost propagators at finite temperature. These two-point GREEN functions represent building blocks of the DYSON-SCHWINGER (*DS*) equations [20, 21, 22, 23] as well as basic components for the functional renormalization group equations (*RGE*) investigations [24, 25]. Therefore, our goal is to provide data serving as input for these non-perturbative methods. Moreover, the propagator behavior data might also serve to confirm or to reject confinement scenarios as proposed by GRIBOV and ZWANZIGER [26, 27, 28] and KUGO and OJIMA [29, 30]. On the other hand, the zero temperature gluon and ghost propagators were intensively investigated within *LQCD* mainly for the LANDAU gauge, see [31, 32, 33, 34, 35, 36, 37, 32] and references therein. However, these propagators are less investigated at finite temperature. In fact, the $SU(2)$ gauge group for the LANDAU gauge was the scope of a few papers [38, 39, 40, 41, 42, 43, 44, 45]. The $SU(3)$ gauge group is less studied within pure gauge theory, see [46, 47, 48, 43, 49]. Our results are published in [49] aiming to fill this gap providing valuable data for pure gauge theory. Furthermore, the $SU(3)$ gluon and ghost propagators in the presence of dynamical fermions are even less studied [50, 51]. Therefore, we decided to study the fermionic case with the help of the lattice twisted mass discretization, as presented in our paper [52]. Regarding the ghost propagator, most of the papers support a temperature independent behavior for the ghost propagator as in [53, 54, 55, 56] and references therein. Still, we show in [49] that small fluctuation appear in the region of small momenta and at higher temperatures. Our full *QCD* results at finite temperature for the gauge group $SU(3)$ are in qualitative agreements with [42, 43]. We have also studied the impact of the GRIBOV problem on the ($SU(3)$ at $T = 0$) gluon propagator using a new criteria to select uniquely the gauge. Namely, we select gauge copies with minimal FADDEEV-POPOV eigenvalues. These gauge copies aim to make the ghost propagator more singular in comparison to gauge copies with maximum gauge functional. In principle, this comparative study aim to clarify which solution of *DS* equations might be supported by *LQCD* when the GRIBOV ambiguity is removed.

The structure of this thesis is as follows: Firstly in chapter II, the necessary theoretical background connected to *QCD* at finite temperature is introduced after a basic review of the framework of *QCD*. In brief, we introduce the classical formalism of *QCD* with the corresponding fields and symmetries. Then, we move on to the finite temperature case by virtue of the MATSUBARA formalism. Furthermore, a discussion of the nature of the *QCD* phase transition is given thanks to the concept of order parameters. At the end of this chapter the present status of art of the gluon and ghost propagator is presented. In chapter III we present the lattice and mathematical definitions of the gauge fields and the different lattice action discretizations used throughout this work. Moreover, we define the GRIBOV problem and discuss our strategy to deal with it. Lattice definitions of the observables of interest, namely the POLYAKOV loop, the gluon and ghost propagators are given in chapter IV. Our results are presented in chapters V, VI and VII. Actually, in chapter V we focus on different aspects of the gluon and ghost propagator in

pure gauge *QCD* at finite temperature. For this we relied on the standard WILSON pure gauge action. First and foremost we study different lattice artifacts as momenta pre-selection and even the POLYAKOV loop sector effects. We were also able to locate the critical temperature T_c thanks to the POLYAKOV loop susceptibility. In fact, the critical (inverse) coupling β_c used in this study is suggested by an extrapolation function proposed in [57], and the POLYAKOV loop study locating T_c is namely a check for the value of β_c. These prerequisites prepared the ground to multiple upcoming studies as the finite volume and finite lattice spacing effects. The GRIBOV ambiguity was also a target of investigations in order to understand how our momenta regime is affected by such a problem. After that we extrapolate our data to the continuum limit $a = 0$. At the end of the day we establish the continuum limit and get the continuum data in hand. We found out that our data reach indeed the continuum limit being at the same time important input data to the DYSON-SCHWINGER and the renormalization group equations. Quite recently authors in [58] took advantage of our data to compute the effective potential of POLYAKOV loop. Hence, FUKUSHIMA et al. were able to perform a thorough thermodynamic study taking into account our parametrization of the gluon and ghost propagators at finite T. Regarding sensitivity issues around the critical temperature T_c we propose "new order" parameters constructed out the longitudinal component of gluon propagator, namely D_L. These new objects turn out to react stronger than D_L around T_c, and hence might be of interest for further investigations using different volumes and critical temperatures.

Our second concern was to present results in chapter VI for full *QCD*, i. e. including fermions, for the special case of two number of flavors $N_F = 2$. In order to achieve this investigation we considered configurations provided by the tmfT collaboration, see [52]. These configurations are thermalized thanks to a combination of the SYMANZIK action as an improved pure gauge action and the so-called twisted mass action for the fermion part. One advantage of such twisted mass actions is to provide an automatic $O(a)$ improvement when tuning the hopping parameter κ to its critical value κ_c. Thanks to these configurations we are able to compute the gluon and ghost propagators as functions of the momentum and temperatures. Moreover, we fit again the gluon propagators data with GRIBOV-STINGL fitting formula giving good χ^2. This latter fit allowed us to show the gluon propagators as function of the temperatures for a few interpolated momenta. In fact our temperatures are chosen in a way to cover the crossover region where the expected temperatures where deconfinement and chiral symmetry breaking might happen. On the other hand the ghost propagator does show a weak reaction to temperatures variation as expected from its scalar tensorial structure.

Within chapter VII, and as a third subject of investigations, we get a closer look into the GRIBOV problem in $SU(3)$ pure gauge *QCD* at $T = 0$. It is already a notorious problem that the multiple DYSON-SCHWINGER solutions for the gluon and ghost propagators generally need to be confirmed thanks to lattice results. In general, these latter lattice results support the so-called *decoupling* solution [59, 60, 61]. Still, this solution does not satisfy important confinement scenarios as the KOGU-OJIMA scenario. We believe that this situation might be clarified thanks to a careful study of the GRIBOV ambiguity thanks to a new approach. Our goal here is to give some indications that namely standard gauge fixing prescriptions (using e. g. methods as *simulated an-*

nealing) might be confronted to our new criteria giving at the end different results on the lattice. In other words, we compare exclusively the gluon propagator using two different criteria to fix the gauge copies, namely simulated annealing (gauge copies with the highest gauge functional) vs. a new method picking up gauge copies with the smallest FADDEEV-POPOV (FP) eigenvalue for fixed configuration. This latter choice of the gauge copies using the FP eigenvalues defines the gauge uniquely. Finally, we sum up our results and draw a conclusion.

CHAPTER 2

Introduction to *QCD* at finite T

WITHIN this introductory chapter we review first basic elements of *QCD* at finite temperature T. Fields and gauge symmetries are also presented to fix notations and symbols used throughout this thesis. First, we adopt the path integral as the most usual quantization approach of *QCD*, and provide standard results on how *QCD* is regularized and renormalized. The second part of this chapter translates *QCD* concepts to the finite temperature case thanks to the so-called: MATSUBARA formalism. Finally, we discuss order parameters as there are the POLYAKOV loop and the chiral condensate, and their relevance within the phase diagram of *QCD*. To end up we give the status of art of the gluon and ghost propagators at $T > 0$ and define them mathematically in the continuum space-time.

2.1 Reviewing QCD

2.1.1 Fields, symmetries and classical action

Strong interactions in nature are described mathematically by the so-called quantum chromodynamics (*QCD*). Within this theory bound states as hadrons arise as particle excitations of the fundamental constituents, namely: quarks and gluons. In brief, *QCD* is a quantum field theory (*QFT*) which accounts for six type of quarks, called quarks flavors: up (u), down (d), strange (s), charm (c), bottom (b) and top (t). To have a basic understanding of their elementary properties please have a look to Table 2.1. Mathematically, *QCD* is also describing the gluons using eight 4-vector potentials A^a_μ, with $a = 1,\ldots,8$ or in a matrix notation as

$$A_\mu = A^a_\mu \lambda^a, \tag{2.1}$$

where λ^a are the 3×3 linearly independent GELL-MANN matrices (see Appendix 8), a and μ are the color and LORENTZ indices respectively. In the fundamental representation of the LIE group

Particle	Mass[MeV/c^2]	Electric charge	Baryon number	Spin
u	1.5-3.0	2/3	1/3	1/2
d	3-7	-1/3	1/3	1/2
s	95±25	-1/3	1/3	1/2
c	(1.25±0.09).10^3	2/3	1/3	1/2
b	(4.20±0.07).10^3	-1/3	1/3	1/2
t	(174.2±3.3).10^3	2/3	1/3	1/2
g	0	0	0	1

TABLE 2.1: Some elementary properties of quarks and gluons. The electric charge and the spin are given as multiples of the electron charge $|e|$ and $\hbar$

$SU(3)$ these λ^a represent the generators of the group satisfying both relations: $\mathrm{Tr}(\lambda^a\lambda^b) = \delta^a_b/2$ and the commutation relation $[\lambda^a, \lambda^b] = if^{abc}\lambda^c$. Here, the quantities f^{abc} are called the *constant structure* of the gauge group, here $SU(3)$, and δ^a_b are the usual KRONECKER symbol. Each quark (fermion) flavor corresponds to three (color) DIRAC 4-spinor fields ψ^c with $c = 1,2,3$. The quark fields look like in general as

$$\psi \equiv \psi^{\mu,c}_f. \tag{2.2}$$

Here, $f = 1,\ldots,6$ (the flavor number) and $\mu = 1,\ldots,4$ (the DIRAC indices). The fundamental principle of *QCD* is the local gauge invariance. This principle, together with the general requirement of locality, LORENTZ invariance and renormalizability strictly constraints the form of the Lagrangian $\mathscr{L}_{QCD}$. The simplest form of the Lagrangian in Euclidean four-dimensional space-time reads

$$\mathscr{L}_{QCD} = -\frac{1}{4}F^a_{\mu\nu}F^{a\mu\nu} + \sum_{\psi=u,d,s,c,b,t} \overline{\psi}(iD_\mu\gamma^\mu - m_\psi)\psi, \tag{2.3}$$

where $D_\mu = \partial_\mu - ig_0A_\mu$ is the gauge covariant derivative. The sum is defined over all the flavor quarks ψ^f and anti-quarks $\overline{\psi}^f$, and γ^μ denotes the DIRAC gamma matrices (see Section 8). The gluon field strength tensor is denoted as $F_{\mu\nu} = \frac{i}{g_0}[D_\mu, D_\nu]$ with g_0 is the bare coupling constant and m_ψ representing the bare mass for each quark flavor. In general, the structure of $F_{\mu\nu}$ looks like

$$F^a_{\mu\nu} = \partial_\mu A^a_\nu - \partial_\nu A^a_\mu + g_0 f^{abc}A^b_\mu A^c_\nu. \tag{2.4}$$

Here and in the following, the latin indices (a,b,c) represent the color indices taking the values $1,\ldots,N_c^2-1$ (adjoint representation), where N_c is in general the number of color (equals to 3 for the $SU(3)$ color gauge group case). On the other hand, the greek indices μ and ν symbolize the usual LORENTZ indices running from 1 to 4. According to Eq. (2.3) and Eq. (2.4) one may

observe the gluons self-interaction as well as interactions between quarks and gluons. This self-interaction of the gluons within Eq. (2.4) is essentially due to the non-abelian structure of $SU(3)$, i. e. the structure constants f^{abc} for the LIE algebra $su(3)$ are not equal to zero. The quark and anti-quark fields representing the matter fields are connected through

$$\overline{\psi} \equiv \psi^{\dagger}\gamma_0. \tag{2.5}$$

These latter fields transform as usual under the fundamental representation of the $SU(3)$ color group, i. e. the color indices runs over $c = 1,\ldots,(N_c = 3)$ with the γ_0 matrix is obviously the DIRAC matrix corresponding to a zero (temporal) LORENZ index. The classical *QCD* action may be defined as a four dimensional space-time integral of the Lagrangian density Eq. (2.3)

$$S_{QCD} = \int dt \int d^3x \mathscr{L}_{\mathrm{QCD}}. \tag{2.6}$$

Here is (x,t) the space-time point. This action (Eq. (2.6)) is invariant by definition under the following set of $SU(3)$ local gauge transformations of (anti-)quarks and gluon fields

$$\begin{aligned} A_\mu &\longrightarrow A^{\omega}_{\mu} = g_\omega A_\mu g^{\dagger}_{\omega}, \\ \psi &\longrightarrow \psi^{\omega} = g_\omega \psi, \\ \overline{\psi} &\longrightarrow \overline{\psi}^{\omega} = \overline{\psi} g^{\dagger}_{\omega}. \end{aligned} \tag{2.7}$$

The $SU(3)$ local gauge transformations g_ω are parametrized by the real functions $\omega(x)$ as

$$g(x) = \exp(i\omega^a(x)\lambda^a/2), \tag{2.8}$$

where the GELL-MANN matrices λ^a (see Appendix 8) are acting on the color indices of the (anti-)quark field. Due to the previous set of color gauge symmetry the quark-gluon and gluon-gluon interaction strength are determined by the same universal coupling constant g_0. Consequently, this fact constraints the the number of independent Z-factors introduced within the regularization scheme. Regularization and renormalization shall be discussed more in detail in Section 2.1.3. For the sake of completeness, we recall as well the infinitesimal form of the local gauge transformations Eq. (2.7) yielding

$$\delta A^a_\mu = \partial^a_\mu + g_0 f^{abc}\omega^b A^c_\mu = D^{ab}_\mu \omega^b, \tag{2.9}$$

$$\delta\psi = -ig_0\omega^a\lambda^a\psi, \tag{2.10}$$

$$\delta\overline{\psi} = +ig_0\omega^a\lambda^a\overline{\psi}. \tag{2.11}$$

Here and in general, we define the infinitesimal gauge transformation for the a generic gauge field $\Psi \to \Psi^{\omega}$ as follows [62]

$$\delta\Psi \equiv \omega^b \frac{\partial}{\partial \omega_b \Psi^{\omega}} \mid_{\omega=0} =: \omega^b \delta_b \Psi(x). \tag{2.12}$$

In the next section, we focus first on the quantization of *QCD* using the path integral approach. Furthermore, we discuss the FADDEEV-POPOV method in order to introduce the physical fields content for quantizing *QCD* with a particular interest to the LANDAU gauge.

2.1.2 The quantization path integral formalism

The quantization of *QCD* using either the path integral or the canonical quantization method is not a trivial task. The complexity comes from the fact that the *QCD* Lagrangian (Eq. (2.3)) is invariant under local gauge transformations. However, such problems are not present when dealing with gauge invariant observables, and especially on the lattice, where integrals over the compact gauge group (as $SU(3)$) become automatically finite.

In the continuum, one usually generalizes the classical Lagrangian Eq. (2.6) adding extra terms (extra fields). This guarantees that expectation values of gauge invariant observables are independent of the gauge condition. However, along this quantization process, the gauge invariance is lost, and another symmetry takes place, namely, the *BRST* symmetry.

To quantize a classical theory, one needs to choose a quantization procedure suitable to the nature of the physical problem. Different quantizations methods treat the fields and the computation of the n-point functions (the GREEN functions) differently. For example, the canonical quantization method regards the fields as operators, and the GREEN functions are computed as vacuum expectation values. Most interesting for us is the path integral formalism taking the fields as c-numbers, and the GREEN functions defined as functional integrations of products of fields over all of their (weighted) possible functional forms. Within this latter formalism the action remains classical without the introduction of any auxiliary fields.

In the following, we concentrate on the path integral formalism. Classical *QCD* is quantized using the functional integration formalism integrating over the (anti-)quark and the gauge bosons fields. The Grassmannian integral on the (anti)quark fields is Gaussian, and might be performed instantly leaving only integration over gluon fields. Therefore, we concentrate in the following only on integrations over the gauge boson fields A.

As well said before, the fields $A^{(\omega)}$ and A are related by a gauge transformation Eq. (2.8), and thus they are physically equivalent. We say that the gauge fields are belonging to the same orbit. In fact, this orbit is spanned by all the gauge transformed fields at each space-time point. So, in principle, in order to quantize a gauge theory one performs an integration over gauge transformations belonging to different equivalence classes, i. e. different orbits of the gauge fields. This procedure avoids to take into account the redundancies of the gauge field within the same orbit whose in general present extra difficulties for the quantization. In the literature such quantization method selecting unique representative for each orbit is called the FADDEEV-

POPOV (*FP*) quantization method [63, 64]. In general, one usually constructs the generating functional

$$Z[j,\overline{\omega},\omega] = \int [\mathscr{D}A\mathscr{D}\psi\mathscr{D}\overline{\psi}]\,\Delta_f[A]\,\delta\left(f[A]\right)\,e^{-\int d^4x\mathscr{L}_{\rm QCD}+\int d^4x\left(A^a_\mu j^a_\mu+\overline{\omega}\psi+\overline{\psi}\omega\right)}, \tag{2.13}$$

where j, $\overline{\omega}$ and ω are the corresponding sources of the gluons, quarks and anti-quarks fields. Δ_f is the *FP* determinant whose definition is given a bit below in Eq. (2.17). The integration over the representative of each orbit is done using the general relation, i. e. the gauge fixing condition

$$f[A;\mathrm{x}] = 0, \tag{2.14}$$

at each space-time point x. In our particular case, we focus on the LANDAU gauge, i. e. on the gauge condition $\partial_\mu A_\mu = 0$, as we shall see later on. We assume for the moment that the path integral measure is well defined in Eq. (2.13). In case Eq. (2.14) is satisfied only once for each gauge orbit we call the gauge condition *ideal* [65]. If this is not the case the gauge condition is called *non-ideal*[1], and integration over the fields would be ambiguous. Indeed, this problem occurs specially beyond perturbation theory where the coupling constant becomes significant.

Different solutions to Eq. (2.14) are called GRIBOV copies, and the space spanned by unique representatives of each orbit is the *fundamental modular region* (FMR) Λ. Therefore, in principle, an integration over Λ of the type

$$\int_\Lambda [\mathscr{D}A] \quad e^{S_{\rm QCD}[A]} \tag{2.15}$$

is well defined. However, an analytical construction of such space is not trivial. On the lattice, for example, such construction is based on the study of maxima (or minima depending on the definition) of the gauge functional in order to get as close as possible to the (unknown) absolute global gauge transformation. The general strategy of the *FP* method is to start with the introduction of the **FADDEEV-POPOV determinant** $\Delta_f[A]$ defined with Eq. (2.13) by means of invariant integration

$$\Delta_f[A]\int \mathscr{D}\omega(x)\prod_x \delta\left(f\left[A^{(\omega)}(x)\right]\right) = 1, \tag{2.16}$$

yielding in the general case

$$\Delta_f^{-1}[A] = \sum_{i:\,f\left[A^{(\omega_i)}\right]=0} \det{}^{-1}\frac{\delta f\left[A^{(\omega_i)}\right]}{\delta\omega}. \tag{2.17}$$

[1] One needs to note that even popular gauge fixing conditions as the LANDAU gauge are in fact non-ideal. The success of the LANDAU gauge in the perturbative regime comes from the fact that the coupling is small yielding small fluctuations around the unit gauge transformation.

The LANDAU gauge is a particular case of Eq. (2.14) [2], namely

$$f[A]: \quad \partial_\mu A_\mu = 0. \tag{2.18}$$

Therefore, in this case, one obtains the following expression for the FP determinant

$$\Delta_{\text{Landau}}[A] = \det\left(\Delta + ig_0 \partial_\mu A_\mu\right) = \int [\mathscr{D}c\mathscr{D}\bar{c}]\, e^{-\int d^4x d^4y \bar{c}^a(x).\mathscr{M}^{ab}_{FP}(x,y)c^b(y)}. \tag{2.19}$$

The anti-commuting fields c and $\bar{c}$ defined in the adjoint representation of the gauge group are called **FADDEEV-POPOV ghosts**, and

$$\mathscr{M}^{ab}_{FP}(x,y) = -\partial^x_\mu D^{ab}_{x,\mu}[A]\delta^{(4)}(x-y) \tag{2.20}$$

is the so-called **Faddeev-Popov matrix**. One may generalize the aforementioned generating functional Eq. (2.13) to the general case of covariant gauges [3] as

$$f[A]: \quad \partial_\mu A_\mu = \mathfrak{a}(x), \qquad \mathfrak{a}(x) \in \mathfrak{su}(N_C). \tag{2.21}$$

Note, Δ_f is the same as in the LANDAU gauge case Eq. (2.19). Integrating on $\mathfrak{a}(x)$ with some Gaussian weight having a dispersion ξ yields for the generating functional

$$Z[j,\overline{\omega},\omega,\overline{\sigma},\sigma] = \int [\mathscr{D}A\mathscr{D}\psi\mathscr{D}\overline{\psi}\mathscr{D}c\mathscr{D}\bar{c}]\, e^{-\int d^4x \mathscr{L}_{eff}[A,\psi,\overline{\psi},c,\bar{c}]+\Sigma}, \tag{2.22}$$

$$\mathscr{L}_{eff}[A,\psi,\overline{\psi},c,\bar{c}] = \mathscr{L}_{\text{QCD}} - \frac{(\partial_\mu A_\mu)^2}{2\xi} - \bar{c}^a(x)(\delta^{ab}\Delta + ig_0 f^{abc}A^c_\mu \partial_\mu)c^b(x) \tag{2.23}$$

$$\Sigma = \int d^4x \left(A_\mu j_\mu + \overline{\omega}\psi + \overline{\psi}\omega + \overline{\sigma}c + \bar{c}\sigma\right). \tag{2.24}$$

Putting $\xi = 0$ corresponds to the LANDAU gauge. The gauge fixing term in Eq. (2.22) can be expressed as a result of Gaussian integration on an auxiliary field $B^a(x)$. As a result, this bring us to an effective Lagrangian form $\mathscr{L}_{eff} \equiv \mathscr{L}_{\text{BRST}}$

$$\mathscr{L}_{\text{BRST}} = \mathscr{L}_{QCD} - \frac{\xi}{2}(B^a)^2 + B^a\partial_\mu A^a_\mu + \bar{c}^a(\delta^{ab}\Delta - ig_0 f^{abc}\partial_\mu A^c_\mu)c^b. \tag{2.25}$$

Hence, we are ending up with an effective Lagrangian invariant under the so-called **BRST transformations** [66, 67, 68].

The **BRST transformations** are the remnant of the classical gauge transformations resulting from replacing the gauge parameters by Grassmann variables. These transformations are global ones. The virtue of the **BRST transformation** is to allow simpler ways of derivation of

[2] We suppose for the moment that the LANDAU gauge is unique. This is nearly the case in perturbation theory since one assumes the coupling to be small in this regime.

[3] The LANDAU gauge is a special case of the family of covariant gauges.

the SLAVNOV-TAYLOR identities [69, 70] as a direct consequence of the gauge invariance. These identities were the cornerstone of the general proof of the renormalizability of non-abelian gauge theories by 'T HOOFT and VELTMAN [6] in 1972.

2.1.3 Regularization and renormalization

General approach

QCD as defined so far needs special care at the level of perturbative theory (PT). Expanding the GREEN functions of *QCD* in terms of the coupling within PT brings extra technical difficulties dealing with loop integrals. The involved mathematical expressions actually diverge as the cutoff of the internal momenta is sent to infinity. Hopefully, thanks to the renormalizability of *QCD* one can absorb all the divergences (at any order) in a suitable redefinition of a finite number of parameters in the Lagrangian, and also into the normalization of the *Green* functions. Thereby, calculations at any order of PT in *QCD* would lead to finite results after renormalization. Thus, the renormalized *QCD* becomes a predictable theory, and results might be confronted to experiments.

In order to define completely *QCD* [4] one needs to compute the whole set of GREEN functions (n-points functions). These functions might be defined through the path integral formalism introduced in Section 2.1.2 as functional derivatives with respect to the general sources $\mathscr{J}_i^{a_i}(x)$

$$\langle \Phi_1^{a_1}(x_1)\cdots\Phi_n^{a_n}(x_n)\rangle = \left.\frac{\delta^n Z[\mathscr{J}]}{\mathscr{J}_1^{a_1}(x_1)\cdots\mathscr{J}_n^{a_n}(x_n)}\right|_{\mathscr{J}_1^{a_1},\ldots,\mathscr{J}_n^{a_n}=0} \tag{2.26}$$

where i counts the number of fields Φ and a_i denotes the collection of indices including LORENTZ, DIRAC and the flavor indices. Now, using Eq. (2.22), this latter formula may be rewritten in a compact path integral form as

$$\langle \Phi_1^{a_1}(x_1)\cdots\Phi_n^{a_n}(x_n)\rangle = \frac{1}{Z[0]}\int [\mathscr{D}\Phi]\ \Phi_1^{a_1}(x_1)\cdots\Phi_n^{a_n}(x_n)\, e^{-S[\Phi]} \tag{2.27}$$

where $Z[0]$ stands for the partition function while switching off the sources. In fact, connected n-point functions can be generated from the functional $W[\mathscr{J}] = \log(Z[\mathscr{J}])$ by successive differentiations as in Eq. (2.26). A further step would be to transform $W[\mathscr{J}]$ according to the LEGENDRE transformation yielding the effective action

$$\Gamma[\Phi] := sup\left(-W[\mathscr{J}] + \int \mathscr{J}\Phi\right), \tag{2.28}$$

where $\mathscr{J} = \mathscr{J}[\Phi]$ is meant to extremize $\int -W[\mathscr{J}] + \mathscr{J}\Phi$ with Φ denoting the expectation values $\langle\phi\rangle$. This last effective action generates the 1PI (one particle irreducible) GREEN functions

[4] Not only *QCD*, but in general any quantum field theory.

by differentiating with respect to Φ like

$$\langle \Phi_1^{a_1}(x_1)\cdots\Phi_n^{a_n}(x_n)\rangle_{1\mathrm{PI}} = \left.\frac{\delta^n\Gamma[\Phi]}{\Phi_1^{a_1}(x_1)\cdots\Phi_n^{a_n}(x_n)}\right|_{\Phi^0}. \tag{2.29}$$

This latter expression needs to be evaluated at vanishing sources at the end, i. e.

$$\Phi_i^0 = \left.\frac{\delta W}{\delta \mathscr{J}_i}\right|_{\mathscr{J}=0}. \tag{2.30}$$

As explained before, these GREEN functions being in general not gauge-invariant pose problem in the perturbative range of *QCD* where the coupling is supposed to be small. Actually, momenta loops integrations yields infinite quantities, and a renormalization prescription is necessary.

Prior to renormalize *QCD* one needs first the regularize it. Regularizing *QCD* may be done invoking several regularization schemes, e. g. the PAULI-VILLAR and the dimensional regularization methods. However, more interesting for us is the lattice regularization of *QCD*. This method introduces an ultraviolet cutoff $\Lambda = a^{-1}$. This cutoff renders instantly all the momentum loops integrations finite. So, in principle, any computation of the GREEN functions on the lattice should not suffer from such kind of divergences.

After regularizing *QCD*, for example by introducing the lattice cutoff λ, we renormalize our GREEN functions. This is achieved by introducing the so-called Z-factors formally into the bare Lagrangian in Eq. (2.3). Concretely, this amounts to define a renormalized effective Lagrangian L^r_{eff} [71] as

$$\begin{aligned} L^r_{eff} &= Z_3\,\frac{1}{2}A^a_\mu\left(-\partial^2\delta_{\mu\nu} - \left(\frac{1}{Z_3\xi_r}-1\right)\partial_\mu\partial_\nu\right)A^a_\nu \\ &+ \widetilde{Z}_3\,\overline{c}^a\partial^2 c^a + \widetilde{Z}_1\,g_r f^{abc}\,\overline{c}^a\partial_\mu\left(A^c_\mu c^b\right) - Z_1\,g_r f^{abc}\left(\partial_\mu A^a_\nu\right)A^b_\mu A^c_\nu \\ &+ Z_4\,\frac{1}{4}g_r^2 f^{abe}f^{cde}A^a_\mu A^b_\nu A^c_\mu A^d_\nu + Z_2\,\overline{\psi}\big(-\gamma_\mu\partial_\mu + Z_m m_r\big)\psi \\ &- Z_{1F}\,ig_r\,\overline{\psi}\gamma_\mu T^a\psi A^a_\mu \end{aligned} \tag{2.31}$$

with the renormalized parameters g_r, m_r, ξ_r are connected to their bare values g_o, m_o, ξ_o with the relations

$$g_o = Z_g g_r, \tag{2.32}$$
$$m_o = Z_m m_r, \tag{2.33}$$
$$\xi_o = Z_3\xi_r\,. \tag{2.34}$$

Moreover, theses fields appearing in the quantized Lagrangian Eq. (2.25) (in the LANDAU gauge)

have also to be rescaled as

$$A^a_\mu \to Z_3^{1/2} A^a_\mu, \tag{2.35}$$

$$\psi \to Z_2^{1/2} \psi, \tag{2.36}$$

$$c^a \to \widetilde{Z}_3^{1/2} c^a. \tag{2.37}$$

We mention also that the renormalized G_r and regularized G_{reg} GREEN functions are related to each other as follows

$$G_r(p_1,\ldots,p_n;g_r,m_r,\xi_r) = Z_G \cdot G_{\text{reg}}(p_1,\ldots,p_n;\Lambda,g_o,\xi_o,m_o). \tag{2.38}$$

In this last equation Z_G denotes in general some combination of the Z-factors who in general are depending on the cutoff. Still, the renormalized GREEN functions must not depend on the cutoff, but rather on the scale of the theory. This scale might be in principle experimentally determined. In principle, the Z-factors introduced so far are independent from each others a consequence of the SLAVNOV-TAYLOR identities. These latter identities constraint the number of independent Z factors, and is a consequence of the universality of the bare coupling g_o in *QCD*.

It is worth to note that GREEN functions need as said before to be renormalized, and the Z-factors correspondingly somehow to be computed as well. However, there are different renormalization schemes in order to determine the Z-factors. The difference between these schemes is essentially the way how the divergences are absorbed when rescaling the parameters. We concentrate in this thesis on the so-called *MOM* scheme [5].

Within the *MOM* scheme, the Z-factors are determined such that the two and three point function equal their corresponding tree-level expressions at some momentum μ. The momentum point μ is called the renormalization (or sometimes subtraction) point. During this thesis, our results regarding the gluon and ghost propagators are renormalized choosing $\mu = 5\,GeV$ for the results for pure gauge theory while $\mu = 2.5\,GeV$ is reserved for our fermionic investigations. For more details on our renormalization procedure we refer to Section 4.4.

2.1.4 The functional method approaches to *QCD*

Beside *LQCD*, some of the most interesting non-perturbative approaches to study the behavior of the gluon and ghost propagators in *QCD* (in the continuum) are the so-called functional methods. In particular, the DYSON SCHWINGER equations (*DSE*) and the functional renormalization group equations (*FRGE*) are two of such methods. We give hereafter an introduction to the *DSE* equations. We start with a derivation of these equations, and then we interpret their simple solutions for the case of the gluon and ghost propagators. After that, we give also an overview of the renormalization group techniques emphasizing their role in both infrared and ultraviolet regions of *QCD*.

[5] There are also other renormalization subtraction schemes such as the *MS* and $\overline{MS}$ schemes.

The DYSON-SCHWINGER equations (*DSE*) approach

Basically, the *DSE* equations correspond to a functional, continuum approach to the quantum theory beyond perturbation theory. These equations are viewed as the equations of motion for exact propagators and vertices. The starting observation to derive the *DSE* is to make the assumption that the functional integral of a total derivative vanishes

$$0 = \int [d\phi] \frac{\delta}{\delta \phi} \left(e^{[-S[\phi] + \int \mathscr{J} \phi]} \right). \tag{2.39}$$

This latter equation might be rewritten as

$$\left(\mathscr{J}_i - \left. \frac{\delta S[\phi]}{\delta \phi_i} \right|_{\phi \to \frac{\delta}{(\delta \mathscr{J})}} \right) Z[\mathscr{J}] = 0. \tag{2.40}$$

Here, the subscript i collects all type of indices as the space time, color and DIRAC degrees of freedom. Moreover, the field ϕ_i might correspond to one of the following fields: $A^a_\mu, \bar{c}^a, c^a, \overline{\psi}, \psi$. Now, using the following identities

$$\mathscr{J}_i = \frac{\delta \Gamma[\Phi]}{\delta \Phi_i}, \tag{2.41}$$

and

$$F[\frac{\delta}{\delta \mathscr{J}_i}] Z[\mathscr{J}] = F[\frac{\delta}{\delta \mathscr{J}_i}] e^{W[\mathscr{J}]}, \tag{2.42}$$

with Γ is the effective action defined in Eq. (2.28), and using the derivative with respect to the source terms as

$$\frac{\delta}{\delta \mathscr{J}_i} = \frac{\delta \Phi_j}{\delta \mathscr{J}_i} \frac{\delta}{\delta \Phi_j} = \left(\frac{\delta^2 W}{\delta \mathscr{J}_i \delta \mathscr{J}_j} \right) \frac{\delta}{\delta \Phi_i}, \tag{2.43}$$

one gets the interesting form

$$\frac{\delta \Gamma[\Phi]}{\delta \Phi_i} = \frac{\delta S}{\delta \phi_i} [(\frac{\delta^2 W}{\delta \mathscr{J}_j \delta \mathscr{J}_k}) \frac{\delta}{\delta \Phi_k} + \Phi_j]. \tag{2.44}$$

Furthermore, arbitrary 1PI (one-particle irreducible) correlators correspond to differentiating Eq. (2.44) with respect to the fields, and putting the sources equal to zero at the end. This yields finally a tower of infinite integral equations coupling GREEN functions to each other. In order to be solved one needs to truncate this system of equations at some level. We remark that all the terms of perturbation theory might be totally recovered reiterating these equations indefinitely. The most interesting *DSE* equations for us are the ones corresponding to the quark, gluon and

ghost fields. For instance, the quark propagator reads in terms of the effective action Γ as

$$S(x,y) \equiv \langle T\,\psi(x)\bar{\psi}(y)\rangle_{connected} = \left(\frac{\delta^2\Gamma}{\delta\Psi(y)\delta\bar{\Psi}(x)}\bigg|_{\Psi^0}\right)^{-1} \tag{2.45}$$

Moreover, the renormalized $S(p,\Lambda)$ and unrenormalized $S(p,\mu)$ quark propagators are related in momentum space via the Z_2-factor as

$$S(p,\Lambda) = Z_2(\mu,\Lambda)\,S(p,\mu), \tag{2.46}$$

where λ denotes the cutoff parameter and μ the renormalization point. In order to get the *DSE* equation for the full renormalized quark propagator we combine Eq. (2.44) (differentiating with respect to Ψ and $\overline{\Psi}$) together with Eq. (2.45) and Eq. (2.46). After some algebra[6], the *DSE* for the quark field is given by

$$S^{-1}(p,\mu) = Z_2(\mu,\Lambda)\,S_0^{-1}(p,\Lambda) + \Sigma(p,\mu), \tag{2.47}$$

where the subscript (0) denotes the bare propagator and $\Sigma(p,\mu)$ symbolizes the self energy. In terms of equations the bare quark propagator and its bare mass are

$$S_0^{-1}(p,\Lambda) = \not{p} + m_0(\Lambda), \tag{2.48}$$

$$m_0(\Lambda) = Z_m(\mu,\Lambda)\,m_r(\mu). \tag{2.49}$$

Here m_r denotes the renormalized quark mass. On the other hand, the self energy $\Sigma(p,\mu)$ describing the quark-gluon interaction is given by

$$\Sigma(p,\mu) = Z_{1F}(\mu,\Lambda)\,g_r(\mu)^2 C_f \int \frac{d^4q}{(2\pi)^4}\gamma_\mu S(q,\mu)\Gamma_\nu(k,l,\mu)D_{\mu,\nu}(k,\mu), \tag{2.50}$$

where the CASIMIR factor is given by $C_f = \frac{N_c^2-1}{2N_c}$. This self energy is a composition of the DIRAC matrices γ_μ (see Appendix 8), the full quark propagator $S(q,\mu)$, the 1PI $q\bar{q}g$-vertex $g_s(\mu)\Gamma_\nu(k,l,\mu)$ and the full gluon propagator $D_{\mu\nu}(k)$. The gluon propagator momentum is denoted by $k = (p-q)$ and the average momentum by $l = (p+q)/2$. As usual g_r denotes the strong coupling. We observe from Eq. (2.47) the quark *DSE* are composed of fundamental building blocks as there are the full quark, the gluon propagator and the $q\bar{q}g$-vertex. The quark *DSE* might be viewed diagrammatically in Fig. 2.1. Further functional derivatives of the expression Eq. (2.44) with respect to a suitable number of fields ϕ, and subsequently setting all sources to zero, lead actually to the DYSON-SCHWINGER equation for any desired full n-point function.

Obviously, in order to get the *DSE* for the gluon and ghost propagators, and also for the ghost-gluon vertex function one needs to differentiate with respect to the corresponding set of fields

[6] Readers interested in more details are referred to the textbooks [72, 73] or the reviews [74, 71].

FIGURE 2.1: A diagram representing the quark DYSON-SCHWINGER equation. The left hand side represents the inverse dressed quark propagator. The right hand side denote the inverse bare propagator and a dressing loop containing dressed quark and gluon propagators and one bare and one dressed quark-gluon vertex. This figure was taken from [75].

$(A^a_\mu, c^a, \overline{c^a})$. In general, the *DS* equations are presented in terms of diagrams. In Fig. 2.2 we show the diagrams corresponding to the gluon and ghost propagators.

The most interesting impact of the *DSE* equations comes out of the study of *QCD* in the infrared region of momenta Actually, the starting point is to focus on ghost-gluon vertex *DSE* depicted in Fig. 2.3. In fact, in the LANDAU gauge it is shown that the ghost-gluon vertex becomes bare in the limit of low momenta. This conclusion has been drawn already by TAYLOR long ago in 1971 [70], and has been confirmed recently by numerical studies of the ghost-gluon vertex on the lattice and in the *DSE*-approach [76, 77, 78]. This property may survive up to mid-momentum regime [78]. Within the LANDAU gauge and the property of the gluon-ghost vertex to remain bare at the infrared one finds asymptotic solutions for the *DS* equations for the gluon and ghost propagators. In fact, *DSE* admit a self-consistent power law solution in the infrared for the ghost and gluon propagators. Since one may write

$$\begin{aligned} G(p^2) &= -\frac{J(p^2)}{p^2}\,, \\ D_{\mu\nu}(p^2) &= \left(\delta_{\mu\nu} - \frac{p_\mu p_\nu}{p^2}\right)\frac{Z(p^2)}{p^2}\,, \end{aligned} \tag{2.51}$$

one finds power laws for the ghost and gluon dressing functions J and Z with the exponent κ:

$$J(p^2) \sim (p^2)^{-\kappa}, \tag{2.52}$$

$$Z(p^2) \sim (p^2)^{2\kappa}. \tag{2.53}$$

as described in [79, 20]. It is worth to observe that the self-consistency of these solutions forces an interrelation of the exponents such that they depend only on an unique parameter κ. This kind of solutions are called *scaling* solutions. On the other hand, the numerical value of κ is constrained according to several criteria. For instance, the KUGO-OJIMA confinement scenario

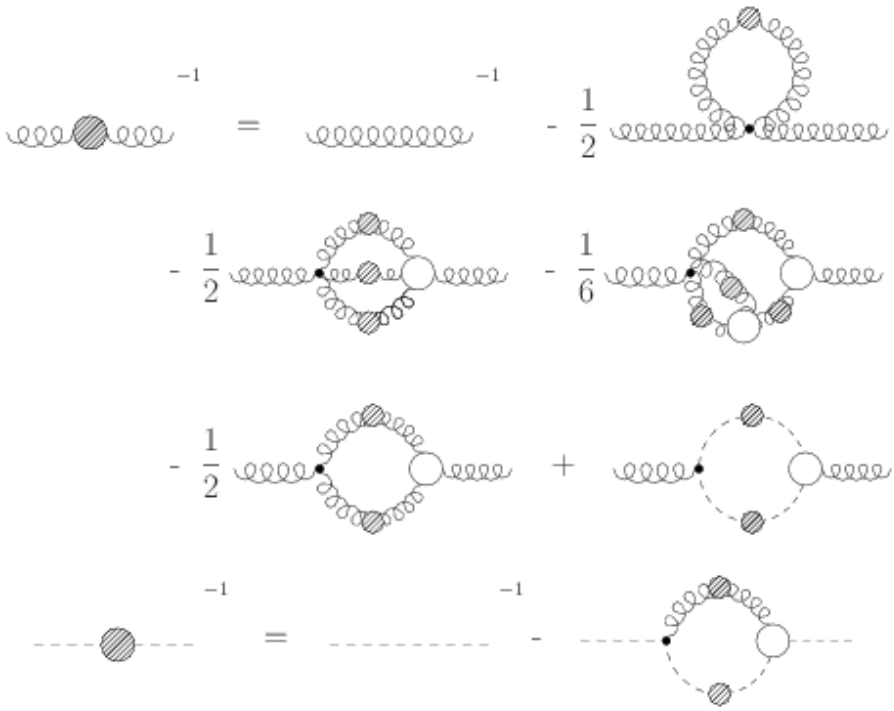

FIGURE 2.2: A diagram representing the DYSON-SCHWINGER equation for the gluon and ghost propagator, where filled circles denote dressed propagators and empty circles denote dressed vertex functions. This figure was taken from [75].

translates into the condition $\kappa > 0$, while the ZWANZIGER conditions impose $\kappa > 0.5$ for the gluon propagator. Those conditions stress that the ghost propagator should be more singular as a simple pole, whereas the gluon propagator is less singular. In a general analysis of the *DSE* solutions one shows in fact that κ must be positive in agreement with the previous predictions [80]. Other investigations depending on the details of the ghost-gluon vertex give also slightly different values for κ (around 0.595) [81] confirming values from [27]. Even more interesting is the agreement from the renormalization group equations which is going to be reviewed in the next section [25, 82]. At the end, all these investigations lead to the same conclusion, namely the gluon propagator needs to vanish in the infrared in agreement with ZWANZIGER horizon condition. In fact, there is a unique solution satisfying a power law ansatz, see [83, 84]. Moreover, ZWANZIGER pointed out that infrared asymptotic solution to the *DSE* done so far has been implicitly chosen to satisfy the supplementary condition [79, 81, 85]. Therefore, in order to find the physical solutions one needs to impose proper infrared boundary conditions. Similar studies were done within the renormalization group equations methods observing a convergence to a unique solution and concluding that DSE and FRGE solutions are in one to one correspon-

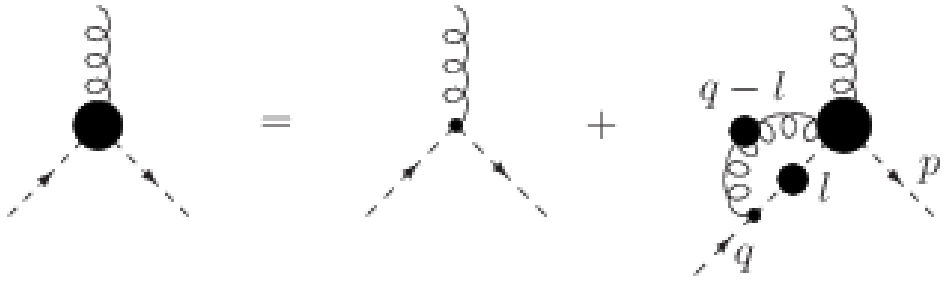

FIGURE 2.3: A diagram representing the DYSON-SCHWINGER equation for the ghost-gluon vertex, where the filled circles indicate dressed GREEN functions, *i.e.* propagators and vertices. A wiggly line denotes a gluon propagator, whereas a dashed line stands for a ghost propagator. This figure was taken from [75].

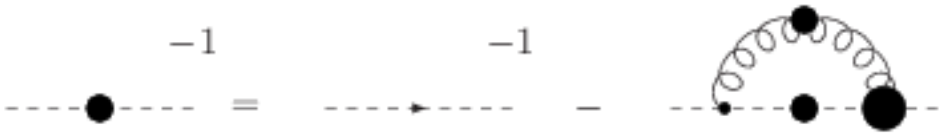

FIGURE 2.4: A diagram representing the DYSON-SCHWINGER equation for the ghost propagator (on the l.h.s.). This latter propagator is the sum of the inverse of the bare ghost propagator and a loop diagram containing dressed ghost and gluon propagators connected by one bare and one dressed ghost-gluon vertex. This figure was taken from [75].

dence. On the lattice, the scaling behavior of the *DSE* with $\kappa > 0$ is in general not possible to be obtained as in the case of a three dimensional theory [86]. Except for the strong coupling limit [87, 88], lattice computations are in favor to the so-called *decoupling* solutions

$$Z(p^2) \sim (p^2)^{1/2}, \tag{2.54}$$

$$G(p^2) \sim (p^2)^0, \tag{2.55}$$

even for large lattices [59, 60, 61]. This latter type of solutions is not in agreement with the KUGO-OJIMA confinement scenario. One needs also to mention that both the FRGE and DSE methods produce the one-parameter family of scaling and decoupling solution as shown in [89]. Indeed, lattice investigations motivated by the existence of multiple solutions within functional methods as the *scaling* and the *decoupling* solutions would judge which solution might be realized.

In this context, we believe that the gauge fixing process on the lattice might be a key ingredient

to clarify this situation. Therefore, it might happen that modifying the gauge fixing method one might end with a solution agreeing with confinement criteria as KUGO-OJIMA's for example. In this spirit, we have studied the gluon propagator (at $T = 0$) for moderate small momenta using other gauge fixing criteria. In fact we think that the GRIBOV copies problem mostly present in the infrared might be the source of getting exclusively decoupling solutions on the lattice so far, and at the same time, to be in contradiction with confinement criteria. In fact, the different solutions (deviating around 1 GeV) are results of different boundary conditions at zero momentum, namely $J = 0$ and $J =$ finite, excluding strongly the GRIBOV effects. As a result, we propose a new procedure to select gauge copies in such a way to avoid the GRIBOV ambiguity. That is why, we take into account gauge copies lying as close as possible to the GRIBOV horizon, i. e. with the lowest FP operator eigenvalues. This process will map uniquely to a unique gauge copy, and therefore, no ambiguity due the fields redundancy need to be taken into account. For a full discussion of this problem we refer to Section 3.4.2.

In general, in order to resolve the *DSE* one needs to make truncations at some level of the theory. That is, in order to manage towers of infinite integral equations one needs to neglect higher order n-point functions. In fact, this truncation is absolutely not trivial as there is no general prescription how to do it. In fact, one needs to proceed taking into account the symmetries of the theory as dictated by WARD-TAKAHASHI and TAYLOR-SLAVNOV identities [69, 70]. So far, we presented the *DSE* for the case of zero temperature. That is, *QCD* in vacuum. However, we will see in section Section 2.2 how temperature dependent concepts at finite temperature ($T \neq 0$) are introduced. The mathematical arena we are basing our finite temperature considerations on the so-called MATSUBARA formulation of *QCD*. Within this formalism we show how the partition function is defined, and also how the periodicity of the field influence the energy spectrum. For the sake of completeness and after presenting the formalism, we derive, and comment out the example of the *DS* equation of the quarks field at $T > 0$.

The functional renormalization group (FRG) methods: The CALLEN's equations

A physical quantity must be a priori independent of the renormalization point. As said before, the renormalized GREEN functions depend on the renormalization point μ. This subtraction point μ is not unique, and then different renormalized GREEN functions are obtained for different values of μ. This change of the GREEN function comes from the dependency of the the renormalized parameters g_r, m_r and ξ_r (via the corresponding Z-factors) on μ. However, two renormalized GREEN functions computed on two different subtraction points μ and μ' are related via finite multiplicative factor z

$$G_r\big(p_i; g_r(\mu'), m_r(\mu'), \xi_r(\mu'), \mu'\big) = z(\mu', \mu) \cdot G_r\big(p_i; g_r(\mu), m_r(\mu), \xi_r(\mu), \mu\big), \tag{2.56}$$

where z is depending on μ and μ'. This renormalization factors form an abelian group called the *renormalization group* (*RG*). Therefore, within this context, physical observables need to be renormalization group invariants. This is in general not the case for the GREEN functions whose

depend on the renormalization point. In fact, the key observation to derive the *renormalization group equations* is to stress that the unrenormalized GREEN function (depending on the bare parameters g_o, m_o and ξ_o) does not depend on μ. This last property phrased in equation looks like

$$0 = \mu \frac{d}{d\mu} G(p_i; g_o, \xi_o, m_o, \Lambda). \tag{2.57}$$

Now using this last equation together with

$$G_r(p_1, \ldots, p_n; g_r, m_r, \xi_r) = Z_G \cdot G_{\text{reg}}(p_1, \ldots, p_n; \Lambda, g_o, \xi_o, m_o), \tag{2.58}$$

and using the chain differentiation rule[7] one obtains

$$\left(\mu \frac{\partial}{\partial \mu} + \beta \frac{\partial}{\partial g_r} + \beta_{\xi_i} \frac{\partial}{\partial \xi_r} - \gamma + m_r \gamma_m \frac{\partial}{\partial m_r} \right) G_r = 0. \tag{2.59}$$

Therefore, one defines the *RG* functions (see [90]) as

$$\beta\left(g_r, \frac{m_r}{\mu}, \xi_r\right) := \mu \frac{\partial g_r}{\partial \mu}\bigg|_{g_o, m_o, \xi_o, \Lambda \text{ fixed}} \tag{2.60a}$$

$$\gamma_m\left(g_r, \frac{m_r}{\mu}, \xi_r\right) := \frac{\mu}{m_r} \frac{\partial m_r}{\partial \mu}\bigg|_{g_o, m_o, \xi_o, \Lambda \text{ fixed}} \tag{2.60b}$$

$$\gamma\left(g_r, \frac{m_r}{\mu}, \xi_r\right) := \mu \frac{\partial \ln Z_G}{\partial \mu}\bigg|_{g_o, m_o, \xi_o, \Lambda \text{ fixed}} \tag{2.60c}$$

$$\beta_\xi\left(g_r, \frac{m_r}{\mu}, \xi_r\right) := \mu \frac{\partial \xi_r}{\partial \mu}\bigg|_{g_o, m_o, \xi_o, \Lambda \text{ fixed}} \tag{2.60d}$$

The meaning of these equations is obviously to translate how the renormalized GREEN function varies under a change of the renormalization point μ. In particular, one important feature of the LANDAU gauge is that it is a renormalized group fixed point. It has been already shown that the β-function is gauge independent [91], i. e.

$$\beta(g_r, \xi_r) = \beta(g_r). \tag{2.61}$$

Moreover, one supposes that $m_\mu \gg m_r$ [8]. The evolution on μ of the *RG* functions $\beta(g_r)$, $\gamma_m(g_r)$ and $\gamma(g_r)$ (see Eq. (2.60a), Eq. (2.60b) and Eq. (2.60c)) is determined by the solution of the

[7] One must keep in mind that the renormalized GREEN function G_r depends on μ explicitly, but also implicitly because of the dependency of renormalized parameters g_r, m_r and ξ_r on μ.

[8] As it holds in a mass-independent renormalization scheme for example.

differential equations (Eq. (2.60a) and Eq. (2.60b)) as

$$\frac{m(\mu')}{m(\mu)} = \exp\left\{\int_{g_r(\mu)}^{g_r(\mu')} dh \frac{\gamma_m(h)}{\beta(h)}\right\}, \tag{2.62}$$

$$\frac{\mu'}{\mu} = \exp\left\{\int_{g_r(\mu)}^{g_r(\mu')} \frac{dh}{\beta(h)}\right\}. \tag{2.63}$$

In general, the GREEN function also transform under a *RG* transformation with a finite factor [62]

$$z(\mu',\mu) = \exp\left\{\int_{g_r(\mu)}^{g_r(\mu')} dh \frac{\gamma(h)}{\beta(h)}\right\}. \tag{2.64}$$

The *RG* functions are quite unknown, and approximations to these functions are relying on perturbative expansions in g_r. Therefore, these approximations are only valid in the perturbative regime of *QCD*. To give an example, let us focus on the case of the β-function. As we know, the β-function is depending on g_r which is related to the bare coupling g_o as

$$g_r = Z_3^{3/2} Z_1^{-1} g_o\,.$$

The renormalization constants, Z_3 and Z_1, are defined at a subtraction point $p = \mu$ in terms of the bare (transverse) gluon propagator and the bare three-point vertex, respectively. Now, relying on the two-loop order expansion of the Z-factors, and plugging it into Eq. (2.60a) for $g_r(\mu)$ one ends with an expansion for the β-function [92]

$$\beta[g_r(\mu)] = -\beta_0 \frac{g_r^3(\mu)}{16\pi^2} - \beta_1 \frac{g_r^5(\mu)}{128\pi^4} + O(g_r^7(\mu)), \tag{2.65}$$

where

$$\beta_0 = 11 - \frac{2}{3} N_f\,, \tag{2.66a}$$

$$\beta_1 = 51 - \frac{19}{3} N_f\,, \tag{2.66b}$$

where N_f is the number of quark flavors as usual. Obviously, this expansion is valid only for small g_r. Moreover, this procedure to get the form $\beta(g_r)$ is depending on which scheme the Z-factors are defined in, and also on the definition of running coupling. Still, the first two terms β_0 and β_1 are shown to be the only renormalization-scheme independent terms. Therefore, we understand from here that most predictions of the *RG* equations go to the ultraviolet asymptotic momenta regime. As we are interested in predictions related to the gluon an ghost propagators let us focus on the *RG* equations expectations for these particular GREEN functions. Under the ass-

umption of large value of the scale λ and setting $\mu' = \lambda\mu$ one get from Eq. (2.56) and Eq. (2.64)

$$G_r(\lambda p_i, g_r, \lambda\mu) = \lambda^D \mu^D f(p_i \cdot p_j/\mu^2) = \lambda^D G_r(p_i, g_r, \mu),$$

where D is the dimension of G and f is dimensionless. Since G is LORENTZ invariant f must be a function of the scalar product $p_i \cdot p_j$. To lowest order in PT the anomalous dimension $\gamma(g_r)$ is given by the expansion $\gamma(g_r) = c_0 g_r^2 + O(r g_r^4)$ [62] where c_0 is the zeroth-order coefficient. Using c_0 and the corresponding coefficient $b_0 = \frac{\beta_0}{16\pi^2}$ from Eq. (2.66b) of the β-function, we obtain from the definition$z(\lambda) = z(\lambda\mu, \mu)$ Eq. (2.64) to lowest order in PT [62]

$$z(\lambda\mu, \mu) \simeq \exp\left\{\int_{g_r(\mu)}^{g_r(\lambda\mu)} \frac{c_0}{b_0}\frac{dh}{h}\right\} = \left[\frac{gr(\lambda\mu)}{g_r(\mu)}\right]^{c_0/b_0} \left[1 + O(g_r^2)\right] \tag{2.67}$$

$$\propto \left[\ln\lambda\right]^{-\delta} \qquad \lambda \to \infty \tag{2.68}$$

where $\delta := c_0/(2b_0)$. For the gluon and ghost propagators in the quenched case ($N_f = 0$) these exponents are $\delta_D = 13/22$ and $\delta_G = 9/44$, respectively. Therefore, the corresponding dressing functions, Z and J, behave in the far ultraviolet momentum region like

$$Z(p^2) \sim \left(\ln\frac{p^2}{\Lambda^2}\right)^{-\delta_D} \quad \text{and} \quad J(p^2) \sim \left(\ln\frac{p^2}{\Lambda^2}\right)^{-\delta_G}.$$

Besides the ultraviolet momenta region, *FRGE* methods are also predicting an infrared behavior for the propagators in the infrared region. Moreover, as seen in Section 2.1.4 *DSE* also bring useful informations on the propagators in the infrared region. In fact, a very sensible issue is whether the solutions from the *DSE* and *FRGE* are compatible in the infrared. We were already observing that solving the *DSE* imposes somehow to perform truncations. Moreover, it has been shown that the solutions provided by the *FRGE* and the ones of *DSE* agree exactly in the infrared as shown in [83, 93] and approximatively at the mid-momentum range [89].

So far, our analysis was always connected to the zero temperature case, and we are not going to describe the *FRGE* at finite T. Still, we should say that one of the most common use of them (at $T \neq 0$) is the study of coupling constant as a function of the temperature, see [94, 95, 96, 97, 98, 99] and references therein.

In the next section, we move on to the so-called MATSUBARA formalism of *QCD*. This is our key tool to analyze temperature effects on the propagators. We will also review briefly how the *DSE* already developed in the vacuum ($T = 0$) might be translated into the finite temperature framework. To do this, propagators will be given proper modifications at finite temperature, where the Euclidean space-time symmetry breaks down due to the heat-bath.

2.2 *QCD* at finite T

2.2.1 Path integrals and the MATSUBARA formalism

The path integral in the case of (imaginary time) finite temperature is commonly connected to statistical quantum theory. Indeed, for a classical statistical system in a heath bath with a temperature T the partition function looks like

$$Z(T) = \mathrm{Tr}[e^{\hat{H}/(k_B T)}] = \mathrm{Tr}[e^{\beta \hat{H}}], \tag{2.69}$$

where $\hat{H}$ is the Hamiltonian operator, and β symbolizes the inverse temperature $\beta = 1/(k_B T)$, with the BOLTZMANN constant k_B [9]. We follow the usual notation, and set always in the subsequent developments $k_B = 1$. Therefore, the temperature is given by

$$\beta = 1/T. \tag{2.70}$$

The trace in Eq. (2.69) restrict the fields to be periodic (bosons) or anti-periodic (fermions) in time. That is,

$$\Psi(\vec{x}, t+\beta) = \pm\Psi(\vec{x}, t), \tag{2.71}$$

where the sign is depending whether the field Ψ is a boson (+) or a fermion (-). In addition, in Eq. (2.13) one assumes that the time extent becomes infinite in the partition function[10]. This is not anymore the case at finite temperature where one set the time interval to be $[0, \beta]$. Therefore, the Euclidean space is compactified to $\mathbb{R}^3 \times [0, \beta]$. Furthermore, the partition function Eq. (2.69) might be transformed into a path integral over (anti) periodic configurations yielding [100]

$$Z(T) = \int [\mathscr{D}\Psi] e^{-S_E[\Psi]}, \tag{2.72}$$

where

$$S_E[\Psi] = \int_0^\beta dt \int_{\mathbb{R}^3} d^3x \mathscr{L}(\Psi(t, \vec{x}), \partial_\mu \Psi(t, \vec{x})). \tag{2.73}$$

Here, the measure $[\mathscr{D}\Psi]$ and the action $S_E[\Psi]$ are discretized on the lattice. Within this discretization the extent of the time direction is limited up to β. The time extent in units of the lattice spacing is $a \cdot N_\tau$ whereas the spatial extent is $a \cdot N_\sigma$ [100]. Hence,

$$\beta = a \cdot N_T = \frac{1}{T}. \tag{2.74}$$

[9] The inverse temperature and the inverse gauge coupling both denoted β lead sometimes to a confusion. During this section, and unless stated otherwise, we refer always to β as the inverse temperature

[10] This is equivalent to setting $T = 0$.

According to this last equation, the case of $T \longrightarrow 0$ corresponds to the limit $\beta \longrightarrow \infty$. Therefore, the case we were considering in Section 2.1.2 corresponds to zero temperature case where the spatial and time extents are equal, i.e. a symmetric lattice. We note that along our lattice investigations and in order to reduce finite volume effects commonly present on a finite lattice, one takes the aspect ratio N_σ/N_τ to be large. Subsequently, one performs the continuum limit of the theory $a \longrightarrow 0$ at fixed temperature and spatial physical volume, i. e. holding $a \cdot N_\sigma$ and $a \cdot N_\tau$ fixed.

Other aspects to mention are the physical implications of the (anti-)periodicity of the fields within the so-called MATSUBARA formalism defined in Eq. (2.71). In fact, if one defines a FOURIER transformation of a periodic function in imaginary time direction, i. e. satisfying $f(\tau) = f(\tau + \frac{1}{T})$, by

$$f(\tau) = T \sum_{n=-\infty}^{n=+\infty} e^{-i\omega_n} f(i\omega_n), \tag{2.75}$$

one finds that only an energy discrete spectrum is allowed with respect to the time direction. That is, only energies values of the form

$$\omega_n = n \cdot \frac{2\pi}{\beta} = 2\pi n \cdot T. \tag{2.76}$$

The integer multiples ω_n are called commonly the MATSUBARA frequencies. However, there are different MATSUBARA energy levels for bosons and fermions. For bosons (periodic fields) the MATSUBARA energies are of the form $\omega_{\mathbf{boson}} = 2\pi n \cdot T$, with an integer n related to the lattice structure $-N_\tau/2 + 1 \leq n \leq N_\tau/2$. The situation is rather different for fermions ψ (and also $\overline{\psi}$) which obey anti-periodicity condition (in time direction)

$$\psi(\tau) = -\psi(\tau + 1/T), \tag{2.77}$$
$$\overline{\psi}(\tau) = -\overline{\psi}(\tau + 1/T). \tag{2.78}$$

Here the energy levels are of the form $\omega_{\mathbf{fermion}} = (2n+1) \cdot \pi T$. Therefore, the smallest energy corresponds to πT. As usual, within the MATSUBARA formalism the fourth component of the Euclidean momenta p_4 is identified to multiples of the MATSUBARA frequencies. In our finite temperature investigations we analyzed exclusively data with zero MATSUBARA frequency. Hence, only time components momenta with zero values were taken into account. Some conventions in the MATSUBARA formalism read

$$p_4 \longrightarrow -\omega_n, \tag{2.79}$$
$$\not{p} = -\omega_n \gamma_4 + \gamma \cdot \mathbf{p}. \tag{2.80}$$

It is also worthwhile to note that within the MATSUBARA formalism one needs to replace the

integral over the fourth component of the Euclidean four vector with sums over MATSUBARA (discrete)frequencies as follows

$$\int \frac{d^4p}{(2\pi)^4} f(-ip_4, \mathbf{p}) \to -T \sum_{n_p} \int \frac{d^3p}{(2\pi)^3} f(i\omega_{n_p}, \mathbf{p}). \tag{2.81}$$

Based on these rules one can easily convert the zero temperature *DSE* to the case of finite temperature. In order to illustrate this point let us take the example of the *DSE* for quark fields [11]in *QCD* already derived in Eq. (2.47). In fact, at finite temperature the *DSE* [101] for the quark field looks like

$$S^{-1}(i\omega_n, \mathbf{p}, \mu) = Z_2(\mu, \Lambda) S_0(i\omega_n, \mathbf{p}, \Lambda) + \Sigma(i\omega_n, \mathbf{p}, \mu), \tag{2.82}$$

with the self-energy defined in Eq. (2.50). To get this formula (valid at $T > 0$) one apply the following substitution $p_\mu = (p_4, p) = (-\omega_n, p)$. Moreover, we have also considered $S(Q, \mu) = S(i\omega_n, p, \mu)$ and correspondingly $\Gamma_\nu(K, L, \mu)$ and $D_{\mu\nu}(K, \mu)$. Here, $D_{\mu\nu}$ and Γ_ν are the gluon propagator and the $q\bar{q}g$-vertex function at finite temperature. Note that we do not present the tensorial structure of the vertex function as being of no interest for us in this thesis, see [101]. However, the gluon propagator is one of the important targets of our study. Therefore, we refer for a proper definition of this quantity (at finite T) to Section 2.5.

In the following section we focus on a study of the order parameters of *QCD* at finite T. We start first with the POLYAKOV loop studying its role as an order parameter in pure gauge theory. Next, we move to the chiral limit of *QCD*, and introduce the chiral condensate as an order parameter for full *QCD*. A theoretical understanding of these order parameters allows one to have a comprehensive picture of the *QCD* phase diagram discussed later on.

2.3 Order parameters in *QCD* at finite T

2.3.1 The POLYAKOV loop

The pure gauge sector of *QCD* is an interesting area where one supposes the quarks fields to be infinitely heavy. This special situation also called the quenched approximation of *QCD* is less computing power demanding in order to be investigated within lattice *QCD* in comparison to the full *QCD* case. Moreover, confinement might also be present even in this quenched approximation. Therefore, a proper understanding of the deconfinement here should in principle bring up valuable informations and a good start to move to the full case in presence of fermions.

Another key property within this context is the existence of a (de)confinement phase transition. This last property is already expected in the continuum, and was the focus of lattice investigations as well. To be able to investigate this transition one needs to rely on order parameters guided by the symmetries of the action. In particular, the ideal order parameter of quenched *QCD*

[11]This particular *DSE* is also called sometimes the gap equation of *QCD* in the scientific literature

is called thePOLYAKOV loop [18]. In order to have an understanding of this quantity let us start with a system without fermions, i. e. pure *Yang-Mills* theory. First, the canonical Euclidean partition function as seen before reads

$$Z(T) = \mathrm{Tr}[e^{\beta\hat{H}}], \tag{2.83}$$

where $\hat{H}$ is the Hamiltonian operator, and the trace applied on gauge invariant physical states. At this step it is interesting to observe that the exponential $[\exp(-\beta\hat{H})]$ is similar to the evolution operator $[\exp(-i\hat{H}t)]$ where β plays the role of the Euclidean time interval it. Now, switching to the path integral formulation one can also write

$$Z = \int [\mathscr{D}A_\mu] \exp(-S_{\mathrm{Eucl}}[A]), \tag{2.84}$$

with the gauge fields A_μ and the Euclidean action $S_{\mathrm{Eucl}}[A]$

$$S_{\mathrm{Eucl}}[A] = -\frac{1}{2}\int_0^\beta d\tau \int d^3x \,\mathrm{Tr}(F_{\mu\nu}F_{\mu\nu}). \tag{2.85}$$

Here and in the following we suppose that measure $\mathscr{D}A_\mu$ to be mathematically defined. Moreover, the fields obey periodic boundary conditions in Euclidean time direction

$$A_\mu(\vec{x}, \tau + \beta) = A_\mu(\vec{x}, \tau). \tag{2.86}$$

The action $S_{\mathrm{Eucl}}[A]$ already defined in Eq. (2.85) is invariant under the transformations

$$A^g_\mu = g(A^\mu - ig^\dagger \partial_\mu g)g^\dagger, \tag{2.87}$$

where $g \in SU(N_c)$ with N_c is the number of colors. In order to fulfill the boundary conditions in Eq. (2.86) the gauge transformations must be of the form

$$g(\vec{x}, \tau + \beta) = g(\vec{x}, \tau), \tag{2.88}$$

or more importantly

$$g(\vec{x}, \tau + \beta) = hg(\vec{x}, \tau), \tag{2.89}$$

with $h \in SU(N_c)$. This last non trivial transformation is called sometimes the *twisted* gauge transformation and is a direct consequence of the structure of the action. Moreover, if h are global transformations and commuting with gauge fields this would still respect the boundary

conditions as shown

$$\begin{aligned} A^g_\mu(\vec{x},\tau+\beta) &= g(\vec{x},\tau+\beta)[A_\mu(\vec{x},\tau+\beta) - ig(\vec{x},\tau+\beta)^\dagger \partial_\mu g(\vec{x},\tau+\beta)]g(\vec{x},\tau+\beta)^\dagger \\ &= hg(\vec{x},\tau)[A_\mu(\vec{x},\tau) - ig(\vec{x},\tau)^\dagger h^\dagger \partial_\mu (hg(\vec{x},\tau))]g(\vec{x},\tau)^\dagger h^\dagger \\ &= hA^g_\mu(\vec{x},\tau)h^\dagger \\ &= hh^\dagger A^g_\mu(\vec{x},\tau) \\ &= A^g_\mu(\vec{x},\tau). \end{aligned} \tag{2.90}$$

There, h is an element of the center group of $SU(N_c)$, i. e. the set of all elements of $SU(N_c)$ which commute with each others. Therefore, this is why this symmetry is called sometimes the center group symmetry. Such elements of the center group are proportional to the unit $SU(N_c)$ matrix $\mathbb{I}$ and might be parametrized as

$$h = z \cdot \mathbb{I}, \tag{2.91}$$

with $z = \exp\left(\frac{2\pi i n}{N_c}\right) \in \mathbb{Z}_{N_c}$. Therefore, from the mathematically point of view the center of $SU(N_c)$ is isomorphic to $\mathbb{Z}_{N_c}$.

The system becomes a bit more involved when treating fermions. Adding dynamical fermions to our previous *Yang-Mills* theory brings extra difficulties to keep the center group as a symmetry of the action. In fact, in order to see that in more details let us consider the quark field [12] and the anti-periodic boundary conditions in Euclidean time direction as

$$\psi(\vec{x},\tau+\beta) = -\psi(\vec{x},\tau),$$

which transform under the gauge transformations $g(x)$ as

$$\psi(x) \to \psi(x) \to g(x)\psi(x).$$

Therefore, if one wants to keep the gauge transformed quark under Eq. (2.89) always compatible with the anti-periodicity condition, that is

$$\begin{aligned} \psi(\vec{x},\tau+\beta)^g &= g(\vec{x},\tau+\beta)\psi(\vec{x},\tau+\beta) \\ &= -zg(\vec{x},\tau)\psi(\vec{x},\tau) \\ &= -z\psi(\vec{x},\tau)^g, \end{aligned} \tag{2.92}$$

the only solution would be to take $z = \mathbb{I}$, and thus the center group symmetry is destroyed in the presence of the fermions. In other words, one says that the center symmetry is explicitly broken when including dynamical fermions. Back to YANG-MILLS theory one defines the POLYAKOV

[12] Here we consider the fermions fields in the fundamental representation of $SU(N_c)$

loop $l(\vec{x})$ through the color operator trace in the fundamental representation given by

$$l(\vec{x}) = \frac{1}{N_c}\,\mathrm{Tr}_c(L(\vec{x})), \tag{2.93}$$

where $L(\vec{x})$ is the POLYAKOV loop operator

$$L(\vec{x}) = \mathscr{P}\exp(i\int_0^\beta d\tau A_4(x)), \tag{2.94}$$

where $\mathscr{P}$ is the path ordering of the exponential, and β stands here for the inverse temperature $\beta = 1/T$. An interesting relation to the free energy $F_{q\bar{q}}$ might be found computing the thermal expectation value of a product of two POLYAKOV loop operators, namely

$$\langle l(\vec{x})l(\vec{y})^\dagger\rangle_\beta = e^{-\beta F_{q\bar{q}}(\vec{x},\vec{y},T)}. \tag{2.95}$$

We point out that in the limit of large distances between two static color sources q and $\overline{q}$, i. e. $|x-y| \to \infty$, the correlation goes to zero. Therefore, at the temperature T one finds that the free energy $F(q)$ of a single static quark

$$F_\infty = \lim_{r\to\infty} F_{q\bar{q}}(r = |\vec{x}-\vec{y}|, T) = -T\log|\langle l\rangle|^2 \neq 0, \tag{2.96}$$

where the $\langle l\rangle = e^{-\beta F_q}$. We interpret physically the equations above as follows: in the confined phase the free energy of a single quark diverges, whereas in the deconfined phase the free energy remains finite. Therefore, the expectation values of the POLYAKOV loop takes zero values in the confined phase and non-zero otherwise

$$\langle l\rangle = \begin{cases} 0 & \Rightarrow \text{confinement,} \\ \neq 0 & \Rightarrow \text{deconfinement.} \end{cases} \tag{2.97}$$

This last property is of not course fulfilled when dealing with fermions having well defined masses. In this case confinement can not be really proven according to this order parameter criteria. This change of situation is mostly due to screening effects tending to produce particle-antiparticle quark pairs, and therefore ending with a finite free energy. Thus, the picture of confinement we present here connected to infinitely heavy masses separated static quarks is not valuable when dealing with fermions with finite masses. Still, the POLYAKOV loop may act as an approximate order parameter in presence of heavy massive quarks.

After this brief review of the POLYAKOV loop one understands that one can probe a system by a test quark with an infinitely heavy static charge. This non trivial behavior of the POLYAKOV loop is indeed a consequence of their non trivial transformation under the center group

symmetry. That is,

$$\begin{aligned} l(\vec{x})^g &= \frac{1}{N_c}\mathrm{Tr}_c[\mathscr{P}\exp(i\int_0^\beta d\tau A_4(x)^g)] \\ &= \frac{1}{N_c}\mathrm{Tr}_c[g(\vec{x},\tau+\beta)\mathscr{P}\exp(i\int_0^\beta d\tau A_4(\vec{x},\tau))g(\vec{x},\tau)^\dagger] \\ &= \frac{1}{N_c}\mathrm{Tr}_c[zg(\vec{x},\tau)\mathscr{P}\exp(i\int_0^\beta d\tau A_4(\vec{x},\tau))g(\vec{x},\tau)^\dagger] \\ &= zl(\vec{x}). \end{aligned} \tag{2.98}$$

Therefore, the POLYAKOV loop transforms non trivially under the center group $\mathbb{Z}_{N_c}$ as soon as the POLYAKOV loop picks a non-zero expectation values in the deconfined phase. In fact, the deconfined phase correspond to higher temperatures, and therefore the center symmetry is spontaneously broken at this regime. Concretely, what we compute in our lattice investigations are the discretized version of the continuum definition of the POLYAKOV loop we have see so far, that is

$$L = \frac{1}{N_\sigma^3}\sum_n \mathrm{Tr}\prod_{N_4=0}^{N_\tau-1} U_4(\vec{n},n_4), \tag{2.99}$$

where N_τ, N_σ are the temporal and spatial lattice extents respectively, and $U_4(\vec{n},n_4)$ are the link variables at each lattice point $(\vec{n},n_4)$ pointing in the time direction. Therefore, as L is a complex number we take only its real part to study it as a function of the temperature T. We will introduce in more details these lattice definitions in the next Chap. 3.

2.3.2 The chiral condensate

In order to start to discuss the chiral condensate it would be worthwhile to start with a proper understanding of the so-called *chiral symmetry*. In simple words, this latter symmetry happens in the special case where the quarks masses are supposed equal to zero. This mass limit is called in the literature the *chiral limit*. What makes this limit physically interesting is the fact that the quarks (u,d and s) masses are small compared to typical hadrons masses. Moreover, the other three quarks, namely the top, charm and bottom quarks are very heavy compared to the first three. Therefore, in the regime of low energies these latter can be considered to be infinitely heavy and their dynamic to be neglected. Hence, the study of the chiral limit corresponding to vanishing quark masses is worth to do, and present a nice first approximation of the real world in this regime.

As mentioned before in the chiral limit there is an emerging symmetry of the *QCD* action called the *chiral symmetry*. To make things clearer let us start our analysis defining the projection

operators

$$P_{R,L} = \frac{1}{2}(1 \pm \gamma_5), \tag{2.100}$$

with $\gamma_5 = i\gamma_0\gamma_1\gamma_2\gamma_3$ in the MINKOWSKI space, see Appendix 8. Using this last operator one defines left- and right-handed quarks as

$$\psi_{R,L} = P_{R,L}\psi. \tag{2.101}$$

The Lagrangian in the case of vanishing quark masses is invariant under the following transformations

$$\psi_{R,L} \longrightarrow e^{i\theta^a_{R,L}\lambda^a/2}\psi_{R,L}. \tag{2.102}$$

This symmetry is represented by the transformation group $SU(N_F)_R \otimes SU(N_F)_L$. Moreover, according to NOETHER theorem the corresponding conserved currents look like

$$J^{\mu,a}_{R,L}(x) = \overline{\psi}_{R,L}\gamma^\mu \frac{\lambda^a}{2}\psi_{R,L}. \tag{2.103}$$

These right and left currents might be combined into a vector and an axial current vectors as follows

$$V^a_\mu = J^a_{R,\mu} + J^a_{L,\mu}, \tag{2.104}$$

$$A^a_\mu = J^a_{R,\mu} - J^a_{L,\mu}. \tag{2.105}$$

The left- and right-handed quarks are mixed into the Lagrangian thanks to the mass term. Therefore, this mass term breaks explicitly the chiral symmetry and the aforementioned currents follow different conservation laws. In fact, the vector current is conserved while the axial one is not. This latter non-conservation property is translated into equations as

$$\partial_\mu A^\mu = i\overline{\psi}\{M, \frac{\lambda^a}{2}\}\gamma_5 \neq 0. \tag{2.106}$$

Furthermore, the chiral symmetry is also spontaneously broken. This is due to the non-invariance of the *QCD* vacuum under chiral transformations while the Lagrangian remains chiral symmetric. Indeed, if one considers the ground state to be symmetric under the chiral symmetry, this would mean that the vector and axial charges must annihilates the vacuum, i. e.

$$Q^V_a|0\rangle = Q^A_a|0\rangle = 0. \tag{2.107}$$

Therefore, in this case there should be in principle parity partners with equal masses for the vector and axial-vector mesons. However, this is not what happens in nature, and a mass gap for

example between the ρ ($m_\rho = 0.77\,\mathrm{GeV}$) and a_1 ($m_{a_1} = 1.23\,\mathrm{GeV}$) mesons is well established. These experimental observations justify the fact that the vacuum is annihilated by the vector charge whereas this is not the case for the axial charge, i. e.

$$Q_a^V|0\rangle = 0, \tag{2.108}$$

$$Q_a^A|0\rangle \neq 0. \tag{2.109}$$

Thereby, the symmetry group of *QCD* due to the spontaneous breaking of the chiral symmetry boils down as follows

$$SU(N_f)_L \otimes SU(N_f)_R \longrightarrow SU(N_f)_{R+L} = SU(N_f)_V. \tag{2.110}$$

The spontaneous breakdown of the chiral symmetry generates according to the GOLDSTONE theorem massless excitations called GOLDSTONE bosons. The quantum states corresponding to these bosons are of the form $|\phi_a\rangle = Q_a^A|0\rangle$, and since $[H, Q_a^A] = 0$ the states $|\phi_a\rangle$ must be energetically degenerate with the vacuum $|0\rangle$. The number of this states is eight in the case of $SU(3)$ since Q_a^A is an axial charge. Due to the mass term as said before the chiral symmetry is also explicitly broken. Therefore, it results light GOLDSTONE bosons rather than being massless.

The order parameter which account for the spontaneous breaking of the chiral symmetry is the so-called the *chiral condensate*, and is defined as

$$\langle\overline{\psi}\psi\rangle = \langle 0|\overline{\psi}\psi|0\rangle = -i\,\mathrm{Tr}\lim_{y\to x} S_F(x,y), \tag{2.111}$$

where $S_F(x,y) = -i\langle 0|T\,\psi\overline{\psi}|0\rangle$ is the FEYNMAN propagator and T is the time ordering operator. After discussing different symmetries within *QCD* in the previous sections let us now summarize the status of the symmetries present in the real world. Hence, we start with the symmetry group

$$SU(N_c) \otimes U(N_f)_V \otimes U(N_f)_A, \tag{2.112}$$

with $SU(N_c)$ is the local symmetry gauge group where the two other ones are global symmetries. As already known from group theory $U(N_f)$ might be decomposed into $U(N_f) = U(1) \otimes SU(N_f)$ getting then

$$\begin{aligned} &SU(N_c) \otimes U(N_f)_V \otimes U(N_f)_A \\ &\qquad\Downarrow \\ &SU(N_c) \otimes U(1)_V \otimes SU(N_f)_V \otimes U(1)_A \otimes SU(N_f)_A. \end{aligned} \tag{2.113}$$

Note that $U(1)_V$ corresponds to the conservation of the baryon number and is not broken whereas $U(1)_A$ is broken and called the $U(1)_A$-*anomaly*. This particular anomaly is connected to the mass splitting between the η and η'. After such analysis, the gauge group shown in Eq. (2.114) boils down to $SU(N_c) \otimes SU(N_f)_V$ where the last part is connected to the chiral symmetry for

vanishing quark masses. In general, the chiral symmetry is explicitly broken for non-vanishing quark masses, and might be also spontaneously broken. Thereby, taking into account the chiral spontaneous breakdown and the anomaly of $U(1)_A$ at the same time one ends with

$$\begin{aligned} &SU(N_c)\otimes U(N_f)_V \otimes U(N_f)_A \\ &\qquad \Downarrow \\ &SU(N_c)\otimes U(1)_V \otimes SU(N_f)_V. \end{aligned} \tag{2.114}$$

Moreover, as said before for different non-vanishing quark masses the chiral symmetry is also explicitly broken. This amounts to

$$\begin{aligned} &SU(N_c)\otimes U(1)_V \otimes SU(N_f)_V \\ &\qquad \Downarrow \\ &SU(N_c) \otimes U(1)_V. \end{aligned} \tag{2.115}$$

Concluding, one understands that at the end there is only the gauge symmetry and the $U(1)_V$ which remain. This latter symmetry corresponds according to NOETHER theorem to the conservation of the baryon number. Thus, the baryonic symmetry should be a part of our real world or any realistic *QCD* model as well as the gauge symmetry $SU(N_c)$.

■ 2.4 Nature of the phase transition in *QCD*

One important question which comes to one's mind when dealing with phase transitions of *QCD* is the nature of these latter. Therefore, it is quite natural to ask which kind of phase transition one expects in *QCD*.

Throughout the present section we review different aspect of the chiral and deconfinement phase transitions. It is quite interesting to note that these latter transitions show dependencies with the quark masses and the flavor numbers. Thus, this leads quite naturally to a rich and a complex picture of the whole image we had so far on chiral symmetry, confinement and their interplay in *QCD*. Here, we focus on the main transition features summarized in Fig. 2.5. This latter plot (called sometimes in the literature the COLUMBIA plot) shows the conjectured phase transitions at vanishing potential. Moreover, this plot shows the chiral and deconfinement phase transitions as a function of the flavor and quark masses as discussed in [101]. First, let us concentrate on the chiral symmetry restoration region within the COLUMBIA plot. Thanks to the universality class properties a first model for chiral symmetry restoration was adressed in [103]. The universality principles guided also to construct models which mimic *QCD* in many apects. However, such models need to reproduce the restoration of the symmetry $SU(N_F)_{R+L} \longrightarrow SU(N_F)_R \otimes SU(N_F)_L$, where the temperature effects are neglected. If one takes into account all effects into considerations, then a first order transition is expected for three degenerate chiral flavors. Moreover, a crossover and a second order transitions are expected for

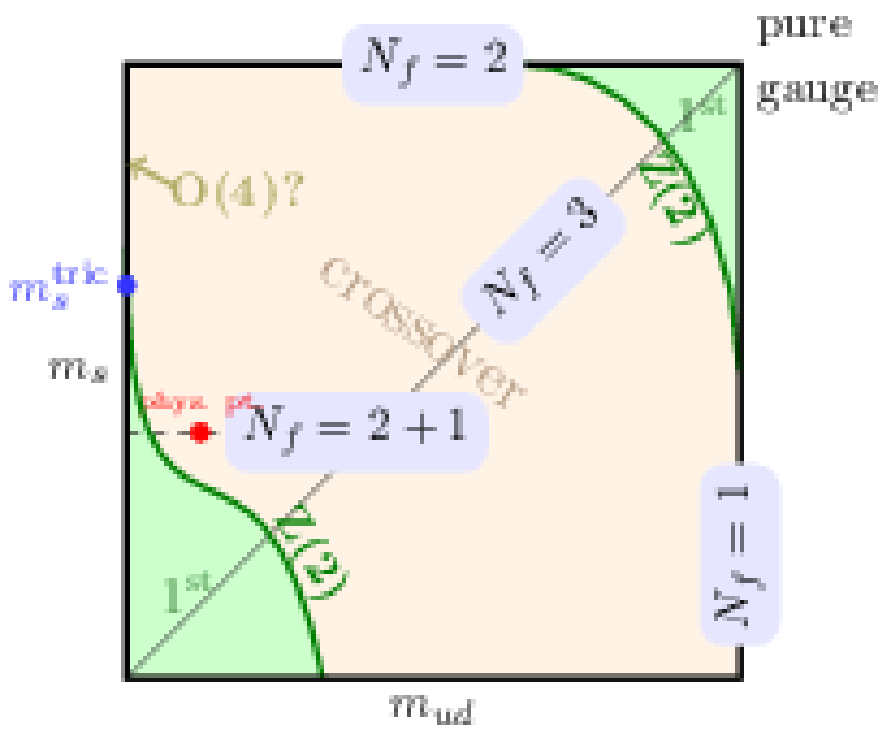

FIGURE 2.5: The expected phase diagram in the plane of quarks masses at vanishing quark chemical potential. This picture called more popularly the Columbia picture was taken from [102].

a single massless quark and two massless flavors respectively. We also observe that the region of the first order transition for three light quarks ends with a second order phase transition line. This line belongs to the ISING universality class with $Z(2)$ symmetry [104]. The dependency of this line however as a function of the quark masses is not well defined. Moreover, it is suggested [103] that the phase transition for $N_F = 2$ chiral quarks is a second order phase transition with $O(4)$ critical behavior. This relies on the symmetry group arguments $SU(2)_L \otimes SU(2)_R \simeq O(4)$ spontaneously broken to $SU(2)_{L+R} \simeq O(3)$.

Now, if one assumes $U(1)_A$ restoration at temperature below or near the chiral critical temperature one then is led to a first order phase transition. The reason for that is that pseudo-scalar meson flavor singlet gets a topological mass from the $U(1)_A$ which makes it heavier. This fact would drive the transition first order. Still, this first order and even the $O(4)$ critical behavior have not been proven definitively, see [105, 106]. In addition, there is also an interesting point called the tri-critical strange quark mass m_s^{tric} in the left side of Fig. 2.5. This point represent a region where the transition from $O(4)$ critical line to the $Z(2)$ critical might occur. However,

even the existence of this point is still unresolved [106].

Arrived at this point, let us discuss the deconfinement according to the *Columbia* picture. In the quenched approximation of *QCD*, namely, in the absence of quarks (or in the limit of infinitely heavy static quarks) occurs a first order phase transition in $SU(3)$ gauge theory. This region is located in the upper right part of the Fig. 2.5. This first order transition is well established by lattice gauge theory investigations [107]. Furthermore and always seen from Fig. 2.5, the region of first order deconfinement phase transition ends at a second order deconfinement phase transition line lying in the $Z(2)$ universality class. The corresponding model is the so-called *Potts* model with a complex scalar field and invariance under $2\pi/3$ rotations in the complex plane.

In this thesis, we investigate the case of quenched $SU(3)$ *QCD* and the phase order transition thanks to the POLYAKOV loop as an order parameter corresponding to the study of the upper right corner region of the *Columbia* plot. In a second project, we study also the regime of intermediate quarks masses $N_F = 2$ (quark up and down) using three values of pion masses corresponding to the upper line of the Fig. 2.5. As one might expect from this plot, at moderate quark masses the transitions are crossovers rather than strict phase transitions. Moreover, it is also expected that the physical quark masses lie into the crossover region.

Remark, that the chiral condensate and the POLYAKOV loop in their corresponding limits show typically a rapid change around the critical transition temperatures. Thanks to these order parameters responses it is already stated that the chiral transition might happen at $T_\chi = 147 - 164\,MeV$ whereas deconfinement occurs at the $T_{\text{deconf}} \sim 165\,MeV$, see [108] and references therein. Still, these values and the nature of the phase transition are a hot topic under discussion within the scientific community.

■ 2.5 The gluon and ghost propagators at $T > 0$

Even if the gluon and ghost propagators are a quite basic quantities in *QFT*, they remain very useful for plenty of reasons. Apart from that, a *QFT* is generally soluble only knowing all its GREEN functions. A special case of these latter are the propagators which play also an interesting physical role connected to confinement for example in *QCD*. Moreover, the gluon and ghost propagators represent the building blocks of the *DS* equations for example as discussed before. Recently, powerful non-perturbative approach has been developed based on *DSE* [20, 21, 22, 23] in parallel to the functional *RGE* investigations [24, 25].

The main focus was first to find a field theoretical, model-independent description of quark and gluon confinement in terms of the infrared behavior of gauge-variant GREEN's functions, in particular of the LANDAU or COULOMB gauge gluon and ghost propagators. The physical prediction of such propagators should confirm or reject confinement scenarios as proposed by GRIBOV and ZWANZIGER [26, 27, 28] and KUGO and OJIMA [29, 30]. The LANDAU gauge at zero temperature was the focus of the *DSE* and *FRGE* (see, e. g. [89] and citations therein) and also the subject of intensive lattice investigations (see [31, 32, 33, 34, 35, 36, 37, 32] and references therein).

At finite temperature the gluon and ghost propagators are less investigated. In fact some papers were devoted the $SU(2)$ pure gauge gluon propagators in LANDAU gauge (see, e.g. papers [38, 39, 40, 41, 42, 43, 44, 45]). The finite temperature studies started in 1995 with HELLER and al. [38] who had for example to determine the electric and the magnetic gluon mass at high temperature. There, the phenomenon of the 'dimensional reduction' appearing at high temperature for the $SU(2)$ gauge group is also investigated. This actually happens at high temperatures reducing a four-dimensional theory to a three-dimensional interacting theory. Latter on, authors in [40] compared the 4D and 3D gluon propagators and found a matching of the two results down to $2T_c$. The infrared limit of the gluon and the ghost propagators show also interesting results thanks to huge volume lattice investigations [45]. There one observes that the longitudinal gluon propagator $D_L(p)$ is enhanced, with an apparent plateau value in the infrared, while the transverse propagator $D_T(p)$ gets progressively more infrared-suppressed. This result is also supported by our work [49] going up to the physical volume of $(2.7\,fm)^3$ for the $SU(3)$ gauge group case.

For the case of $SU(3)$ pure gauge theory the gluon propagators are less studied, see [46, 47, 48, 43, 49]. This also applies for the studies of $SU(3)$ gluon propagators in the presence of dynamical fermions [50, 51]. In fact the reference [50] takes into account the number of flavors $N_F = 2$ as we do in our study except that we use a twisted mass fermionic action as our main discretization as described later on. Most of the papers support a temperature independent behavior for the ghost propagator as in [53, 54, 55, 56] and references therein. Still, we were able [49] to observe small fluctuation in the region of small momenta and at higher temperatures. In the case of full QCD at finite temperature for the gauge group $SU(3)$ our results are in qualitative agreements with [42, 43].

After presenting the status of art of the gluon and ghost propagator let us now turn to the theoretical definition of the gluon and ghost propagators in QCD at finite T. The gluon propagator generic form in real space is the time ordered expectation value of two gluon fields

$$\langle A^a_\mu(x)A^b_\nu(0)\rangle \equiv \langle 0|T(A^a_\mu(x)A^b_\nu(0))|0\rangle, \tag{2.116}$$

where T denotes the time ordering. The FOURIER transform of this latter gives

$$D^{ab}_{\mu\nu}(p^2) = -i\int d^4x\cdot e^{ipx}\langle A^a_\mu(x)A^b_\nu(0)\rangle. \tag{2.117}$$

On the other side, the ghost propagator form is

$$\langle c^a(x)\bar{c}^b(0)\rangle \equiv \langle 0|T(c^a(x)\bar{c}^b(0))|0\rangle, \tag{2.118}$$

and the Fourier transform reads

$$G^{ab}(p^2) = -i\int d^4x\cdot e^{ipx}\langle c^a(x)\bar{c}^b(0)\rangle. \tag{2.119}$$

At finite temperature ($T \neq 0$), the Euclidean symmetry is broken and the gluon propagator splits into two structures [109], namely a transverse D_T and a longitudinal D_L components to the time direction as follows

$$D^{ab}_{\mu\nu}(p) = \delta^{ab}(P^T_{\mu\nu} D_T(p_4^2, \vec{p}^{\,2}) + P^L_{\mu\nu} D_L(p_4^2, \vec{p}^{\,2})), \tag{2.120}$$

where the fourth momentum component p_4 is the so called MATSUBARA frequency. The projectors within the Landau gauge are defined as

$$\begin{aligned} P^T_{\mu\nu} &= (1-\delta_{\mu 4})(1-\delta_{\nu 4}) \left(\delta_{\mu\nu} - \frac{p_\mu p_\nu}{\vec{p}^{\,2}} \right), \\ P^L_{\mu\nu} &= \left(\delta_{\mu\nu} - \frac{p_\mu p_\nu}{p^2} \right) - P^T_{\mu\nu}. \end{aligned} \tag{2.121}$$

In the next chapter, we introduce our lattice framework. We also present our lattice actions used in this work. Next, the continuum theory is commented and how to reach such a limit from our lattice simulations. Last but not least, we discuss the GRIBOV problem and ways to deal with it.

CHAPTER 3

QCD at $T > 0$ on the lattice

We introduce basic definitions related to the lattice regularization of *QCD*. We first introduce gauge fields and gauge transformations on the lattice. Then, we specify our two lattice actions of interest, namely the standard plaquette WILSON action and also the one used for full *QCD* consisting of a sum of the SYMANZIK and the twisted mass actions. Next, we discuss the concept of continuum limit and the prescription adopted to reach it on the lattice. At the and, the GRIBOV problem is posed together with the gauge fixing techniques we used. There, we clarify the problem of GRIBOV copies and propose our procedure to deal with it.

3.1 General introduction

Lattice *QCD* (*LQCD*) provides the way par excellence to handle problems in the non perturbative regime of *QCD*. This is basically done by introducing a new scale in the theory, namely a cutoff a^{-1}, where a is the lattice spacing. Indeed, *LQCD* is basically a discretization of the Euclidean space-time into a lattice of points separated with distance a. Therefore, this cutoff regularizes *QCD* which becomes finite. We refer the reader to standard textbooks for more details on the subject [14, 15] and [16, 17].

In fact, perturbation theory (PT) ceases at some regime of energy/temperature to work and purely non-perturbative phenomena as confinement or chiral symmetry restoration are not taken into account. Still, PT was successful to test *QCD* at high energy regime, i. e. small distances [1, 2, 3], where the asymptotic freedom might happen. Actually, this latter property motivated to consider the quark-gluon plasma as a weakly interacted system [5, 4]. This suggests that the effective *QCD* potential used in thermodynamical models should be small as a function of high temperature/density. Still, infrared divergences, known as the LINDE problem, might also prohibit the computation of thermodynamic quantities [8]. Therefore, naive perturbation

theory might be replaced by improved perturbation techniques, as the dimensional reduction [9, 110, 111] and Hard Thermal Loop (HTL) resummation [9, 10, 11, 12] for example.

However, these improved methods seem to work only for relatively higher temperature ($\gtrsim 3T_c$). Therefore, to study the infrared properties of *QCD* one needs to investigate with the help of *LQCD* at finite temperature T [1] for example. Moreover, an extra feature of *LQCD* is the possibility to use Monte-Carlo (MC) simulation techniques to evaluate the observables. These latter are defined with the MC framework in terms of the path integrals are interpreted as sample statistical averages in the equilibrium within *LQCD*.

In the following we introduce the *LQCD* including basic gauge fields and transformations. Furthermore, we also present the type of lattice actions we used during this present work. This next section is also meant to fix notations and conventions for the upcoming discussions.

3.1.1 Gauge fields and gauge symmetries

The general starting point to study *QCD* at finite temperature is namely to consider the grand canonical partition function for many-particles ensemble at temperature T defined previously as

$$Z = tre^{-\beta(\tilde{H}-\mu\tilde{N})}, \tag{3.1}$$

where, $\tilde{H}$ is HAMILTON operator of the system and $\beta = 1/T$ [2]. Here, $\tilde{N}$ is the number operator corresponding to some charge as there are the baryon number, the electric charge..., and μ is the chemical potential. Let us assume for this general discussion $\mu \neq 0$ despite our thesis results concern only the zero chemical potential case. the partition function Z Eq. (3.1) might be rewritten in terms of the path integral as

$$Z = \int_{bc} \mathscr{D}\psi\mathscr{D}\overline{\psi}\mathscr{D}A_\mu \, exp[-\int_0^\beta d\tau \int d^3x \mathscr{L}], \tag{3.2}$$

with $\mathscr{L}$ is the Lagrangian density and τ is the inverse temperature, i. e. the Euclidean imaginary time. bc denotes the boundary conditions for the fields. That is, periodic boundary conditions for the gauge fields A_μ, while anti-periodic for the quark fields ψ and $\overline{\psi}$. In *LQCD* the Euclidean continuum space-time is discretized to hyper-cubic grid of lattice sites x. The quark fields ψ and $\overline{\psi}$ in Eq. (3.2) live on the lattice site $x \equiv (x_0, x_1, x_2, x_3)$. The lattice gauge fields are introduced as links joining two adjacent lattice points x and $x+\hat{\mu}$, where $\hat{\mu}$ is the unit vector in the x_μ direction. We denote these gauge fields as $U_{x,\mu}$ calling them link variables. These fields are introduced in the lattice formulation instead of the gluon field $A_\mu(x)$ in order to maintain the explicit gauge invariance [112]. These link variables takes values in a compact LIE group, here $SU(3)$. The link

[1] We recall that we deal in this thesis exclusively with the zero chemical potential case, namely $\mu = 0$.

[2] We fix the units system to the natural units, i.e. $\hbar = c = k_\beta = 1$

variables [113] are connected to the continuum gluon field $A_\mu(x)$ with [3]

$$U_{x,\mu} \equiv \mathscr{P} \exp\left\{ ig_o \int_0^1 A_\mu(x+at\hat{\mu})\, dt \right\} \simeq e^{iag_o A_\mu(x+\hat{\mu}/2)} + O(a^3). \tag{3.3}$$

Here $\mathscr{P}$ denotes path ordering of the gluon fields along the integration path, and g_o is the bare coupling constant as usual. The thermal expectation value of an observable $\mathscr{O}$ is defined as

$$\langle \mathscr{O} \rangle = \frac{1}{Z} tr[\mathscr{O} e^{-\beta(\hat{H}-\mu\hat{N})}]. \tag{3.4}$$

This latter equations takes the following form in the path integral approach

$$\langle \mathscr{O} \rangle = \frac{\int_{bc} \mathscr{D}\psi \mathscr{D}\overline{\psi} \mathscr{D} A_\mu \mathscr{O} exp[-\int_0^\beta d\tau \int d^3x \mathscr{L}]}{\int_{bc} \mathscr{D}\psi \mathscr{D}\overline{\psi} \mathscr{D} A_\mu exp[-\int_0^\beta d\tau \int d^3x \mathscr{L}]}. \tag{3.5}$$

LQCD at finite T is a an approach providing essentially prediction for the *QGP* simulating the partition function. In fact, several observables might be computed within this framework thanks to Eq. (3.5) using Monte-Carlo simulations methods. In the present study we focus first on results using the WILSON plaquette action described in Section 3.2.1 as the gauge action $S_G[U]$ for pure gauge *QCD*. This amounts to evaluate on the lattice vacuum expectations values [15] of the form

$$\langle \mathscr{O} \rangle = \frac{1}{Z} \int [\mathscr{D}U]\, e^{-S_G[U]}\, \mathscr{O}[U]. \tag{3.6}$$

In fact, Eq. (3.6) provides an evaluation of purely gauge field dependent observables $\mathscr{O}[U]$. However, the situation might be generalized to the case including fermion ψ_{x_i} and $\overline{\psi_{x_i}}$, where x_i are the corresponding lattice sites. Actually, if one considers $\mathscr{O} = \mathscr{O}[\psi, \overline{\psi}, U]$ as[4]

$$\mathscr{O}[\psi, \overline{\psi}, U] = \psi^{a_1}_{x_1} \cdots \overline{\psi}^{b_1}_{y_1} \cdots U_{z_1\mu_1} \cdots .$$

Then, the vacuum expectation values gives

$$\langle \mathscr{O} \rangle = \frac{1}{Z} \int [\mathscr{D}U, \mathscr{D}\overline{\psi}, \mathscr{D}\psi]\, \mathscr{O}[\psi, \overline{\psi}, U]\, e^{-S_{QCD}[U,\overline{\psi},\psi]}\, . \tag{3.7}$$

In general, the *QCD* lattice action is a sum of the gauge action part $S_G[U]$ and a fermionic part $S_F[U, \overline{\psi}, \psi]$

$$S_{QCD} = S_G[U] + S_F[U, \overline{\psi}, \psi]\, . \tag{3.8}$$

[3] This line integral is the lattice version of the parallel transport matrix between adjacent lattice sites, see e.g. [113].
[4] In this equation the index $a_1 \cdots b_1$ denote the color, the spinor and the flavor index.

Moreover, the fermionic part is a bilinear form in the fermion fields ψ and $\overline{\psi}$

$$S_F[U,\overline{\psi},\psi] = \sum_{f,x,y} \overline{\psi}^f_x \, Q_{xy} \, \psi^f_y, \tag{3.9}$$

where, Q is called the fermion matrix acting on fermion fields $\overline{\psi_x}$ and ψ_x. Thereby, the integral in Eq. (3.7) might be performed instantly over the fermionic variables yielding

$$\begin{aligned}\langle \mathscr{O} \rangle &\equiv \left\langle \psi_{x_1} \overline{\psi}_{y_1} \cdots \psi_{x_n} \overline{\psi}_{y_n} \mathscr{G}[U] \right\rangle \\ &= \frac{1}{Z} \int [\mathscr{D}U] \, e^{-S_G[U]} \, \mathscr{G}[U] \sum_{z_1,\ldots,z_n} \varepsilon^{z_1,\ldots,z_n}_{x_1,\ldots,x_n} \, Q^{-1}_{z_1,y_1}[U] \cdots Q^{-1}_{z_n,y_n}[U],\end{aligned} \tag{3.10}$$

where the antisymmetric tensor is defined as $\varepsilon^{z_1,\ldots,z_n}_{x_1,\ldots,x_n} := 1$ ($\varepsilon^{z_1,\ldots,z_n}_{x_1,\ldots,x_n} := -1$) for even (odd) permutations of the lattice sites $x_1,\ldots,x_n$, and zero else. One can re-express the total action called the effective action S_{eff} in Eq. (3.10) as

$$S_{eff}[U] = S_G[U] - \log\det Q[U] \tag{3.11}$$

where $\det Q[U]$ is called the fermion determinant. Therefore, on remark that the pure gauge case (or the quenched approximation) corresponds actually to a fermion determinant equal to one ending up with $S_G[U]$ as the total effective action.

What makes things interesting in *LQCD* is the possibility to apply MC techniques in order to evaluate vacuum expectation values with an effective action S_{eff} as a statistical averages. The first step would be to generates gauge field configurations U^i according to a MARKOV chain process. These configurations, let us say of number N, are thermalized (brought to equilibrium). That is, these are realizations of the Boltzmann distribution

$$\frac{1}{Z} \exp\left\{-S_{eff}[U]\right\} \ .$$

Actually, we take into account configurations which dominate the exponential according to *importance sampling* principle. This latter is in general implemented considering mostly configurations minimizing S_F, i. e. in the equilibrium. Therefore, one computes in *LQCD* statistical averages on such sampled configurations as

$$\langle \mathscr{O} \rangle_U := \frac{1}{N} \sum_{i=1}^{N} \mathscr{O}[U^{(i)}].$$

Only in the limit $N \to \infty$ the ensemble estimator $\langle \mathscr{O} \rangle_U$[5] and the expectation value $\langle \mathscr{O} \rangle$ would match.

[5] In general, this estimator is afflicted with errors of the form $\sigma/\sqrt{(N)}$, where σ is the standard deviation. Moreover, additional systematic errors are present due to finite volume and lattice spacing effects.

Therefore, one concludes that *LQCD* is performing integrations by taking a limit of sums on discrete points. On the lattice N_σ and N_τ denote the number of points in the spatial and the temporal (or the inverse temperature) directions. The (spatial) volume V and the temperature T are given by

$$V = (N_\sigma a)^3, \tag{3.12}$$

and

$$T = \frac{1}{N_\tau a}. \tag{3.13}$$

The finite lattice spacing a imposes an ultraviolet cut-off a^{-1} while the volume V imposes an infrared cut-off at low momenta. Now, let us talk about the gauge transformation on the lattice g_x. As seen before, the effective action in Eq. (3.11) is invariant under the following local gauge transformations set $g_x \in SU(3)$ acting as

$$\psi(x) \to \psi^g(x) = g(x)\psi(x) \tag{3.14}$$

$$\overline{\psi}(x) \to \overline{\psi}^g(x) = \overline{\psi}(x)g^\dagger(x) \tag{3.15}$$

$$U_{x,\mu} \to {}^gU_{x,\mu} = g_x U_{x,\mu}\, g^\dagger_{x+\hat{\mu}}. \tag{3.16}$$

These (arbitrary) gauge transformations need to satisfy the lattice version of the LANDAU gauge presented later on in order to be fixed. In fact, in our MC process one first generate configurations and their gauge transformations. Secondly, we fix the gauge for example to the LANDAU gauge. Thirdly and finally, we measure the propagators as statistical averages using the gauge fixed configurations.

3.2 A closer look to our lattice actions

3.2.1 The gauge WILSON action

At this point we start presenting the lattice gauge action we used for our pure gauge theory investigations. This action is called the WILSON gauge action S_G in honor to its discoverer [114]. It reads as a sum over plaquettes $\square_{x,\mu\nu}$

$$S_G[U] := \beta \sum_x \sum_{1\le\mu<\nu\le 4} \left(1 - \frac{1}{N_c}\,\mathfrak{Re}\,\mathrm{Tr}\,\square_{x,\mu\nu}\right) \tag{3.17}$$

where the plaquette represent the shortest, non-trivial closed loop[6] on the lattice denoted as

$$\Box_{x,\mu\nu} := U_{x,\mu} U_{x+\hat{\mu},\nu} U^{\dagger}_{x+\hat{\nu},\mu} U^{\dagger}_{x,\nu} \, . \tag{3.18}$$

The trace of this plaquette variable is a gauge-invariant object. This lattice discretization is actually the first formulation of lattice gauge theory [114], and it actually approaches the continuum form, namely the YANG-MILLS action Eq. (3.20) in the naive limit $a \to 0$. Here and in the following β represents the inverse coupling

$$\beta := \frac{2N_c}{g_o^2} \tag{3.19}$$

where $N_c = 3$ for $SU(3)$ and g_o is the bare coupling constant.

3.2.2 The improved SYMANZIK gauge action

In this section we are going to talk about another type of pure gauge lattice action, namely the SYMANZIK action. Thanks to the tmfT collaboration this kind of action has been used as well as the twisted mass fermionic action to generate configurations for our full *QCD* investigations. In brief, the SYMANZIK type action belong to a class of actions called *improved actions*. As noticed before, expanding the gauge WILSON action Eq. (3.17) in the limit $a \longrightarrow 0$ (small lattice spacings) and using $U_\mu \sim e^{-igA_\mu(x)}$ the continuum Yang-Mills action is recovered (up to a^2 order)

$$S_{YM} = -\frac{1}{4} \int_0^\beta d\tau \int d^3x F^b_{\mu\nu} F_b^{\mu\nu} + \mathcal{O}(a^2). \tag{3.20}$$

As we see from this latter equation the correction to the continuum action is of order $\mathcal{O}(a^2)$. However, a large set of actions might also have the same continuum form, differencing only by irrelevant terms proportional to higher powers of the lattice spacing a. This fact opens the way to define 'improved' actions, and this is the sense of improvement in this context. The idea behind constructing such actions is to add further counter-terms to S_G Eq. (3.17) in order to eliminate order $\mathcal{O}(a^2)$. One might do this operation repeatedly, and therefore eliminate all desired corrections. This brings us to the concept of the so-called *perfect actions* [115]. Therefore, one understands that the total improved pure gauge action for example is a result of a combination of terms added to the gauge action Eq. (3.17) in order to reduce the discretization effects. Many years ago SYMANZIK in 1985 [116, 117] pointed out that the convergence to the continuum limit might be accelerated thanks to the inclusion of counter-terms of order a (or higher) in the lattice actions and the local operator of interest. For an account of the order a-improvement of lattice *QCD* we advise the reader to consult [118, 119] and references therein.

[6] Into this action the plaquettes are counted with only one spatial orientation.

The pure gauge SYMANZIK action of interest for us looks like

$$S_G^{SYM} = \beta \sum_x [c_0 \sum_{\mu<\nu} (1 - \frac{1}{3} \mathfrak{Re}\ \mathrm{Tr}\, U_{x\mu\nu}^{1\times 1}) + c_1 \sum_{\mu\neq\nu} (1 - \frac{1}{3} \mathfrak{Re}\ \mathrm{Tr}\, U_{x\mu\nu}^{1\times 2})], \tag{3.21}$$

with $c_1 = -\frac{1}{12}$ and the normalization condition $c_0 = 1 - 8c_1$. $U_{x\mu\nu} \in SU(3)$ represent plaquettes variables. $U^{1\times 1}$ represent the usual (1×1) WILSON loop plaquette (denoted $\Box_{x,\mu\nu}$ in the previous section) and $U^{1\times 2}$ planar rectangular (1×2) WILSON loops. The second term in this last equation suppresses short-range fluctuations at cut-off scale, and therefore improves the behavior towards the continuum limit. For a comprehensive account on rectangle plaquette actions, and also other generalized improved action we refer to the papers [120, 120, 116, 117].

3.2.3 The improved twisted mass action

We introduce in this section the fermionic part of the improved action used to provide thermalized configuration we relied on to compute the propagators. The action in question is called the improved *twisted mass* action including dynamical WILSON twisted fermions. This action represent the fermionic part while the gauge part is given by the SYMANZIK action described in the previous section. More interesting for us, namely the case of two mass-degenerate quarks flavors $N_F = 2$, the twisted mass formulation introduces an isospin structure as a mass term. This twisted mass term provides in fact a useful infrared regulator and can be utilized to obtain $\mathcal{O}(a)$ improvement. The twisted mass action for two degenerate fermions consists of the standard WILSON action augmented by a twisted mass term $\overline{\psi} i\mu_0 \gamma_5 \tau^3 \psi$. In this context, the hopping parameter κ and the twisted parameter μ_0 are connected to the bare quark mass as

$$m_0 = \sqrt{\frac{1}{4}(\frac{1}{\kappa} - \frac{1}{\kappa_c})^2 + \mu_0^2}. \tag{3.22}$$

For a maximal twist we have $\kappa = \kappa_c$, where κ_c is the critical hopping parameter. Therefore, the quark mass is defined by μ_0 alone. In general, the WILSON fermions with a twisted mass term evaluated at the maximal twist provide as said before automatic $\mathcal{O}(a)$-improvement, but also the suppression of exceptional configurations. We refer to [121] for a comprehensive report. In general, the twisted mass action looks like

$$S_F[U, \psi, \overline{\psi}] = \sum_x \overline{\chi}(x) \left(1 - \kappa D_W[U] + 2i\kappa a \mu_0 \gamma_5 \tau^3\right) \chi(x)\ . \tag{3.23}$$

The WILSON covariant derivative is given by

$$D_W[U]\psi(x) = \sum_\mu ((r - \gamma_\mu) U_\mu(x) \psi(x + \hat{\mu}) (r + \gamma_\mu) U_\mu^\dagger(x - \hat{\mu}) \psi(x - \hat{\mu})). \tag{3.24}$$

Here the twisted mass is expressed into the physical basis $\{\overline{\psi}, \psi\}$. At the maximal twist it is

better to redefine this basis into the so-called twisted basis $\{\bar{\chi}, \chi\}$ as

$$\psi = \frac{1}{\sqrt{2}}(1 + i\gamma_5\tau^3)\chi \quad \text{and} \quad \overline{\psi} = \overline{\chi}\frac{1}{\sqrt{2}}(1 + i\gamma_5\tau^3)\,. \tag{3.25}$$

In the weak coupling limit, $\beta = 6/g_0^2 \to \infty$, zero quark mass corresponds to $\kappa = 1/8$, setting $r = 1$. For finite coupling this value of κ gets corrections through mass renormalization. The overall renormalized quark mass M is composed of the twisted and untwisted masses as

$$M^2 = Z_m^2\,(m_0 - m_{\rm cr})^2 + Z_\mu^2\mu_0^2 \tag{3.26}$$

where $m_{\rm cr}$ is the critical mass and Z_m is the corresponding Z-factor. Our hopping parameters of interest are based on the values of β provided by the European Twisted Mass Collaboration (ETMC) [122]. k_c for intermediate lattice spacing $a(\beta)$ values were obtained thanks to interpolations as practized in [123, 124].

As usual at finite temperature *QCD*, the imaginary-time extent corresponds to the inverse temperature $T^{-1} = N_\tau a$. To be able to set the physical scale for each β we interpolated the data at the β values of 3.90, 4.05, 4.2 provided by the ETMC collaboration [122]. This allowed us to map each β value to a some lattice spacing a in Fermi for example. We consider during the present investigations lattice spacings $a < 0.09\,fm$ and three sets of pion masses $m_\pi = 316,\ 398\,\text{and}\,469\,\text{MeV}$.

■ 3.3 How to perform the continuum limit?

In order to extract continuum physics from *LQCD* computations one needs to extrapolate the outcoming (originally dimensionless) lattice results to the limit of vanishing lattice spacing $a \longrightarrow 0$. This limit makes sense only after fixing the scale of the theory to some physical meaningful quantity as the temperature. That means the lattice spacing needs to be related somehow to the temperature. This latter is expected to remain fixed in the limit of vanishing lattice spacing. One way to achieve this relationship is to consider the two-loop renormalization group equation

$$a\Lambda \simeq (\frac{6b_0}{\beta})^{-\frac{b_1}{2b_0^2}} exp(-\frac{\beta}{12b_0}), \tag{3.27}$$

and the relation $T = 1/aN_\tau$. Here the two universal coefficients amount to $b_0 = \frac{1}{16\pi^2}(11 - \frac{2}{3}N_f)$ and $b1 = (\frac{1}{16\pi^2})^2[102 - (10 + \frac{8}{3})N_f]$, and Λ is the scale parameter which might be related to other regularization schemes. Here, in our thesis we set the scale for pure gauge theory for example using the NECCO-SOMMER parametrization of $\ln(a/r_0)$ on β [125]. Setting the SOMMER scale to $r_0 = 0.5\,\text{fm}$ allows to determine the physical scale of the lattice spacing a, and employ-

ing such parametrization one may map β to each a. Regarding our unquenched data, the values of r_0/a were provided to us by the tmfT collaboration. These values result from interpolations of the data provided by the ETMC collaboration [122].

Therefore, after mapping somehow a to β one can in principle perform numerical simulations with β as input, for different N_τ, keeping the aspect ratio (N_σ/N_τ) and T fixed. That is, we simulate at different lattice spacings keeping T and the (spatial) volume fixed. Hence, once may at the end of day extrapolate results (for example of the propagators) to $a \longrightarrow 0$ and extract the continuum physics. This is the strategy we applied in the study of the continuum limit of quenched *QCD* as we discuss later. We were able to reach the continuum limit using a lattice size of $48^3 \times 12$ and keeping the physical volume fixed above and below the critical temperature T_c. In fact, extrapolations at different a correspond in our case to a quadratic function of a as the WILSON action has $\mathcal{O}(a^2)$ errors. One other aim was also to extrapolate to the thermodynamic limit $V = (aN_\sigma)^3 \longrightarrow \infty$. This is achieved setting the temperature T and N_τ fixed. In fact, such ideal limit is always limited by the finite size of the lattice. We used in this context a maximal lattice size of $64^3 \times 12$. This enables us to assess finite size effects which are discussed in the results part of the thesis.

To summarize, to extract the continuum physics of an observable $\mathcal{O}$ on the lattice one need to perform the following ordered multiple limits

$$\langle \mathcal{O} \rangle = \lim_{V_{\text{phys}} \to \infty} \lim_{a \to 0} \lim_{N \to \infty} \langle \mathcal{O} \rangle_U \ ,$$

where N denotes the number of configurations, and $V_{\text{phys}} = (N_\sigma \times a)^3$ is the physical spatial 3d space.

3.4 Fixing the LANDAU gauge

Beside the systematic errors which arise in a typical lattice simulation the GRIBOV ambiguity might be the most problematic aspect one needs to deal with. In this particular section we introduce basic elements on how to gauge fix the fields on the lattice and how the GRIBOV problem comes into play. Two popular gauge-fixing methods are used during our simulations, namely *simulated annealing* and *over-relaxation*. Finally, we propose to define the gauge uniquely taking into account the smallest FADDEEV-POPOV (FP) operator eigenvalues. This way one considers gauge copies as close as possible to the so-called GRIBOV horizon [28]. Results on this new proposed method can be found in Chap. 7.

3.4.1 Gauge fixing and gauge functional

In this thesis, we are interested in propagators for the particular case of the LANDAU gauge fixing condition. In general, during the gauge fixing process on the lattice one needs to search for a gauge transformation $g = g_x$ (for a fixed configuration U) which maximizes the gauge

functional $F_U[g]$. This gauge functional might be written for the LANDAU gauge as

$$F_U[g] = \frac{1}{4V} \sum_x \sum_{\mu=1}^{4} \mathfrak{Re}\,\mathrm{Tr}\ {}^g U_{x,\mu} \tag{3.28}$$

with V denotes the lattice volume. The continuum form of this lattice form was already presented in Eq. (2.21). Actually, for the trivial case of $U = \mathbb{I}$ the gauge functional $F_U[g]$ takes the largest value $F_U[g] = 3$ for $g = \mathbb{I}$. Searching a maximum of $F_U[g]$ for other U drive all the ${}^g U_{x,\mu}$ close to the unity. Therefore, our goal during the gauge-fixing process is to find global maxima of $F_U[g]$. In fact $F_U[g]$ has many local maxima whose the number is increasing with the lattice size. The different gauge copies maxima belonging to the same gauge orbit are called GRIBOV *copies* [26]. These gauge copies are all satisfying the same lattice transversality condition, namely

$$(\nabla_\mu A_\mu)(x) \equiv (\nabla \cdot A)(x) := \sum_{\mu=1}^{4} \Big[A_\mu(x + \hat{\mu}/2) - A_\mu(x - \hat{\mu}/2) \Big] = 0 \tag{3.29}$$

Where the lattice gauge potential $A_\mu(x + \hat{\mu}/2)$ is defined in a mid-point link as

$$A_\mu(x + \hat{\mu}/2) := \frac{1}{2i} \left(U_{x,\mu} - U^\dagger_{x,\mu} \right) |_{traceless} \tag{3.30}$$

Moreover, here and in the following we will assume the notation

$$A_{x,\mu} := A_\mu(x + \hat{\mu}/2).$$

For the sake of completeness we should also define the gluon fields in the adjoint representation as

$$A^a_{x,\mu} := A^a_\mu(x + \hat{\mu}/2) = 2 \cdot \mathfrak{Im}\,\mathrm{Tr}\{T^a U_{x\mu}\}. \tag{3.31}$$

This latter equation is needed when computing the gluon propagator. We have used for the implementation of the LANDAU gauge fixing on the lattice two popular methods, namely *simulated annealing* (SA) and *over-relaxation*(OR). In fact we used a combination of both methods (SIM followed by OR) for better efficiency to find g_x as close as possible to the global maximum of $F_U[g]$ as already practized in [126, 127, 128, 31, 32]. Let us in the next section present such methods in more detail.

Simulated annealing and over-relaxation

As said in the previous section, gauge fixing on the lattice amounts to find gauge copies being as close as possible to the global maximum of $F_U[g]$ [129, 130] as already practized in [33, 35, 34, 36, 31, 32]. This prescription has been shown to provide correct results for LANDAU gauge photon and fermion propagators within compact $U(1)$ lattice gauge theory

[131, 132, 133, 134]. Very efficient for this aim is the simulated annealing (SA) algorithm combined with subsequent over-relaxation (OR) iterations [126, 127, 128, 31, 32]. The SA algorithm generates gauge transformations $\{g_x\}$ randomly with a statistical weight $\sim \exp(F_U[g]/T_{sa})$. The "temperature" T_{sa} is a technical parameter which is monotonously lowered in the course of a determined SA simulation sweeps (actually, these are heat-bath updates). Also, for better performance, a few micro-canonical steps are applied after each heat-bath step. Finally, we employ the OR algorithm in order to satisfy the gauge condition Eq. (3.29) with a local accuracy of ε

$$\max_x \mathfrak{Re}\,\mathrm{Tr}[\nabla_\mu A_{x\mu} \nabla_\nu A^\dagger_{x\nu}] < \varepsilon. \tag{3.32}$$

3.4.2 A new proposal to deal with the GRIBOV ambiguity

The ambiguity to find a (absolute) local maxima for the gauge functional corresponds to a problem connected with the nature of LANDAU gauge itself. Several approaches are developed to study the GRIBOV effects on the propagators. The approach we used to the pure gauge sector of *QCD* is called first-best copy (fc-bc) strategy. In general, it consists of comparing the gluon propagator (for example) computed on the first (random) gauge copy generated during the MC process with the best copy, i.e. the copy providing the highest maximum of $F_U[g]$. Our alternative to solve the GRIBOV problem is to consider the vicinity of the GRIBOV horizon. That is, to take into account gauge fixed configurations having the minimal FP operator eigenvalues. This latter requirement ensures to get a ghost propagator singular behavior. We will discuss these results in Chap. 7.

The FADDEEV POPOV operator and its eigenvalues

Presently we start to introduce basic definitions and concepts we need later on to understand our alternative study of the GRIBOV problem. The master key in our analysis is the FADDEEV POPOV operator and its eigenvalues on the lattice in the LANDAU gauge. Let us start first by defining the one-parameter subgroup of local $SU(3)$ gauge group [135] as

$$g_\omega(\tau, x) = \exp\{i\tau\omega^c_x T^c\} \qquad \tau, \omega^c_x \in \mathbb{R}\,.$$

Here T^c are the generators of the $SU(3)$ group. Let us now assume that g is a local maxima of the gauge functional $f_\omega(\tau) := F_U[g_\omega(\tau)]$, then the first derivative with respect to τ should vanish (in fact for any τ)

$$0 = \frac{\partial}{\partial\tau} f_\omega(\tau)\bigg|_{\tau=0} = \frac{1}{2}\sum_{x,c}\omega^c_x \sum_\mu \left[A^c_{x-\hat{\mu},\mu} - A^c_{x,\mu}\right]\,,$$

therefore one observes from this latter equation that local maxima of the gauge functional automatically satisfy the lattice LANDAU gauge Eq. (3.29). A second derivation with respect to

τ at $\tau = 0$ defines in the LANDAU gauge the FADDEEV-POPOV operator[7] as follows

$$\frac{\partial^2}{\partial \tau^2} f_\omega(\tau)\bigg|_{\tau=0} = \sum_{x,y,c,d} \omega_x^c M_{xy}^{cd} \omega_y^d$$

where

$$M_{xy}^{ab} = A_x^{ab}\,\delta_{x,y} - \sum_\mu \left(B_{x,\mu}^{ab}\,\delta_{x+\hat{\mu},y} + C_{x,\mu}^{ab}\,\delta_{x-\hat{\mu},y} \right) \tag{3.33}$$

with

$$A_x^{ab} = \textstyle\sum_\mu \mathfrak{Re}\,\mathrm{Tr}\left[\{T^a, T^b\}(U_{x,\mu} + U_{x-\hat{\mu},\mu}) \right], \tag{3.34a}$$

$$B_{x,\mu}^{ab} = 2 \cdot \mathfrak{Re}\,\mathrm{Tr}\left[T^b\, T^a\, U_{x,\mu} \right], \tag{3.34b}$$

$$C_{x,\mu}^{ab} = 2 \cdot \mathfrak{Re}\,\mathrm{Tr}\left[T^a\, T^b\, U_{x-\hat{\mu},\mu} \right]. \tag{3.34c}$$

M is a symmetric real matrix which satisfy in the LANDAU gauge

$$M[U] = -\nabla \cdot D[U] = -D[U] \cdot \nabla \quad \Longleftrightarrow \quad \nabla \cdot A = 0$$

where $D[U]$ refers to the covariant derivative [136]. This F-P operator admit eight zero modes. Still, the remaining eigenvalues of the F-P operator are positive. The corresponding gauge field configuration is said to lie within the GRIBOV region. If the lowest non-trivial eigenvalue tends to zero the configuration approaches the so-called GRIBOV horizon. Therefore, the GRIBOV set Ω [28] is defined as a set of local maxima as

$$\Omega := \{U : U \in \Gamma, M[U] \geq 0\},$$

where Γ is the set of transverse configurations U, namely satisfying $\nabla \cdot A(U) = 0$. From this GRIBOV region one might construct the fundamental modular region FMR [136] constituted with all global maxima of $F_U[g]$ defined as

$$\Lambda := \{U : F_U(\mathbb{I}) \geq F_U[g] \quad \text{for all } g\}.$$

It has been proven on the lattice that such FMR is a GRIBOV-copies free region except on its boundary where GRIBOV copies might be encountered [136]. Still, a prescription to construct such FMR spaces is not a priori a trivial task. The aforementioned F-P eigenvalues have a direct influence on the ghost propagator behavior as this propagator might be given a spectral representation in terms of these eigenvalues. In fact, an enhanced density of eigenvalues near zero causes the ghost propagator to diverge stronger than $1/q^2$ near zero momentum [28]. Actually,

[7] The second derivative is called also the Hessian of $F_U[g]$.

the ghost propagator might be reconstructed as a spectral representation as

$$G_n(q^2) = \sum_{i=1}^{n} \frac{1}{\lambda_i} \vec{\Phi}_i(k) \cdot \vec{\Phi}_i(-k) \tag{3.35}$$

with $\vec{\Phi}_i(k)$ being the Fourier transform of the i-th eigenmode (k denotes the lattice momentum) [137, 138]. Therefore, If all $n = 8V$ eigenvalues and eigenvectors were known, the ghost propagator $G(q^2)$ would be completely determined. Therefore, considering small FP eigenvalues render the ghost propagator more singular. Therefore, we focus in this investigation only on the gluon propagator at $T = 0$. An important remark in [137, 138] is that the FP eigenvalues (or the density of lowest eigenvalues) are shifted to zero when moving to higher lattice volumes. This behavior is in agreement with ZWANZIGER paper [28]. We are not going to examine the behavior of the ghost propagator (as a function of the FP eigenvalues) as we already know that it enhances for smaller eigenvalues in the infrared momentum region.

How to face the GRIBOV ambiguity?

Even if the approach consisting of finding maxima closer to the global one by maximizing the value of $F_U[g]$ is quite admitted we believe in fact that the FP eigenvalues might also play a rôle. In fact, we have already seen that these (lower) eigenvalues are dominating the infrared behavior of the ghost propagator in [137, 138], and one observes a singular behavior of the ghost propagator.

The conventional method based on maximizing the gauge functional is subject to the GRIBOV ambiguity when different local maxima are taken into account. This situation spoils an unique definition of the gauge, and no criteria is possible to distinguish different GRIBOV copies giving at the end different propagators results (mainly in the infrared). Furthermore, lattice results using the gauge functional approach show a plateau ending with a finite zero momentum gluon propagator even for physical volumes larger than $13^4\, fm^4$ [61]. On the other hand, solutions of a truncated set of DYSON-SCHWINGER equations (*DSE*) for gluon and ghost propagators in LANDAU gauge predict two type of different solutions, namely the scaling and the decoupling solutions [20, 139, 71, 81, 27]. These two types of solutions start to deviate from each other below the region of 1 GeV. In the ultraviolet region of momenta these solution are indistinguishable. These two solutions are the consequence of different boundary conditions on the ghost dressing function at zero momenta [89, 140]. Therefore, fixing these boundary conditions is equivalent to not take the GRIBOV problem seriously. For the moment lattice investigation support coupling solutions contradicting the KUGO-OJIMA confinement criterion [29]. We think that if one is able to define a free GRIBOV problem procedure on the lattice one may observe the 'real' physical solution of the DSE.

In Chap. 7 we propose to concentrate on a new criteria which enable us to choose in an unique way, which gauge transformation needs to be taken into account. We consider in fact only gauge configurations with the lowest positive FP eigenvalues. This set of gauge configuration is actually

a subset of the GRIBOV region, and might intersects with the fundamental modular region. In this respect, we have studied in this respect the correlation between the highest $F_U[g]$ and lowest positive FP eigenvalues, and no strict correlation have been observed. Indeed, this is a fortunate situation as this actually means that the ghost propagator might diverge stronger as a result of our new criteria for example. Moreover, this also shows that both criteria (hightest F vs. minimal λ) might provide independent results.

For the gluon propagator it is already known that the influence within the gauge functional approach is weak [137, 138] following the fc-bc method. But still, in this last references no comparison between best copies (in the sense of highest gauge functional] to gauge copies with lowest FP eigenvalues have been done. We shall discuss results of our new approach for the $SU(3)$ gauge group for symmetric lattices ($T = 0$) in Chap. 7.

CHAPTER 4

Lattice observables at $T > 0$

HERE we introduce basic definitions of the POLYAKOV on the lattice. We also define the gluon and ghost propagators at finite temperature. This brings us two define the two independent components of the gluon propagator, namely: the transverse (D_T) and longitudinal (D_L) components on the lattice. We discuss at the end of this chapter renormalization issues for these propagators.

4.1 The POLYAKOV loop on the lattice

As we know confinement is the realization of a global $Z(3)$ center symmetry. When this symmetry does break a phase transition from a confining state to a deconfined plasma occurs. This phenomena was first observed in [141]. The lattice analogous of the POLYAKOV loop defined previously in the continuum (Eq. (2.93)) looks like

$$L(\vec{n}) = \mathrm{Tr} \prod_{N_4=0}^{N_\tau - 1} U_4(\vec{n}, n_4), \tag{4.1}$$

where $\vec{n} = (n_1, n_2, n_3, n_4)$ is the lattice site and $n_4 = t$. The average of this POLYAKOV loop is related to the free energy of a static quark F_q as already remarked with

$$\langle L(\vec{n}) \rangle = e^{-\frac{F_q}{T}}. \tag{4.2}$$

In fact $|\langle L \rangle|$ is an order parameter for confinement-deconfinement phase transition since the static q-$\bar{q}$-potential $F_{q\bar{q}}(\vec{n})$ satisfies

$$F_{\vec{q}q}(\vec{n}) \longrightarrow 2F_q, \tag{4.3}$$

for $\vec{n} \longrightarrow \infty$ in the confining phase. Therefore, $|\langle L(\vec{n})\rangle|$ satisfies

$$\begin{aligned} \text{Confinement} &\Leftrightarrow |\langle L(\vec{n})\rangle| = 0, \\ \text{Deconfinement} &\Leftrightarrow |\langle L(\vec{n})\rangle| \neq 0. \end{aligned}$$

Since the POLYAKOV line transforms under $Z(3)$ transformation as

$$L(\vec{n}) \longrightarrow e^{\frac{2\pi i}{3} j} L(\vec{n}), \qquad j \in \{0,2\}, \tag{4.4}$$

the free energy diverges as long as the center symmetry is satisfied. $F_{q\bar{q}}$ remains finite when the center symmetry is spontaneously broken. We interpret this as a manifestation of deconfinement.

■ 4.2 The lattice gluon propagator

On the lattice the gluon propagator (at zero temperature) is defined in momentum space as

$$D^{ab}_{\mu\nu}(q) = \left\langle \widetilde{A}^a_\mu(k)\widetilde{A}^b_\nu(-k)\right\rangle, \tag{4.5}$$

where $\langle\cdots\rangle$ represents the average over configurations, and $\widetilde{A}^a_\mu(k)$ denotes the Fourier transform of the gauge-fixed gluon field [1]

$$A_\mu(x+\hat{\mu}/2) = \frac{1}{2iag_0}(U_{x\mu} - U^\dagger_{x\mu})\,|_{traceless} \tag{4.6}$$

depending on the integer-valued lattice momentum k_μ ($\mu = 1,\ldots,4$), and $U_{x\mu}$ are $SU(3)$ links. The lattice momenta k_μ are related to the physical momentum (for the WILSON plaquette action) as

$$q_\mu(k_\mu) = \frac{2}{a}\sin\left(\frac{\pi k_\mu}{N_\mu}\right), \quad k_\mu \in \left(-N_\mu/2, N_\mu/2\right], \tag{4.7}$$

where $(N_i, i = 1,2,3;N_4) \equiv (N_\sigma;N_\tau)$ characterizes the lattice size.

For non-zero temperature it is convenient to split the propagator into two components, the transverse D_T ("chromomagnetic") (transverse to the heat-bath rest frame) and the longitudinal D_L one ("chromoelectric"), respectively,

$$D^{ab}_{\mu\nu}(q) = \delta^{ab}(P^T_{\mu\nu}D_T(q_4^2,\vec{q}^2) + P^L_{\mu\nu}D_L(q_4^2,\vec{q}^2)), \tag{4.8}$$

where q_4 plays the role of the MATSUBARA frequency, which will be put to zero later on. For the Landau gauge, the tensor structures $P^{T,L}_{\mu\nu}$ represent projectors transverse and longitudinal relative to the $(\mu = 4)$-direction already defined in Eq. (2.121). For the propagator functions $D_{T,L}$ we

[1] In our case satisfying the lattice transversality Landau gauge condition $\nabla_\mu A_\mu = 0$.

find

$$D_T(q) = \frac{1}{2N_g}\left\langle \sum_{i=1}^{3} \widetilde{A}_i^a(k)\widetilde{A}_i^a(-k) - \frac{q_4^2}{\vec{q}^{\,2}}\widetilde{A}_4^a(k)\widetilde{A}_4^a(-k) \right\rangle \tag{4.9}$$

and

$$D_L(q) = \frac{1}{N_g}\left(1+\frac{q_4^2}{\vec{q}^{\,2}}\right)\left\langle \widetilde{A}_4^a(k)\widetilde{A}_4^a(-k)\right\rangle, \tag{4.10}$$

where the number of generators $N_g = N_{\text{color}}^2 - 1$ for $N_{\text{color}} = 3$. The zero-momentum propagator values can be defined as

$$D_T(0) = \frac{1}{3N_g}\sum_{i=1}^{3}\left\langle \widetilde{A}_i^a(0)\widetilde{A}_i^a(0)\right\rangle, \tag{4.11}$$

$$D_L(0) = \frac{1}{N_g}\left\langle \widetilde{A}_4^a(0)\widetilde{A}_4^a(0)\right\rangle. \tag{4.12}$$

■ 4.3 The ghost propagator

The Landau gauge ghost propagator is given by

$$\begin{aligned} G^{ab}(q) &= a^2\sum_{x,y}\langle e^{-2\pi i(k/N)\cdot(x-y)}[M^{-1}]_{xy}^{ab}\rangle, \\ &= \delta^{ab}\,G(q), \end{aligned} \tag{4.13}$$

where $q \neq 0$ and $(k/N)\cdot(x-y) \equiv \sum_\mu k_\mu (x-y)_\mu / N_\mu$. M denotes the lattice FADEEV-POPOV operator [2], already defined in Eq. (3.33) and Eq. (3.34). For our simulations and in order to invert M we use the conjugate gradient (CG) algorithm with plane-wave sources $\vec{\psi}_c$ with color and position components $\psi_c^a(x) = \delta_c^a \exp(2\pi i(k/N)\cdot x)$ to solve the equations $M_{xy}^{ab}\phi^b(y) = \psi_c^a(x)$ [142, 143]. In fact we exploit the formula

$$G^{ab}(q^2(k)) = \frac{1}{V}\left\langle \sum_{x,y}\left(M^{-1}\right)_{xy}^{ab} e^{ik\cdot(x-y)}\right\rangle_U .$$

Where the ensemble average is translation invariant. Since G^{ab} has the following tensorial struc-

[2] This operator definition is corresponding to the gauge field definition in Eq. (4.6) and the related gauge functional in Eq. (3.28)

ture $G^{ab}(q) = \delta^{ab} G(q^2)$ [142, 143] we are interested to compute the scalar function

$$G(q^2(k)) = \frac{1}{N_c^2 - 1} \sum_a G^{aa}(q^2(k)) = \frac{1}{N_c^2 - 1} \langle \mathrm{Tr}\, \mathscr{M}^{-1}(k) \rangle_U , \tag{4.14}$$

where $\mathscr{M}^{-1}(k)$ is the Fourier transform of the inverse FP operator M^{-1} in momentum space defined as

$$\left(\mathscr{M}^{-1}\right)^{ab}(k) = \frac{1}{V} \sum_{x,y} e^{-ik\cdot x} \left(M^{-1}\right)^{ab}_{xy} e^{ik\cdot y}, \tag{4.15}$$

and

$$k \cdot x \equiv \sum_{\mu=1}^{4} 2\pi \frac{k_\mu x_\mu}{L_\mu} \tag{4.16}$$

is the product of lattice momentum k and lattice site x. L_μ denotes the lattice extension in direction μ. As we are interested in non-zero momenta we apply the conjugate gradient method to solve the following sparse linear system

$$[M\psi_b]^{cz} \equiv \sum_{a,x} M_{cz,ax} \psi_b^{ax} = \xi_b^{cz}(k) \tag{4.17}$$

using a fixed source ξ_b with $8V$ complex components $\xi_b^{cz}(k) := \delta^{cb} e^{ik\cdot z}$. Here, c and z label the vector components of ξ_b, while index b specifies the sources. The inverse FP in Eq. (4.15) might be written as a function of the solutions of the system Eq. (4.17) like

$$\left(\mathscr{M}^{-1}\right)^{ab}(k) = \frac{1}{V} \sum_{x} e^{-ik\cdot x} \cdot \psi_b^{ax}(k) \; . \tag{4.18}$$

with $\psi_b^{ax}(k)$ representing the $8V$ vector components. Therefore, the problem numerically boils down to solve systems of the form

$$[M\mathsf{c}_b(k)]^{cz} = \delta^{cb} \cos(k\cdot z) \tag{4.19}$$

$$[M\mathsf{s}_b(k)]^{cz} = \delta^{cb} \sin(k\cdot z), \tag{4.20}$$

where ψ_b^{ax} is decomposed to $\psi_b^{ax} = \mathsf{c}_b^{ax} + i\,\mathsf{s}_b^{ax}$. Thereby, the inverse FP operator might be rewritten as

$$\begin{aligned}\left(\mathscr{M}^{-1}\right)^{ab}(k) = \frac{1}{V} \sum_{x,y} \quad & \cos(k\cdot x)\mathsf{c}_b^{ax}(k) + \sin(k\cdot x)\mathsf{s}_b^{ax}(k) \\ & + i\left[\cos(k\cdot x)\mathsf{s}_b^{ax}(k) \; - \sin(k\cdot x)\mathsf{c}_b^{ax}(k)\right].\end{aligned} \tag{4.21}$$

Back to the ghost propagator defined in Eq. (4.14) together with Eq. (4.21) and exploiting the property of the symmetry of the FP operator, one gets

$$\mathrm{Tr}\,\mathscr{M}^{-1}(k) = \sum_{a,x,y} \cos(k\cdot x)\cdot \mathsf{c}_a^{ax} + \sin(k\cdot x)\cdot \mathsf{s}_a^{ax}$$

where c_a^{ax} and s_a^{ax} are solutions to the two independent linear systems given in Eq. (4.19) and (Eq. (4.20)). Therefore, once the values of c_a^{ax} and s_a^{ax} are found numerically one gets directly the value of ghost scalar function from Eq. (4.14).

■ 4.4 Renormalizing the propagators

Throughout this thesis we renormalize our gluon propagator defined as $\langle A_\mu^a(x)A_\nu^b(y)\rangle$ and the ghost propagator $\langle c^a(x)\bar{c}^b(y)\rangle$ within the *MOM* scheme. In fact the *MOM* scheme defines the Z-factors such that the fundamental two-point and three-point functions equal their corresponding tree-level expressions at some momentum μ, the so-called the renormalization point. The LANDAU gauge gluon propagator expressed in momentum space looks like

$$D_{\mu\nu}^{ab}(p,\mu) = \delta^{ab}\left(\delta^{\mu\nu} - \frac{p_\mu p_\nu}{p^2}\right)\frac{Z(p^2,\mu^2)}{p^2} \tag{4.22}$$

with Z is the dressing function of the gluon propagator. This dressing function measure the deviation from the tree-level structure (corresponding to $Z\equiv 1$).

On the other hand, the ghost propagator has the following tensorial structure in Landau gauge

$$G^{ab}(p,\mu) = \delta^{ab}\,\frac{J(p^2,\mu^2)}{p^2}. \tag{4.23}$$

Where J is the dressing function of the ghost propagator.

As said before, within the *MOM* scheme the renormalization constants, for instance of the gluon and ghost fields Z_3 and $\widetilde{Z}_3$, are defined by requiring the renormalized expressions to equal their tree-level form at some (large) momentum μ. That is, we renormalized the gluon (D_T and D_L) and ghost (G) propagators imposing their dressing functions to be equal to one at the momentum subtraction point $p=\mu$.

$$p^2 D_T(p)|_{p=\mu} = 1, \tag{4.24}$$
$$p^2 D_L(p)|_{p=\mu} = 1, \tag{4.25}$$
$$p^2 G(p)|_{p=\mu} = 1. \tag{4.26}$$

The Z factors Z_3 and $\widetilde{Z}_3$ are defined as

$$D^{ab}_{\mu\nu}(p;\Lambda,g_o,m_o,\xi_o)\Big|_{p^2=\mu^2} =: Z_3\ \delta^{ab}\left(\delta^{\mu\nu}-\frac{p_\mu p_\nu}{\mu^2}\right)\frac{1}{\mu^2}, \tag{4.27}$$

and

$$G^{ab}(p;\Lambda,g_o,m_o,\xi_o)\Big|_{p^2=\mu^2} =: \widetilde{Z}_3\ \delta^{ab}\frac{1}{\mu^2}, \tag{4.28}$$

where $D^{ab}_{\mu\nu}(G^{ab})$ denotes the unrenormalized gluon(ghost) propagator. Actually, it is well expected that at high temperature these two components, D_T and D_L should behave independently of the temperature. This has a direct consequence on the values of Z_T and Z_L factors, which should coincide at this high temperature regime. This was observed by us [49] in pure gauge theory confirming a rough matching of the Z values as well as in the full QCD case [52]. We will come back to these points in the results part of this thesis.

Hence, the renormalization constants can be determined by calculating the corresponding unrenormalized (regularized) GREEN function. Their values depend on the chosen renormalization point μ and also on the bare parameters of the regularized theory. Therefore, fixing the values of Z_3 at some momentum μ thanks to Eq. (4.27) we were able to compute the renormalized gluon propagator (at μ) via multiplicative renormalization according to Eq. (2.38).

We took always $\mu = 5\,GeV$ for our pure gauge investigations based. This choice is done in order to be far enough in the ultraviolet region of momenta (to study the low momenta lattice artifacts conveniently) as well as not being too close to the cutoff. Concerning full QCD we choose the renormalization point to be 2.5 GeV.

CHAPTER 5

Results in the pure gauge sector of *QCD*

WITHIN this chapter, we report on results in the pure gauge sector of *QCD* in LANDAU gauge. In particular, we present gluon and ghost propagators results in the so-called quenched approximation of *QCD*. Prior to this, we start first by specifying the lattice samples we used during our investigations. Therefore, important different parameters as the critical β_c are discussed and identified. Also we comment on how to map to physical units. Lastly, different systematic effects as the momenta preselection, the POLYAKOV loop sector, finite size and the GRIBOV problem are studied extensively.

5.1 Specification of our lattice samples

During our lattice investigations of the pure gauge sector of *QCD* we generated $SU(3)$ gauge configurations according to a Monte-Carlo process. We thermalized the configurations using the standard WILSON action. In general, each thermalization sweep consist of four micro-canonical over-relaxation steps and one heath-bath. In particular, the system was thermalized with the heat-bath method using the CABIBBO-MARINARI trick [144]. Moreover, $O(2000)$ sweeps were discarded between consecutive measurements of observables. In fact, we took this big number of 2000 sweeps in between in order to reduce the auto-correlation between consecutive measurements. Our strategy here in order to vary the temperature is to keep the scale (β) fixed to the critical value $\beta_c = 6.337$. This latter value corresponds to a quite big $N_\tau = 12$. Moreover, we choose on purpose a quite high β_c to deal with a small lattice spacing, and therefore being close to the continuum limit. Hence, fixing the scale and varying N_τ temperature was able to be changed correspondingly according to Eq. (3.13). In contrast, in order to study finite size effects

T/T_c	N_τ	N_σ	β	$a(\mathrm{GeV}^{-1})$	$a(\mathrm{fm})$	n_{conf}
0.65	18	48	6.337	0.28	0.055	150
0.74	16	48	6.337	0.28	0.055	200
0.86	14	48	6.337	0.28	0.055	200
0.99	12	48	6.337	0.28	0.055	200
1.20	10	48	6.337	0.28	0.055	200
1.48	8	48	6.337	0.28	0.055	200
1.98	6	48	6.337	0.28	0.055	200
2.97	4	48	6.337	0.28	0.055	210
0.86	8	28	5.972	0.49	0.097	200
0.86	12	41	6.230	0.33	0.064	200
0.86	16	55	6.440	0.24	0.048	200
1.20	6	28	5.994	0.47	0.094	200
1.20	8	38	6.180	0.35	0.069	200
1.20	12	58	6.490	0.23	0.045	200
0.86	14	56	6.337	0.28	0.055	200
0.86	14	64	6.337	0.28	0.055	200
1.20	10	56	6.337	0.28	0.055	200
1.20	10	64	6.337	0.28	0.055	200

TABLE 5.1: Temperature values, lattice size parameters, lattice spacing a in units of GeV^{-1} and fm, and the number n_{conf} of independent lattice field configurations used throughout this study.

we fixed the temperature to two reference values (above and below T_c), and changed the lattice spacing (β), and N_σ correspondigly to fix the physical volume according to Eq. (3.12). Our lattice parameters are displayed in Table 6.1. The critical $N_\tau = 12$ provides an interesting range around the critical temperature T_c. The way to localize this critical value is examined in the next section with more detail.

5.1.1 Localization of our critical β_c

In order to be able to study the phase transition one needs to know the scale where it might happen. We fixed during our first investigations of the gluon and ghost propagator the coupling to the critical value $\beta_c = 6.337$. This β-value corresponds to a temperature very close to the critical value T_c of the deconfinement phase transition for $N_\tau = 12$ and a linear spatial extent $N_\sigma a(\beta = 6.337) = 48\ a\ \simeq 2.64$ fm. According to Ref. [57] our β_c has been fixed using interpolations

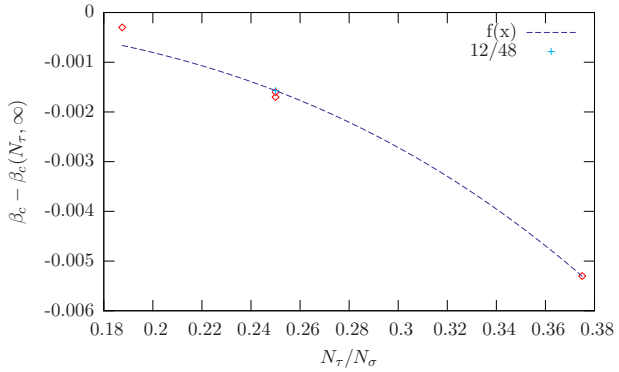

FIGURE 5.1: The difference $\beta_c(N_\tau, N_\sigma) - \beta_c(N_\tau, \infty)$ as a function of the ratio N_τ/N_σ using Eq. (5.1) presented in [57]. The interpolation is done at $N_\tau/N_\sigma = 12/32$.

(see Fig. 5.1) with the help of the fit formula

$$\beta_c(N_\tau, N_\sigma) = \beta_c(N_\tau, \infty) - h\left(\frac{N_\tau}{N_\sigma}\right)^3, \tag{5.1}$$

where $\beta_c(N_\tau, \infty)$ corresponds to the thermodynamic limit and h denotes a fit parameter ($h \lesssim 0.1$).

In fact, our choice $N_\sigma = 48$ guarantees a reasonable aspect ratio over the whole temperature range $T/T_c \equiv 12/N_\tau \in [12/18, 12/4]$ and to reach three-momenta below 1 GeV.

5.1.2 Selecting the momenta and the MATSUBARA frequency

On the lattice, typical lattice artifacts might be reduced by selecting an appropriate set of momenta. For the gluon and ghost propagators the momenta choice is an important issue. We focus first, in order to study systematic hyper-cubic effects, on the influence of the momentum choice on the behavior of the gluon propagator. Thus, both the transverse D_T and the longitudinal D_L gluon propagators are compared on both on-axis and diagonal momenta. We took as a reference our critical $\beta = 6.337$ and found in the lower momentum range only quite small deviations, as observed in Fig. 5.2. In fact, we show the bare transverse and longitudinal gluon propagators as functions of the lattice momenta, where the propagators are computed for the critical inverse coupling $\beta_c = 6.337$. As the fluctuations between the gluon data for the diagonal and on-axis momenta are small, we conclude that the choice of the momenta pre-selection is irrelevant. Nevertheless to be on the safe side we decided for most of our computations to apply the so-called cylinder cut [113] defined by

$$\sum_\mu k_\mu^2 - \frac{1}{4}\left(\sum_\mu k_\mu\right)^2 \leq c, \tag{5.2}$$

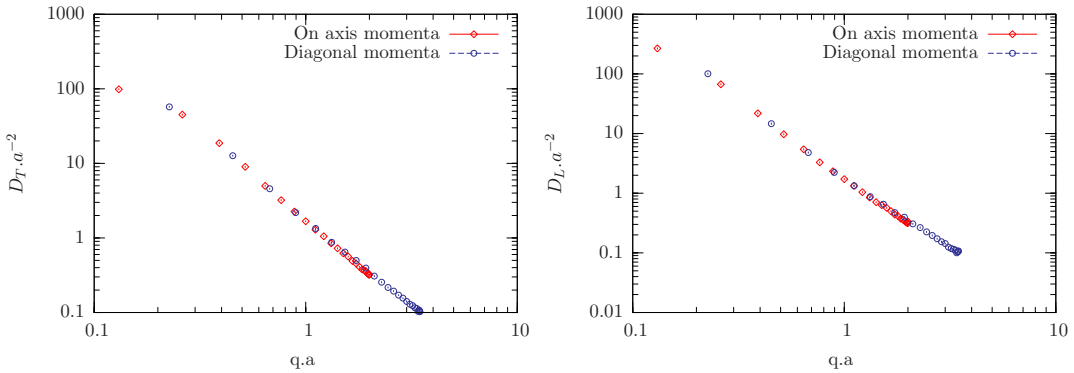

FIGURE 5.2: Comparison of the bare transverse (l.h.s.) and the longitudinal (r.h.s.) gluon propagator for $\beta = 6.337$, $N_\sigma = 48$ on on-axis and diagonal momenta preselections.

meaning that we take only into account momenta lying within the cone described with Eq. (5.2).

The cut parameter was chosen $c = 3$. Additionally, we took momenta with $k_4 = 0$. That is, only zero MATSUBARA frequencies are considered here. This choice of zero MATSUBARA frequencies is motivated by different reasons. The first reason is to be able to reach low momenta, at least around the physical momenta of $1\,GeV$. Therefore, concentrating on zero MATSUBARA frequencies (soft modes) one can access the region of small momenta. The second physical reason to study exclusively the soft modes is that the hard modes ($n \neq 0$) develop a thermal mass $2\pi nT$, and behave as massive particles, see [145, 54, 109, 9] and references therein.

5.1.3 Gauge fixing process

The process we employ here to fix gauge to the LANDAU gauge was based on two gauge fixing methods, namely: simulated annealing (SA) and over-relaxation(OR). The simulated annealing algorithm generates gauge transformations $\{g_x\}$ randomly with a statistical weight $\sim \exp(F_U[g]/T_{sa})$. T_{sa} is a technical parameter ("temperature") which is monotonously lowered. In fact, we start with $T_{sa} = 0.45$ and decrease this parameter down to $T_{sa} = 0.01$ in equal steps applied after each of the 3500 SA simulation sweeps. Fixing the initial and the final SA temperatures to $T_{sa} = 0.45$ and $T_{sa} = 0.01$ correspondingly rely on our study of the gauge functional as a function of these parameters. We observed actually that starting with 0.45 one might see a transition-like behavior of the gauge functional just above this temperature. The final temperature 0.01 was chosen in order to minimize the OR maximal divergence monotonously with respect to the number of iterations. For better performance a few micro-canonical steps are applied after each SA sweep. On the other hand, over-relaxation (see Appendix 8) is an iterative method transforming each gauge configuration to the LANDAU gauge looking for a local gauge transformation $g \equiv \{g_x\}$, which maximizes the gauge functional, and therefore approaching the (unknown) global maximum [146]. The stopping criteria for this iterative gauge fixing process

is the violation of the transversality condition. That is, the gauge fixing process is stopped as one satisfies

$$\max_x \mathfrak{Re}\,\mathrm{Tr}[\nabla_\mu A_{x\mu} \nabla_\nu A^\dagger_{x\nu}] < \varepsilon\,, \quad \varepsilon = 10^{-13} \tag{5.3}$$

Actually, we have always taken a maximum number of OR iterations equal to 80000. Therefore, it has been observed that the OR iterations needed for all temperature cases do not exceed this maximal number. In fact, a combination of SA and OR (simulation annealing finalized with over-relaxation) is proven to be more efficient to bring the gauge fixing process close to the global maximum [126, 127, 128, 31, 32].

5.1.4 Fixing the scale

In order to translate the bare gluon propagator into the physical one needs to fix the scale. To do that, we relied on the SOMMER scale $r_0 = 0.5\ fm$ [147]. This latter value together with the parametrization of $\ln(a/r_0)$ as a function of β [125] enabled us to physically map all the values of β as displayed on Table 6.1 to the corresponding lattice spacings. In fact, this mapping apply only for the reduced set of beta, namely $5.7 < \beta < 6.92$. Still, this range is enough for us to cover the temperatures range of interest.

5.2 The POLYAKOV loop results

The POLYAKOV loop is an important order parameter for *QCD* in the pure gauge sector. In fact, this quantity is an exact order parameter in this sector. That is, it takes different values depending whether the system lies in the confining or the deconfining phase. Ideally, the POLYAKOV loop takes zero values in the confining phase (below T_c) and a finite value otherwise.

In our lattice study we are interested in the POLYAKOV loop in order to check whether our localization of β_c at 6.337 is exact or not. In Section 5.1.1 such localization has been performed thanks to an interpolating formula proposed in [57].

On the lattice, the POLYAKOV loop is defined in Eq. (4.1), and due to the translation invariance on the lattice we take the following spatial average into consideration

$$L = \frac{1}{N_\sigma^3} \sum_n L(\vec{n}). \tag{5.4}$$

In fact, we focus on the real part of the spatial average of the POLYAKOV in Eq. (5.4). Our results are shown in Fig. 5.3. Here, we show the dependence of the absolute value of the real part as a function of the temperature. In order to cover the region around T_c coveniently, we vary the values of the β around the critical value β_c. This allows us to get a good distribution

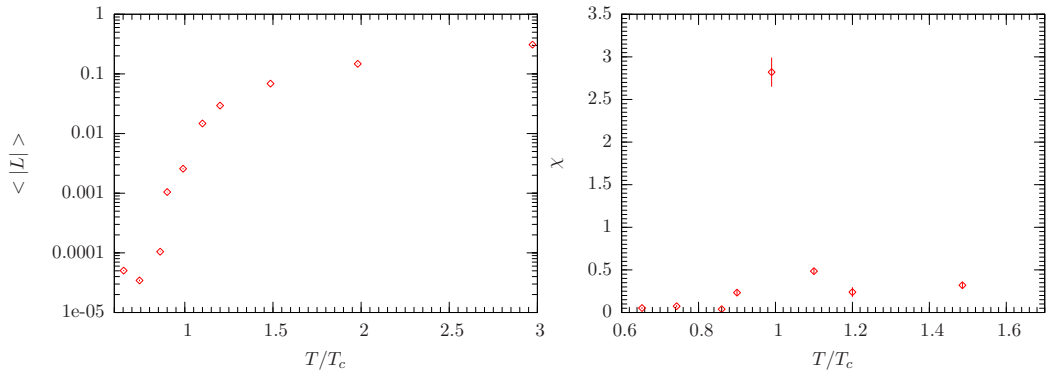

FIGURE 5.3: The temperature dependence of the absolute value of the POLYAKOV loop (l.h.s.) and its susceptibility (r.h.s.). The inverse coupling $\beta = 6.337$ and the spatial extent $n_\sigma = 48$.

of temperatures around T_c to observe occurately what happens around this latter temperature. In fact, We clearly see a brutal bending of the curve around the critical temperature T_c. Moreover, the (real part of) POLYAKOV loop values below the inflexion point are nearly close to zero. However, they are not completely equal to zero most probably due to the finite statistics in our analysis. Above T_c the curve take finite values up the maximal temperature investigated around 3 T_c. This POLYAKOV loop behavior is in agreement with previous studies [141]. Moreover, we are showing in the same previous plot (right side) the susceptibility of the POLYAKOV loop. This informative quantity is defined as follows

$$\chi = N_\sigma^3 \left(\langle L^2 \rangle - (\langle L \rangle)^2 \right). \tag{5.5}$$

This observable is one of the most important tools in statistical physics to study criticality in physical systems. We observe as expected that χ peaks around the critical temperature T_c. This indicates that the localization of our critical $\beta_c = 6.337$ is satisfying. Still, for higher temperature as T_c we still get error fluctuations due to the statistics used. Actually, we have used the *Jackknife* method to evaluate the errors. Therefore, from now we will concentrate on the critical beta $\beta_c = 6.337$ as our reference in the pure gauge sector. One advantage to use such higher critical beta corresponding to a smaller lattice spacing $a = 0.055$ fm intend to approach the continuum limit of the theory, namely $a \longrightarrow 0$. The continuum limit study will be the focus of the upcoming results.

In the next section, we report on the gluon and the ghost propagators as a function of the momentum and temperatures. We concentrate in fact on the components of the gluon, namely: the transverse D_T and longitudinal D_L propagators. These propagators behave as we will see quite differently showing different responses to the phase transition.

5.3 Results on the gluon and ghost propagators at $T > 0$

5.3.1 The T dependence of the gluon and ghost propagators

We start now discussing our results for the gluon and ghost propagators in the pure gauge sector of *QCD*. Before starting such analysis we should notice an important fact about the behavior of the gluon propagator for large β. In particular, for such high values of the couplings the LANDAU gauge gluon propagator is expected to depend on the $Z(3)$-sectors into which the POLYAKOV loop spatial averages can fall [148]. This observations goes also in parallel with what we noticed on the influence of the POLYAKOV sectors on the gluon propagator, and in particular on its longitudinal part. The results of these systematic effects are shown on Fig. 5.9 and discussed there. Therefore, our strategy goes as follows: First, we determine the POLYAKOV sector to which the produced configuration belongs to, then, if (and only if) the sector measured is not the physical sector [1] one multiply the links $U_{x,4}$ in the time direction with a phase rotation $\exp\{\pm 2\pi i/3\}$ to keep the sector physical. This phase rotation corresponds actually to a $Z(3)$-flip in time direction before the gauge fixing procedure is started. Such global flips are equivalent to non-periodic gauge transformations and do not change the pure gauge action.

As for the observables themselves, namely the gluon and ghost propagators, and as stated before, the gluon propagator might be splittable into two components, namely: the transverse D_T ("chromomagnetic") (transverse to the heat-bath rest frame) and the longitudinal D_L one ("chromoelectric") already defined in Eq. (4.9), Eq. (4.10) on the lattice, respectively, with the zero-momentum propagator values defined in Eq. (4.11). On the other hand, the ghost propagator is defined in Eq. (4.13) in the continuum for $q \neq 0$ and $(k/N)\cdot(x-y) \equiv \sum_\mu k_\mu (x-y)_\mu / N_\mu$. The corresponding form of the ghost propagator on the lattice is described in Eq. (4.13). We recall also that momentum q is already defined in Eq. (4.7).

We show in Fig. 5.4 the multiplicatively renormalized propagators $D_L(q)$ and $D_T(q)$ as functions of the three-momentum ($q \equiv |\vec{q}|,\ q_4 = 0$) for $\beta = 6.337$, obtained with $N_\sigma = 48$ and different N_τ, i.e. for temperature values varying from $T = 0.65\,T_c$ up to $T \simeq 3\,T_c$. For details we refer to the upper section of Table 5.1. The renormalization condition is chosen such that $D_{L,T}$ take their tree level values at the subtraction point $q = \mu$. We choose $\mu = 5$ GeV in order to be close to the perturbative range and still reasonably away from our lattice cutoff ($q_{max} = 2\sqrt{3}/a \simeq 12.4$ GeV). We observe from Fig. 5.4 that the temperature dependence of both D_L and D_T becomes weaker with increasing momentum. This weakening proceeds faster for D_T than for D_L. The ultraviolet regions of D_T and D_L turn out to be "phase-insensitive". This affect the values of the Z-factor which do not really react to the temperatures. This observation was also reported in [50]. More precisely, while the temperature changes from its minimal value to our maximal one, the change of D_T is less than 5% for $q > 2.2$ GeV, while for D_L this is guaranteed for $q > 2.7$ GeV. For $T \lesssim T_c$ D_L shows a comparatively weak temperature dependence also at small momenta. This changes drastically as soon as $T \gtrsim T_c$. In contrast to that $D_T(q)$ changes monotonously with T

[1] This means the phases of the corresponding POLYAKOV loop averages to fall into the interval $(-\pi/3, \pi/3]$

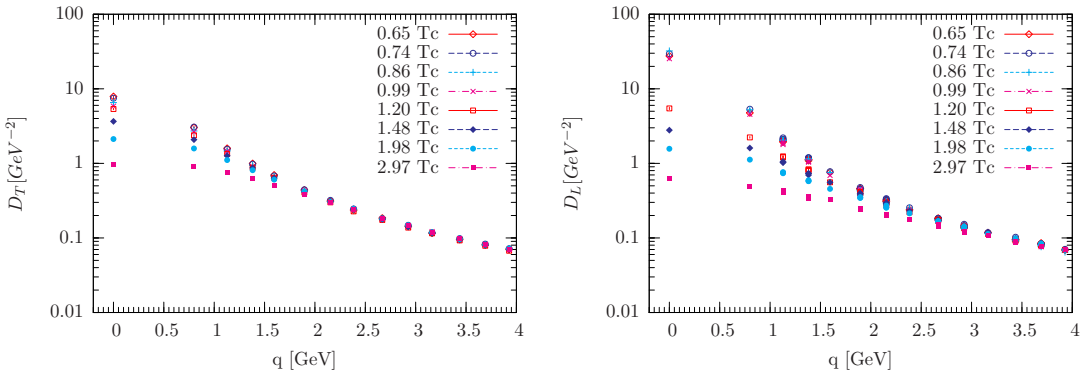

FIGURE 5.4: Temperature dependence of the longitudinal (l.h.s.) and the transverse (r.h.s.) gluon propagator for $\beta = 6.337$ and a spatial lattice size $N_\sigma = 48$.

in the infrared region. This can be seen in more detail from Fig. 5.5. There we show the temperature dependence of $D_L(q)$ (left panel) as well as of $D_T(q)$ (right panel) for six selected momenta in the range up to 1.6 GeV.

One can see that D_L at fixed momentum shows strong variations in the neighborhood of T_c. It is rising with T below T_c and sharply drops around T_c. This behavior looks most pronounced for zero momentum and gets progressively weaker at higher momenta. For the lowest momenta we observe maxima at $T = 0.86\,T_c$. It remains open, whether the maxima are shifted away from the transition temperature with increasing volume. Similar observations have been recently reported [149] for the case of $SU(2)$ gauge theory where the maximum of $D_L(0)$ tend to move away from the transition with decreasing lattice spacing.

In any case, our data confirms that the infrared part of $D_L(p)$ is strongly sensitive to the temperature phase transition [43, 50]. It may serve to construct some kind of order parameters characterizing the onset of the phase transition, as we will propose below. In contrast to that, D_T is ever decreasing and varying smoothly across T_c, showing no visible response to the phase transition at all momenta.

We go on with the investigation of the gluon propagator fitting our data with the so called GRIBOV-STINGL fit formula originally proposed in [26, 150]. This fit formula looks like

$$D(q) = \frac{c\,(1+d\,q^{2n})}{(q^2+r^2)^2+b^2}\,. \tag{5.6}$$

This formula was the subject of previous investigations [151] and recently also in [149]. Our momentum range of interest for the GRIBOV-STINGL interpolation is $[0.6 : 8.0]$ GeV. This range is of a particular interest for the *DSE* where a a working fit function for the gluon propagator is important to be provided. In fact, our fit function with the corresponding fitting parameters play the role of input data for the *DSE*. Moreover, this fit function might be compared to the *DSE*

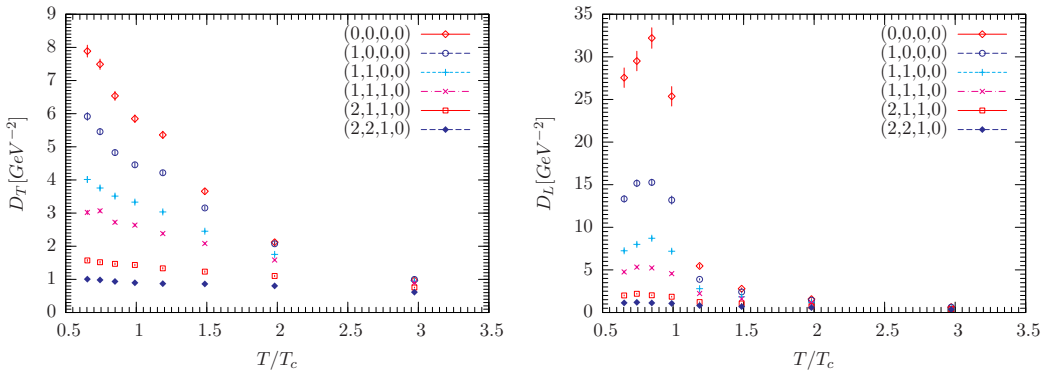

FIGURE 5.5: The longitudinal propagator, D_L, (l.h.s.) and the transverse one, D_T, (r.h.s.) vs. temperature for a few low momenta, the latter represented as (k_1,k_2,k_3,k_4). $\beta = 6.337$ and $N_\sigma = 48$.

Parameters		D_L fits					D_T fits				
T/T_c	N_τ	r^2(GeV^2)	b(GeV^2)	d(GeV^{-2})	c(GeV^2)	χ^2_{df}	r^2(GeV^2)	b(GeV^2)	d(GeV^{-2})	c(GeV^2)	χ^2_{df}
0.65	18	0.372(29)	**0.0**	0.192(8)	4.29(17)	1.49	0.751(24)	**0.0**	0.153(4)	5.40(14)	1.17
0.74	16	0.296(22)	**0.0**	0.206(7)	4.11(13)	1.40	0.756(20)	**0.0**	0.161(3)	5.31(11)	0.99
0.86	14	0.257(22)	**0.0**	0.221(8)	3.70(13)	1.57	0.847(22)	**0.0**	0.152(4)	5.50(12)	1.09
0.99	12	0.359(30)	**0.0**	0.209(10)	3.89(16)	1.83	0.869(26)	**0.0**	0.157(4)	5.45(14)	1.44
1.20	10	1.029(41)	**0.0**	0.155(6)	5.43(21)	1.27	0.951(25)	**0.0**	0.147(4)	5.56(13)	1.17
1.48	8	1.547(47)	**0.0**	0.118(4)	7.12(24)	1.06	0.886(138)	0.810(167)	0.146(11)	5.70(42)	1.46
1.98	6	2.455(75)	**0.0**	0.086(4)	9.55(37)	1.35	0.856(109)	1.398(62)	0.133(8)	6.15(34)	0.93
2.97	4	5.327(159)	**0.0**	0.045(2)	17.15(73)	0.51	0.927(126)	2.559(33)	0.100(6)	7.58(41)	1.01

TABLE 5.2: Results from fits with Eq. (5.6) ($n = 1$) for D_L (l.h.s.) and D_T (r.h.s.) corresponding to the Monte Carlo data shown in Eq. (5.4) ($\beta = 6.337, N_\sigma = 48$). The fit range is $[0.6 : 8.0]$ GeV. The values in parentheses provide the fit errors. The boldface printed b-values indicate that they are fixed to zero.

predictions in order to have a control over the truncations often used to solve these latter.

Expected logarithmic corrections needed for the ultraviolet limit have been neglected here (for a thorough discussion see [113]). We put throughout $n = 1$. In a first attempt we have left b varying. We obtained values compatible with $b = 0$ except for $D_T(q)$ at the highest three temperature values inspected. Therefore, in all other cases we have repeated the fits with fixed $b = 0$ and obtained χ^2_{df}-values reasonably below 2.0. The fit parameters can be found in Table 5.2.[2]

5.3.2 Improving the sensitivity around T_c

Hereafter we perform an original study connected to the sensitivity of the observables around the phase transition. As we have seen in the former section D_L shows a sensitivity when passing

[2]Note that for $b = 0$ Eq. (5.6) is equivalent to the interpolation formula $D(q) = \frac{\gamma}{(q^2+\delta^2)} + \frac{\beta}{(q^2+\delta^2)^2}$.

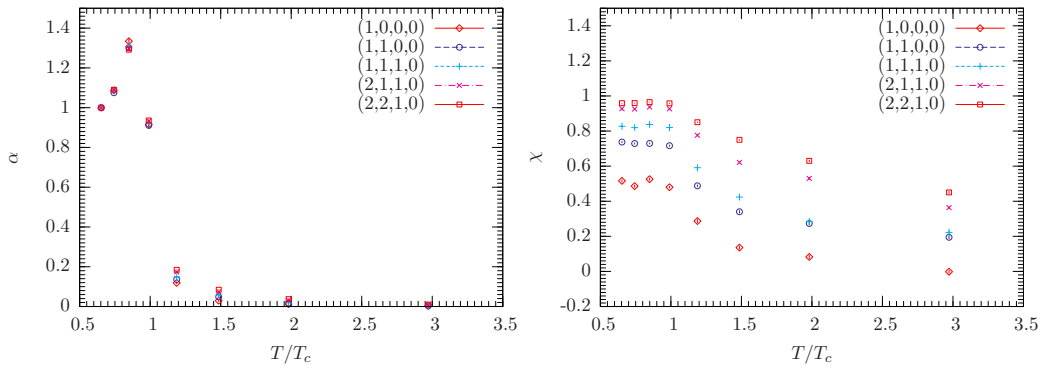

FIGURE 5.6: Temperature behavior of the ratios χ (Eq. (5.7), left panel) and α (Eq. (5.9), right panel) at low momenta as given in the legend, for a spatial lattice size $N_\sigma = 48$ and $\beta = 6.337$.

through the phase transition temperature T_c. This fact motivated us to construct out of D_L additional observables which might strongly react to the phase transition. The original hope was that these observables might be useful for full *QCD* with $N_F = 2$. Nevertheless, the fact that the nature of the phase transitions in the pure gauge *QCD* and the full *QCD* are quite different plays an important role on the efficiency of such 'improved' observables. In fact, it is well know that quenched *QCD* demonstrates a first phase transition while in full *QCD* one expects a crossover.

Still, we have tried to form "observables" constructed from the gluon propagator which can serve as "order parameters" for the deconfinement transition. We tried many functional combinations, and we picked up some of the most interesting for our purposes. First, we plot the ratio

$$\chi = [D_L(0,T) - D_L(q,T)]/D_L(0,T) \tag{5.7}$$

as a function of T/T_c in the left panel of Fig. 5.6.

The first observation is that all the curves labeled by the momentum 4-tuples in the legend show approximate plateau below T_c. Then, passing the phase transition they suddenly fall off with slopes becoming slightly smaller with increasing momentum, but still with visible temperature sensitivity. This means that χ can be used as an indicator for the deconfinement transition[3]. Moreover, the transition can be traced even at rather high momentum. This was not so clear from the lift hand side of Fig. 5.5, where the behavior of D_L at higher momenta looks rather smooth.

A non-trivial consequence from the behavior of χ, at least in the interval $0.65\,T_c < T < T_c$, is a factorization conjecture as

$$D_L(q;T) \simeq A(q) \cdot B(T)\,. \tag{5.8}$$

[3] at least for pure gauge theory.

Then, as long as the temperature T varies in the given interval, the change of D_L can be described by a momentum independent rescaling. This is a rather nontrivial property from which further conclusions can be drawn. For example, in the interpolation formula (Eq. (5.6)) above, we should find the mass parameter r^2 and the parameter d to be (approximately) temperature independent as long as $T < T_c$. This constancy of these parameters is well-established from our fit table (the left panel of Table 5.2).

Another interesting construction we tried along this study is the ratio

$$\alpha = \frac{D_L(0,T) - D_L(q,T)}{D_L(0,T_{min}) - D_L(q,T_{min})}, \quad T_{min} = 0.65\,T_c\,, \tag{5.9}$$

which according to the factorization in Eq. (5.8) should be approximately momentum independent. Indeed, this can be seen from the right panel of Fig. 5.6. Moreover, $\alpha(q,T)$ should resemble qualitatively the temperature dependence of D_L at $q = 0$. Above T_c, however, α falls off reaching very small values at higher temperatures (around $2\,T_c$). Therefore, we conclude that both quantities χ and α behave as indicators for the finite-temperature transition. It remains to be seen, whether they also map out the (pseudo)critical behavior in unquenched *QCD*.

Let us note that our volumes are not large enough to study the infrared asymptotic behavior. Moreover, at the lowest momenta we expect systematic deviations related to finite-size effects, lattice artifacts, and GRIBOV copy effects. This concerns also the parameters χ and α because of their dependence on the value $D_L(q = 0)$. The systematic effects will be discussed in Section 5.3.3, in order to identify the momentum range, where they play only a negligible role, i.e. to define a momentum range free of systematic effects.

Besides the observables α and χ we studied other interesting observables showed in Fig. 5.7. These new quantities are combinations of our D_T and D_L. These quantities exhibit the relative difference between D_T and D_L in a sense to enhance the critical behavior around T_c. We call these two quantities ψ and θ which look like in equations as

$$\psi = 1 - D_T/D_L \tag{5.10}$$

and

$$\theta = (D_L - D_T)/(D_L + D_T) \tag{5.11}$$

From Fig. 5.7 we observe that ψ takes rise below Tc with the temperature reaching some maximum around T_c. This rise of values translate the difference in values between D_T and D_L as one might see in Eq. (5.10). Thus, This difference takes its maximum around T_c showing that D_L is higher than D_T for all momenta. The highest difference occurs in the case of the zero momenta. After such a rise below T_c one observe a dramatic fall down right after T_c and for all momenta. The values of ψ for $T > T_c$ are negative demonstrating that D_T is smaller that D_L in this regime.

Now, concerning the so called ‘asymmetry‘ order parameter in Eq. (5.11). We observe nearly

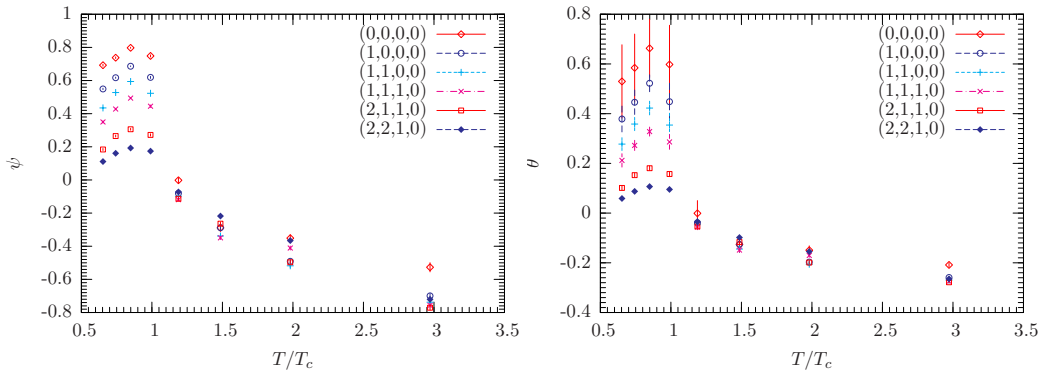

FIGURE 5.7: Additional improved observables reacting to the phase transition. ψ defined as $1 - D_T/D_L$ (l.h.s.) and the so called 'asymmetry' order parameter $\theta = (D_L - D_T)/(D_L + D_T)$ (r.h.s.). All data are obtained at $\beta = 6.337$ on a lattice with spatial size $N_\sigma = 48$.

the same scenario as for ψ. This means, we see a rise for all momenta below T_c and fall down above reaching then negative values. However, all momenta are behaving nearly with the same strength and the errors computed are quite large. Concluding one should say that even if ψ and θ are quite good quantities to determine T_c they take negative values. In other words, the drawback is that these quantities do not take zero values above T_c as an ideal order parameter would do. Therefore, ψ and θ should not be taken as order parameter for pure *QCD*.

To summarize, our gluon propagator results show agreements with findings in other recent investigations [42, 152, 43, 50, 149]. We observed that the strongest response to the phase transition occur in the gluonic chromoelectric sector (the longitudinal propagator) rather than in the gluonic chromomagnetic one (the transverse propagator). Our results are more focused on the mid-range of momenta ($[0.6 : 8.0]$ GeV), namely around 1 GeV, which are interesting for the *DSE* as input data.

Regarding the investigation of the ghost propagator at finite temperature we computed the ghost propagator according to Eq. (4.13), restricting it for simplicity to the diagonal three-momenta and vanishing MATSUBARA frequency, $k_\mu = (k,k,k,0)$ with $k = 1,\ldots,7$. The data are again normalized at $\mu = 5$ GeV, such that the ghost dressing function equals unity at $q = \mu$. The result for the latter function is displayed in Fig. 5.8. In comparison with the gluon propagator we see the ghost propagator to change relatively weakly with the temperature (we are using here the logarithmic scale instead of the linear one as for the gluon results). This is in agreement with the observation in [42]. An increase becomes visible at temperature values $T > 1.4\,T_c$ for the lowest momenta studied (see Fig. 5.8). The relative insensitivity with respect to the temperature is the reason why we will not further consider the ghost propagator in what follows.

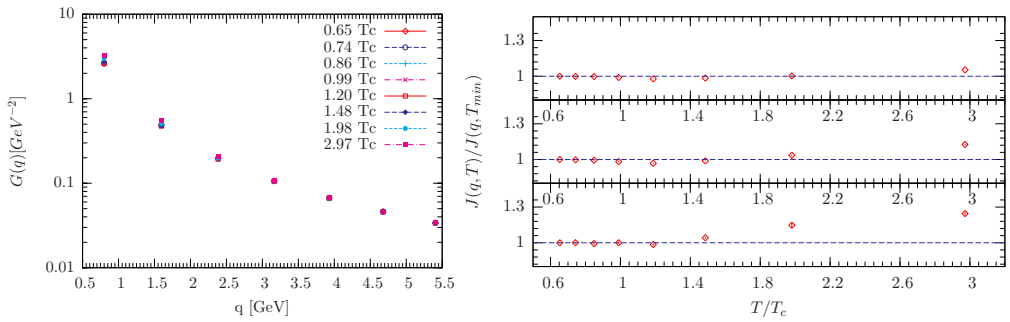

FIGURE 5.8: The momentum dependence of the ghost propagator $G(q)$ in physical units for different temperatures (l.h.s.). The renormalized ghost dressing function $J(q,T)$ for various temperature values (r.h.s.) and its dependence on the temperature shown for the fixed diagonal 3-momenta $((k,k,k,0),k = 1,2,3)$ and normalized with $J(q,T_{min})$ for $T_{min} = 0.65T_c$ (r.h.s.). The lowest panel shows the lowest momentum. All data are obtained at $\beta = 6.337$ on a lattice with spatial size $N_\sigma = 48$.

5.3.3 Study of the systematic effects

Within this section we concentrate on the study of the systematic effects exclusively on the gluon propagator. We start investigating the role of the POLYAKOV sector choice on the values of the components of the gluon propagators, namely: D_T and D_L. Remember, we have already discussed this point at the beginning of Section 5.3.1. We said in brief that this POLYAKOV sector dependence holds for higher couplings. In fact, this original study motivated us to concentrate only on the physical sector of the POLYAKOV loops. Next, we move to a systematic study of the finite volume effects above and below T_c. Lastly, the GRIBOV problem is explored on the lattice giving more insight into the problematic of the choice of gauge copies for the momenta range $[0.6 : 8.0]$ GeV.

5.3.4 The POLYAKOV sector effects

The POLYAKOV loop, as discussed before, represents one of the most important observables in *QCD* at finite temperature. The POLYAKOV loop is defined by Eq. (4.1) as the trace of the ordered product of gauge link variables in time direction. As the POLYAKOV loop (at each spatial) point is a translational invariant quantity one needs also to average it over space indices as defined in Eq. (5.4). This latter complex number quantity might be written for each configuration as

$$L = \mathfrak{Re}(L) + i\,\mathfrak{Im}(L) \tag{5.12}$$

with the phase $\phi = \frac{\mathfrak{Im}(L)}{\mathfrak{Re}(L)}$. Therefore, each gauge configuration map uniquely to some value of ϕ. The POLYAKOV values displayed in the complex plane lie in one of three sectors delimited

by the center elements of the $SU(3)$ group. The physical sector is defined only for phases ϕ satisfying

$$-\pi/3 < \phi < \pi/3. \tag{5.13}$$

The other sectors, namely the second and the third one are considered unphysical. What we did in this work was to compare the effect on the gluon propagator on configurations lying to different POLYAKOV sectors. Here in Fig. 5.9 we compare two sectors, namely the physical sector to the second sector (with $\pi/3 < \phi < \pi$). We use in this case data at T_c with $n_\sigma = 48$. Moreover, the data are presented in physical units. We observe on the right hand side the dramatic change in values for D_L for momenta below 1.8 GeV. This change rises while moving to lower momenta. On the contrary, D_T looks not so effected by the POLYAKOV sector change for all momenta. The strong jump in values for D_L might be explained by the fact that D_L is a function of the temporal gauge links U_4 as well as the POLYAKOV loop itself. Therefore, any jump from sector to another one might affect the values of D_L as it is the case for POLYAKOV loop.

We conclude that the role of the choice of POLYAKOV loop sector is important to get reasonable propagator data. We have seen that the most dramatic reaction happens to the longitudinal propagator D_L, and D_T seems not to be sensible. Still, it is not clear that such difference might also happen in the (de)confined phase of *QCD* especially in the continuum limit, i.e. higher β. This should be an interesting topic to be investigated in the future.

Therefore, we decided for data production always to stick to the physical sector of the POLYAKOV loop. That is, we took in consideration only configurations lying in the physical sector. In practice, after producing configurations randomly according to the Monte-Carlo process we evaluated each corresponding POLYAKOV loop sector. In case the sector is not physical we apply an appropriate rotation $exp(i\theta)$ to the gauge links to come back to the physical sector. Therefore, in our pure gauge investigations we computed our gluon propagators only on configurations in the physical sector[4].

5.3.5 Finite volume effects

In order to assess finite-volume effects is to compare the data shown before in Fig. 5.4 with the ones obtained on even larger spatial volumes while keeping fixed the coupling (at $\beta = 6.337$) and two temperature values, $T = 0.86\,T_c$ (confinement) and $T = 1.2\,T_c$ (deconfinement), respectively. Within this study the linear spatial extent varies from $48a = 2.64$ fm to $64a = 3.52$ fm (see also the middle section in Table 5.1).

In Fig. 5.10 and Fig. 5.11 we show the corresponding plots for D_L and D_T, respectively. In all four cases we observe the effects to be small for momenta above 0.6 GeV.[5] For lower momenta,

[4] This is possible because $Z(3)$ is still a global symmetry of the pure gauge action. This is not anymore the case in the fermionic case.

[5] Below T_c the transverse propagator changes by less than 12 %, the longitudinal one by less than 5 %. Above T_c the transverse propagator varies by less than 8 % and the longitudinal one by less than 11 %.

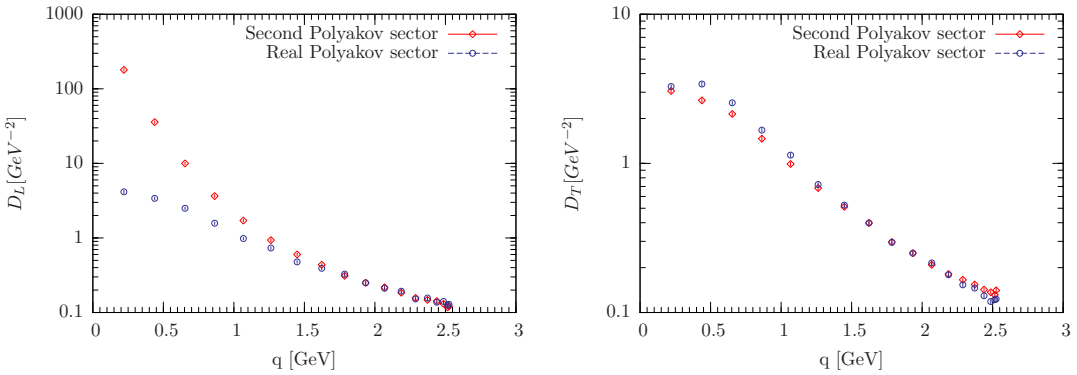

FIGURE 5.9: Comparative study of behavior of D_L (l.h.s.) and D_T (r.h.s.) in physical units evaluated on the physical (real) and the second POLYAKOV sectors. These data correspond to critical temperature T_c.

especially at zero momentum, systematic deviations become more visible. With increasing volume the infrared values of D_L seem to rise, whereas for D_T the opposite is the case. This behavior has already been reported for pure gauge theories in [41, 44] for $SU(2)$ and in [50] for $SU(3)$, respectively.

5.3.6 The GRIBOV ambiguity investigated

The present study of the GRIBOV copies was designed to determine the effect of the choice of the gauge copies to compute gauge-dependent quantities as the gluon propagators. To study GRIBOV copy effects we compare "first", i.e. randomly occurring copies (*fc*) with "best" copies (*bc*) [6]. The copies in question were produced as follows:

we searched for copies within all $3^3 = 27$ $Z(3)$ sectors characterized by the phase of the spatial POLYAKOV loops, i.e. POLYAKOV loops in one of the three spatial directions. For this purpose the $Z(3)$ flipping operations [34, 50] were carried out on all link variables $U_{x,i}$ ($i = 1,2,3$) attached and orthogonal to a 3D hyperplane with fixed x_i by multiplying them with $\exp\{\pm 2\pi i/3\}$. Such global flips are equivalent to non-periodic gauge transformations and do not change the pure gauge action. For the 4th direction, we stick to the sector with $|arg\ P| < \pi/3$ which provides maximal values of the functional Eq. (3.28) at the β-values considered in this section [50]. Thus, the flip operations combine for each lattice field configuration the 27 distinct gauge orbits of strictly periodic gauge transformations into one larger gauge orbit.

The number of copies actually considered in each of the 27 sectors depends on the rate of convergence (with increasing number of investigated copies) of the propagator values assigned to the best copy, in particular at zero momentum. From our experience with $SU(3)$ theory [50]

[6] This strategy is called sometimes in the literature the *fc-bc* method

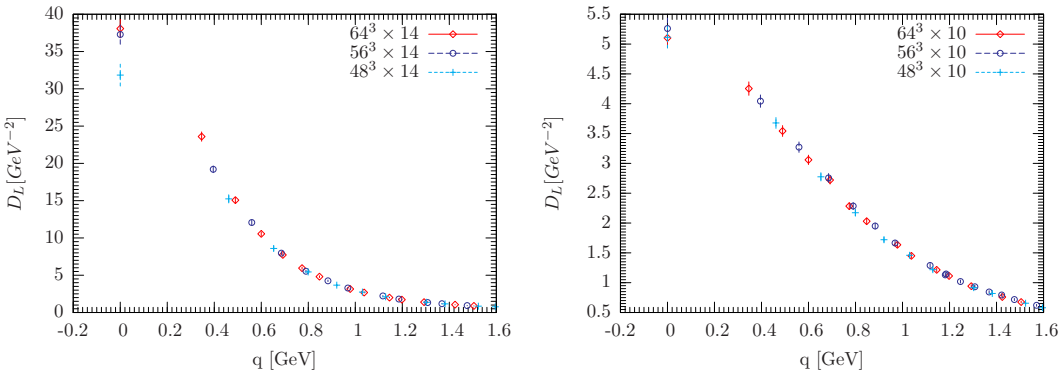

FIGURE 5.10: Finite-size effect study for D_L at $\beta = 6.337$. l.h.s.: $T = 0.86\,T_c$, r.h.s.: $T = 1.20\,T_c$.

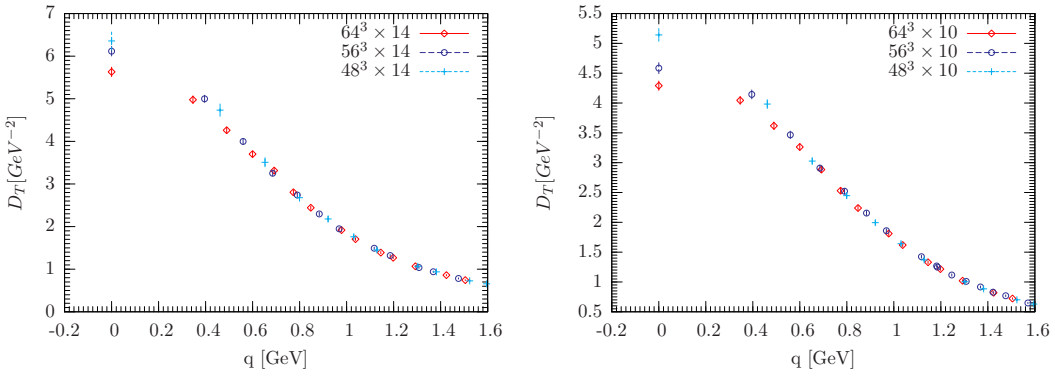

FIGURE 5.11: Same as in Fig. 5.10 but for D_T.

we expect that the effect of considering gauge copies in different flip-sectors is more important than probing additional gauge copies in each sector. For this reason and to save CPU time we have considered one gauge copy for every $Z(3)$-sector; therefore, in total $n_{copy} = 27$ gauge copies for every configuration.

To each copy the simulated annealing algorithm with consecutive over-relaxation was applied in order to fix the gauge. We take the copy with maximal value of the functional Eq. (3.28) as our best realization of the global maximum and denote it as "*bc*".

The parameters of the SA algorithm in the study of GRIBOV copies were slightly different from those described above in Section 5.1.3. 2000 SA combined simulation sweeps with a ratio 11:1 between micro-canonical and heat bath sweeps were applied starting with $T_{sa} = 0.5$ and ending at $T_{sa} = 0.0033$.

Since this procedure is quite CPU time consuming we restricted this investigation to coarser

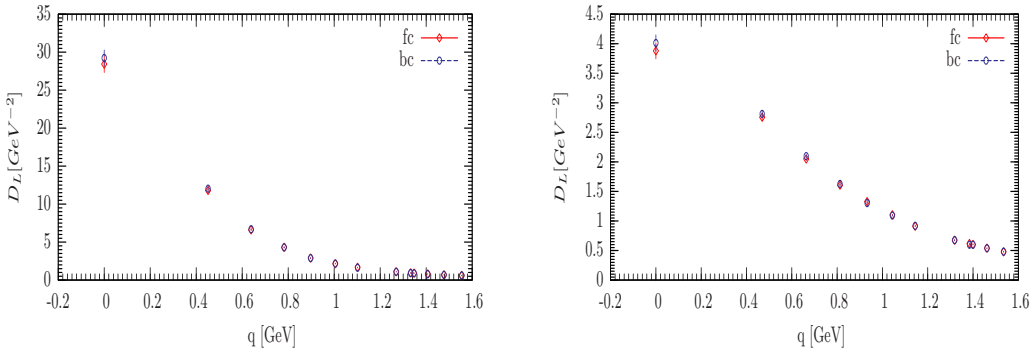

FIGURE 5.12: Comparison of the *bc* with the *fc* GRIBOV copy result for the longitudinal propagator D_L (unrenormalized) (l.h.s.: $T = 0.86\,T_c$, r.h.s.: $T = 1.20\,T_c$).

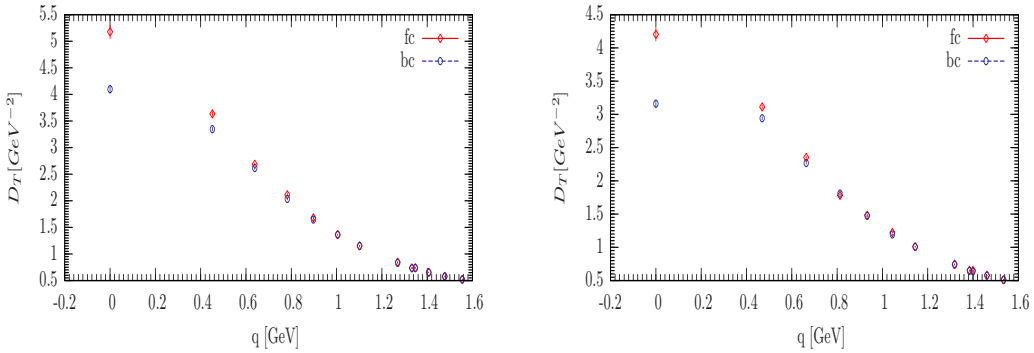

FIGURE 5.13: Same as in Fig. 5.12 but for the transverse propagator D_T (l.h.s.: $T = 0.86\,T_c$, r.h.s.: $T = 1.20\,T_c$).

lattices 6×28^3 and 8×28^3 with larger lattice spacing keeping fixed the temperature to both values $T = 0.86\,T_c$ and $T = 1.20\,T_c$, respectively. Moreover, the physical 3D volume $(2.64\,\mathrm{fm})^3$ were also approximately fixed.

In Fig. 5.12 and Fig. 5.13 we compare *bc* with *fc* results for the gluon propagator components D_L and D_T, respectively. As one can see, D_L is almost insensitive to the choice of GRIBOV copies (at least, for the comparatively small values of N_τ we consider). This observation has been already reported in [44] for the $SU(2)$ case and in [50] for the $SU(3)$ case. On the contrary, the transverse propagator is strongly affected in the infrared region. This behavior is independent of the temperature. Moreover, we see that the transverse gluon propagator values in the infrared become lowered for *bc* compared with *fc* results. These observations resemble those made already in [44] and [50]. To complement our results we have also studied the ratios $D_L(fc)/D_L(bc)$ and $D_T(fc)/D_T(bc)$. The result is shown in Fig. 5.14. We observe that for D_L ratios fall down very

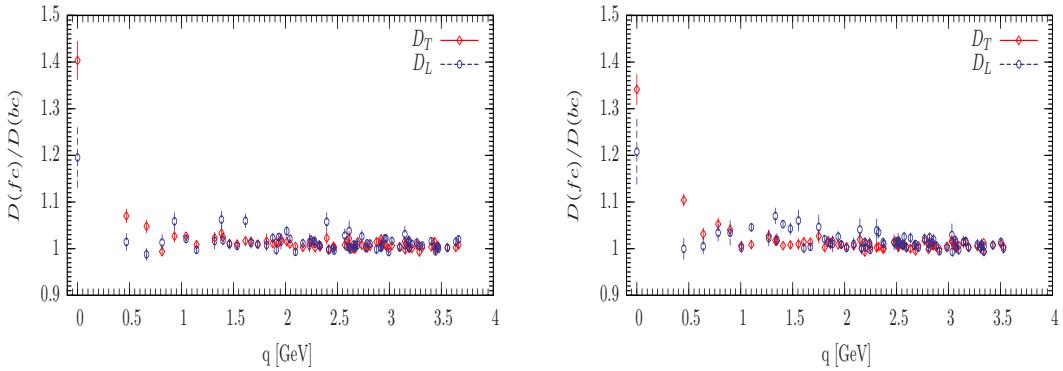

FIGURE 5.14: The ratios $D_L(fc)/D_L(bc)$ and $D_T(fc)/D_T(bc)$ as a function of the physical momenta $q[GeV]$. These data were produced for $\beta = 5.994$ and (n_σ,n_τ)=(28,6). These data correspond to the temperatures $1.20\,T_c$ (r.h.s.) and $0.86\,T_c$ (l.h.s.).

quickly for non-zero momenta. This behavior is the same for the deconfined ($1.20\,T_c$) and the confined ($0.86\,T_c$) phases. These effects are getting smaller with higher momenta. Therefore, except for the zero momenta where we see a deviation of 20 % in the ratio higher momenta might be neglected. Regarding D_T ratios one sees that deviations in ratios reach 40 % in deconfined phase and 35 % in the confined one. However, we observe that above T_c points are not joining the horizontal unity line as fast as the D_L case. That is, D_T is a bit more affected by GRIBOV effects for the low momenta. Still, we point out that a roughly stable behavior with small fluctuations is reached for $p > 800\ MeV$. This looks to be the case for the deconfined and the confined phase as well.

The main conclusion of this section is that GRIBOV copy effects may be neglected for all nonzero momenta in the case of the longitudinal propagator (at least, for comparatively small values of N_τ), and for momenta above 800 MeV in the case of the transverse propagator. The momentum range where the last statement is true might depend on the temperature.

5.3.7 Scaling effects study and the continuum limit

Throughout the present section we show results of the gluon propagator regarding scaling properties and the continuum limit in pure gauge theory. Our strategy is to perform this systematic study moving to smaller values of the lattice spacing keeping the values of other parameters fixed, i.e. studying the gluon propagator following the limit: $\lim_{a\to 0}\lim_{V_{\rm phys}=\rm fixed}\lim_{T=\rm fixed}$. This order of limits is crucial and must not be inverted. Hence, we exploited in this investigation data already presented in Section 5.3.5 at the two fixed temperatures $0.86\,T_c$ and $1.20\,T_c$, and also fixed physical volume to $(2.7\ \text{fm})^3$.

Therefore, in order to check the scaling properties we have used the same reference values for the temperature below and above T_c as discussed before (i.e., $0.86\,T_c$ and $1.20\,T_c$). We kept

Parameters				Z-factors	
T/T_c	β	N_σ	N_τ	$\tilde{Z}_T$	$\tilde{Z}_L$
0.86	5.972	28	8	1.43	1.43
0.86	6.230	42	12	1.45	1.47
0.86	6.337	48	14	1.48	1.53
0.86	6.440	56	16	1.64	1.66
1.20	5.994	28	6	1.46	1.46
1.20	6.180	38	8	1.52	1.52
1.20	6.337	48	10	1.62	1.63
1.20	6.490	58	12	1.62	1.65

D_L fits			
$r^2(\mathrm{GeV}^2)$	$d(\mathrm{GeV}^{-2})$	$c(\mathrm{GeV}^2)$	χ^2_{df}
0.317(20)	0.138(24)	4.67(26)	0.30
0.254(9)	0.224(7)	3.90(8)	0.44
0.262(12)	0.224(11)	3.80(12)	0.42
0.256(7)	0.220(6)	3.86(7)	0.24
0.995(37)	0.153(10)	5.46(24)	0.80
0.985(20)	0.163(6)	5.34(13)	0.28
0.960(19)	0.180(7)	4.96(13)	0.22
1.018(18)	0.162(5)	5.27(11)	0.06

D_T fits			
$r^2(\mathrm{GeV}^2)$	$d(\mathrm{GeV}^{-2})$	$c(\mathrm{GeV}^2)$	χ^2_{df}
0.810(23)	0.148(7)	5.49(17)	1.19
0.835(16)	0.151(5)	5.69(12)	0.52
0.867(18)	0.142(6)	5.62(14)	0.14
0.880(15)	0.143(4)	5.65(11)	0.36
0.894(26)	0.144(7)	5.55(18)	1.10
0.924(22)	0.142(6)	5.71(16)	0.57
0.982(27)	0.133(8)	5.87(21)	0.59
0.963(19)	0.140(5)	5.77(13)	0.45

TABLE 5.3: **Left panel:** Renormalization factors $\tilde{Z}_{T,L}$ of the renormalized propagators $D_{T,L}(q,\mu)$ according to Eq. (5.14). The renormalization point is $\mu = 5\,\mathrm{GeV}$. **Right panels:** Fit parameters and χ^2_{df} for fits of D_L (l.h.s.) and D_T (r.h.s.) using the generic fit function $D(q^2)$ acc. to Eq. (5.6), but with $b = 0$.The fit range is restricted to $[0.6 : 3.0]$ GeV. The fit errors are indicated in parentheses.

also the spatial volume fixed at $(2.7\ \mathrm{fm})^3$, and compared the renormalized propagators at four different values for the lattice spacing $a(\beta)$ (see Table 5.1). Our results are displayed for the momentum range up to 1.5 GeV in Fig. 5.15 for D_L and in Fig. 5.16 for D_T, respectively. Gauge fixing has been carried out as originally described in Section 5.1.3.

We provide the renormalization factors for

$$D_{L,T}(q,\mu) \equiv \tilde{Z}_{L,T}(a,\mu)\, D^{bare}_{L,T}(q,a) \tag{5.14}$$

in the left panel of Table 5.3. As expected the Z-factors of D_L and D_T approximately agree.

From Fig. 5.15 and Fig. 5.16 we see that the scaling violations happen to be reasonably small for momenta above 0.8 GeV. This shows that our choice of $a = 0.055$ fm for $\beta = 6.337$ was already close to the continuum limit.

To determine the a-dependence at five particular physical momenta p we need interpolations of the momentum dependence in between the data points. For the fit within the interval $0.6\,\mathrm{GeV} \leq q \leq 3.0\,\mathrm{GeV}$ we have used again Eq. (5.6) with parameter b fixed to zero. The values of the fit parameters are displayed in the right hand panels of Table 5.3. In all cases we find χ^2-values per degree of freedom around or below unity.

The propagators, interpolated to the set of selected momentum values, are shown in Fig. 5.17 for D_L and in Fig. 5.18 for D_T, respectively, as functions of the lattice spacing a. We show them together with the respective fit curves

$$D(a;p) = D_0 + B \cdot a^2 \tag{5.15}$$

assuming only $O(a^2)$ lattice artifacts. The corresponding fit results are collected in Table 5.4. The respective fit parameters D_0 represent the continuum limit values of the propagators at the preselected momenta.

Our lattice propagator data obtained for $\beta = 6.337$ as discussed in Section 5.3.1 can now be

Parameters		D_L fits		D_T fits	
T/T_c	$p(GeV)$	B	$D_0(GeV^{-2})$	B	$D_0(GeV^{-2})$
0.86	0.70	-1.3(28.1)	7.68(16)	32.3(20.0)	3.20(11)
0.86	0.85	13.5(14.5)	4.63(8)	19.5(14.0)	2.42(8)
0.86	1.00	12.3(7.9)	2.95(4)	11.7(9.8)	1.83(5)
0.86	1.20	7.0(4.1)	1.75(2)	5.9(6.4)	1.27(4)
0.86	1.40	3.0(2.6)	1.12(1)	3.2(4.4)	0.90(2)
1.20	0.70	23.1(9.3)	2.48(5)	30.7(11.0)	2.84(6)
1.20	0.85	15.8(6.5)	1.93(4)	18.5(7.4)	2.19(4)
1.20	1.00	11.8(4.7)	1.49(2)	10.8(4.8)	1.68(2)
1.20	1.20	7.4(3.3)	1.07(2)	5.3(3.0)	1.19(2)
1.20	1.40	4.8(2.2)	0.77(1)	2.4(1.8)	0.86(1)

TABLE 5.4: Results of the fits for D_L (l.h.s.) and D_T (r.h.s.) as a function of the lattice spacing a using the fit function $D(a;p)$ acc. to Eq. (5.15). The errors of the fit parameters are given in parentheses. χ^2_{df} in all cases is close or well below unity. See also Fig. 5.17 and Fig. 5.18.

compared with the values extrapolated to the continuum limit. This is shown in Fig. 5.19. In more detail, we can compare the continuum extrapolated values at some lower momentum – say at $q = 0.70\,\mathrm{GeV}$ – with those obtained from $a(\beta = 6.337) = 0.055\,\mathrm{fm}$ and interpolated to the same momentum. Then we find deviations being smaller than 4 %. Thus, we are really justified to say that the results obtained for $\beta = 6.337$ in the given momentum range are already very close to the continuum limit.

Additionally, the continuum limit extrapolated propagators can be easily fitted with Eq. (5.6). The results are shown in Fig. 5.20.

We conclude that for the higher β-values and the momentum range considered in this thesis we are close to the continuum limit. Moreover, systematic effects as there are finite-volume and GRIBOV copy effects seem to be negligible for momenta above 0.8 GeV.

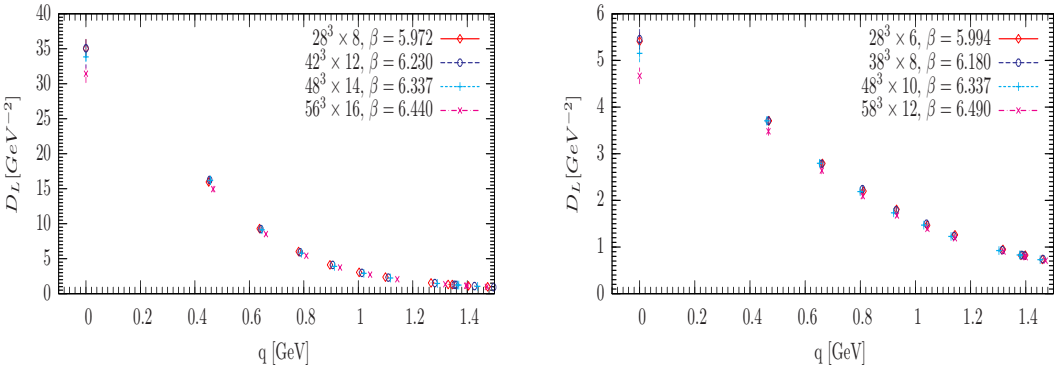

FIGURE 5.15: The longitudinal propagator D_L, renormalized at $\mu = 5$ GeV, obtained for fixed physical volume and temperature but varying $a = a(\beta)$. l.h.s.: $T = 0.86\,T_c$, r.h.s.: $T = 1.20\,T_c$.

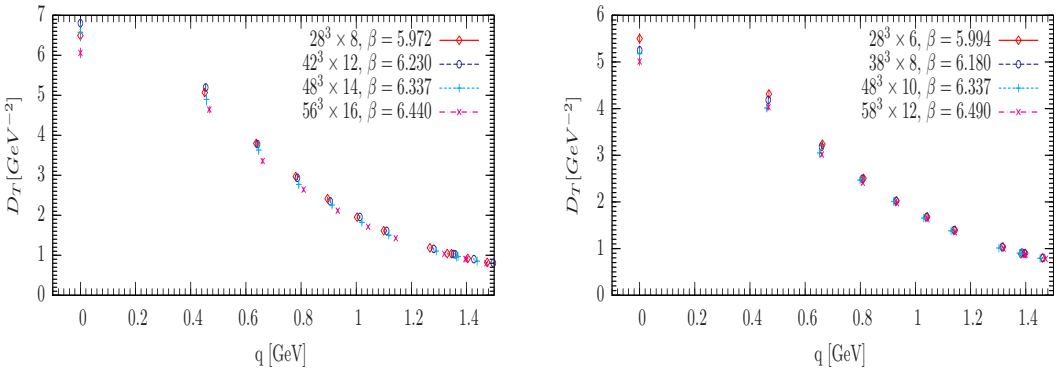

FIGURE 5.16: Same as in Fig. 5.15 but for the transverse propagator D_T. l.h.s.: $T = 0.86\,T_c$, r.h.s.: $T = 1.20\,T_c$

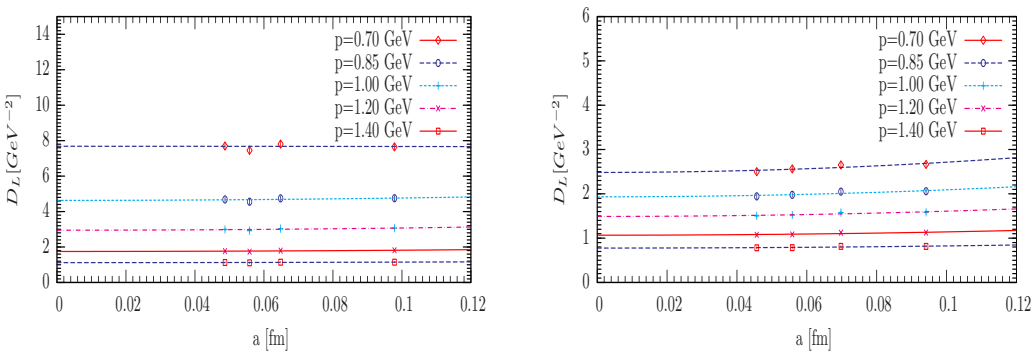

FIGURE 5.17: D_L vs. lattice spacing a for a set of different preselected momenta p. l.h.s. $T = 0.86\ T_c$; r.h.s. $T = 1.20\ T_c$.

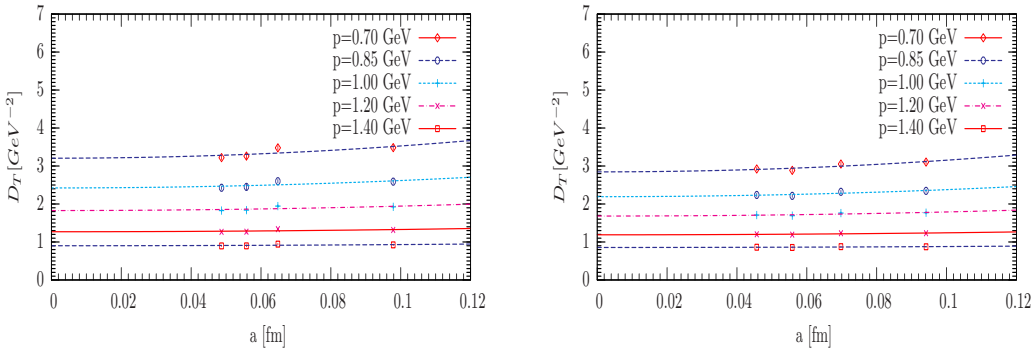

FIGURE 5.18: Same as in Fig. 5.17 but for D_T. l.h.s. $T = 0.86\ T_c$; r.h.s. $T = 1.20\ T_c$.

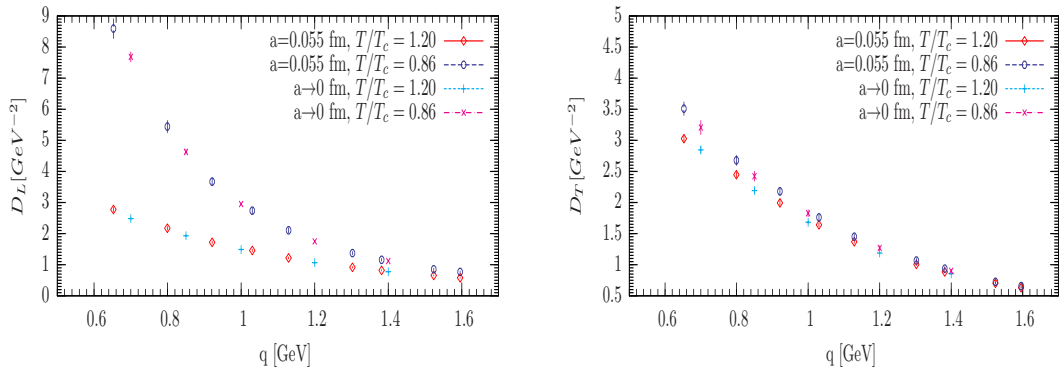

FIGURE 5.19: Comparison of the renormalized propagators $D_L(q)$ (l.h.s.) and $D_T(q)$ (r.h.s.) obtained from the Monte Carlo simulation at $\beta = 6.337$ with some continuum limit extrapolated values.

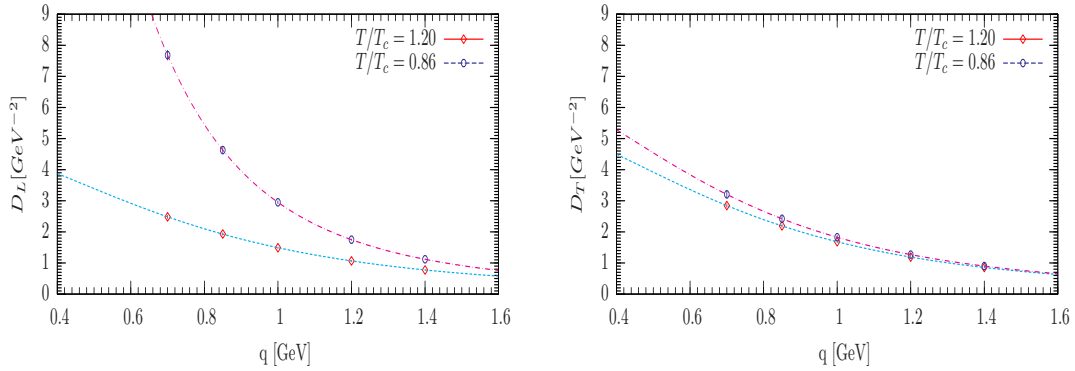

FIGURE 5.20: Continuum extrapolated values of $D_L(q)$ (l.h.s.) and $D_T(q)$ (r.h.s.) together with their respective interpolation curves for two temperature values.

CHAPTER 6

Results for full *QCD*

We investigate the temperature behavior of the LANDAU gauge gluon and ghost propagators in the *QCD* sector of two flavors ($N_F = 2$) maximally twisted mass fermions. We focus on the set of pion masses, $300\ MeV << m_\pi << 500\ MeV$ reaching the smallest lattice spacing of around $0.06\ fm$. We study the dependence of the gluon propagator as a function of the temperature. We show that at lower momenta the gluon propagator behaves smoothly in the crossover region. Still, the longitudinal component D_L seems to react stronger as the transversal part D_T specially for zero momenta. The ghost propagator on the other hand demonstrates only a very weak temperature dependence. A good parametrization to our gluon data was also undertaken thanks to the GRIBOV-STINGL formula for the momenta range $[0.4, 3.0]$ GeV. In fact, this latter range is important for *DSE* whose different solutions deviate from each other around 1 GeV. In general, our data may serve as input for general continuum functional methods. During our present work we relied on the thermalized configurations provided by the tmfT collaboration. These configurations were generated on a four-dimensional lattice of spatial size of $N_\sigma = 32$ and a temporal one of $N_\tau = 12$. Here, one considers *QCD* with a mass-degenerate doublet of twisted mass fermions, cf. the review by [121]. The corresponding gauge action is a combination of a tree-level SYMANZIK improved gauge action and the twisted-mass action for the fermionic part. We refer to Chap. 3 for a precise description of such actions. Our results are presented in [52].

.

6.1 Lattice setting and parameters

As already said, we consider the four-dimensional periodic lattice of spatial size of $N_\sigma = 32$ and a temporal one of $N_\tau = 12$. Configurations were thermalized and provided to us by the tmfT collaboration. We had the task to gauge fix the configuration to the LANDAU gauge using simulated annealing followed by over-relaxation as we did for the pure gauge case. The configurations are

provided at the maximal twist by tunning the hopping parameter to its critical value k_c. Therefore, at maximal twist we get an automatic a-improved fermion formulation [121]. Our hopping parameters of interest are based on the values of β provided by the European Twisted Mass Collaboration (*ETMC*) [122]. Furthermore, k_c for intermediate lattice spacing $a(\beta)$ values were obtained thanks to interpolations as practized in [123].

As usual at finite temperature *QCD*, the imaginary-time extent corresponds to the inverse temperature $T^{-1} = N_\tau a$. To be able to set the physical scale for each β we interpolated the data provided by the *ETMC* collaboration [122] at the β values of 3.90, 4.05, 4.2. This allowed us to map each β value to some lattice spacing a in FERMI for example, and so to be able to construct the momenta and the propagators in physical units. We are reaching during the present investigations lattice spacings $a < 0.09\,fm$. The values of our parameters were already investigated thanks to the chiral condensate and the Polyakov loop and as well as their susceptibilities within the tmfT collaboration [153, 154, 123, 124], and a very smooth behavior was found. Furthermore, one observes signals for a a breakdown of chiral symmetry and a deconfinement transition at slightly different temperatures $T_c = T_\chi$ and $T_{\rm deconf}$, respectively, in agreement with the observation reported in [108].

Our runs parameters are listed on Table 6.1. In this table we show the β values together with the corresponding lattice spacings, the temperature and the independent number of configurations for the three sets of pion masses.

In order to reduce systematic hyper-cubic momentum selection effects, we have applied for most of our computations the so-called cylinder cut [113]. Therefore, we took in considerations only diagonal and first off-diagonal momenta for the gluon propagator and strictly diagonal momenta for the ghost momenta. Moreover, only modes with zero MATSUBARA frequencies are studied, i. e. $k_4 = 0$.

Now, according to refs. [123, 124], we display in Table 6.2 the (pseudo-) critical couplings β_c and the corresponding temperatures T_χ and $T_{\rm deconf}$ for the three pion mass values as obtained from fits around the respective maxima of the chiral susceptibility $\sigma^2_{\bar\psi\psi}$ and from the behavior of the (renormalized) Polyakov loop $\langle \mathfrak{Re}(L)\rangle_R$, respectively

6.2 Results on the gluon and ghost propagators

6.2.1 Fitting the bare gluon and ghost propagators

The temperatures of interest in this work correspond to the temperatures range covering temperatures where the chiral restoration and deconfinement are expected to happen. These two letter phenomena occur at two different temperatures denoted respectively by T_χ and $T_{\rm deconf}$. However, the values of these temperatures within the lattice community are still under discussion. As an example, for *QCD* with 2+1 flavors authors in [155] show a temperature separation of about $20-30\,$MeV between the deconfining and the chiral transition temperatures. This latter result conflicts with data provided by others [156] who claim both temperatures to coincide.

m_π [MeV]	β	a [fm]	T [MeV]	r_0/a	$r_0 \cdot T$	n_{conf}	κ_c	$a \cdot \mu_0$	$\tilde{Z}_T$	$\tilde{Z}_L$	$\tilde{Z}_J$
316(16)	3.8400	$8.77(47)\cdot10^{-2}$	187	4.81	0.40	293	0.162731	0.00391	0.6380(80)	0.6264(108)	0.66862(32)
316(16)	3.8800	$8.25(22)\cdot10^{-2}$	199	5.17	0.43	299	0.161457	0.00360	0.6208(34)	0.6139(50)	0.66939(10)
316(16)	3.9300	$7.65(13)\cdot10^{-2}$	215	5.63	0.47	255	0.159998	0.00346	0.6117(70)	0.6116(103)	0.67264(14)
316(16)	3.9525	$7.39(12)\cdot10^{-2}$	222	5.84	0.49	273	0.159385	0.00335	0.6156(59)	0.6122(84)	0.67252(15)
316(16)	3.9600	$7.31(12)\cdot10^{-2}$	225	5.91	0.49	151	0.159187	0.00331	0.6151(71)	0.6101(102)	—
316(16)	3.9675	$7.22(11)\cdot10^{-2}$	228	5.98	0.50	250	0.158991	0.00328	0.6120(63)	0.6079(114)	0.67388(14)
316(16)	3.9750	$7.14(11)\cdot10^{-2}$	230	6.05	0.50	113	0.158798	0.00325	0.6146(77)	0.5982(126)	—
316(16)	3.9900	$6.98(11)\cdot10^{-2}$	235	6.19	0.52	290	0.158421	0.00319	0.6092(71)	0.6118(97)	0.67536(14)
398(16)	3.8600	$8.51(32)\cdot10^{-2}$	193	4.99	0.42	159	0.162081	0.00617	0.6191(64)	0.6147(98)	0.66730(21)
398(16)	3.8800	$8.25(22)\cdot10^{-2}$	199	5.17	0.43	173	0.161457	0.00600	0.6202(54)	0.6192(76)	—
398(16)	3.9300	$7.65(13)\cdot10^{-2}$	215	5.63	0.47	209	0.159998	0.00561	0.6076(59)	0.6080(84)	0.67005(23)
398(16)	3.9700	$7.20(11)\cdot10^{-2}$	228	6.00	0.50	198	0.158927	0.00531	0.6087(59)	0.6119(89)	—
398(20)	3.9900	$6.98(11)\cdot10^{-2}$	236	6.19	0.52	156	0.158421	0.00517	0.6075(139)	0.6090(231)	0.67293(13)
398(16)	4.0050	$6.82(10)\cdot10^{-2}$	241	6.34	0.53	150	0.158053	0.00506	0.6156(87)	0.6112(115)	0.6784(60)
398(20)	4.0175	$6.69(10)\cdot10^{-2}$	246	6.46	0.54	271	0.157755	0.00498	0.6036(78)	0.6063(101)	0.67504(16)
398(20)	4.0250	$6.62(10)\cdot10^{-2}$	248	6.53	0.54	226	0.157579	0.00493	0.6001(64)	0.6005(94)	0.67517(11)
398(20)	4.0400	$6.47(10)\cdot10^{-2}$	254	6.68	0.56	113	0.157235	0.00483	0.6029(119)	0.6167(178)	0.67519(26)
469(24)	3.9500	$7.42(12)\cdot10^{-2}$	222	5.81	0.48	146	0.159452	0.00779	0.6121(55)	0.6020(82)	0.67142(16)
469(24)	3.9700	$7.20(11)\cdot10^{-2}$	228	6.00	0.50	348	0.158926	0.00752	0.6116(80)	0.6024(110)	0.67128(14)
469(24)	3.9900	$6.98(11)\cdot10^{-2}$	235	6.19	0.52	120	0.158421	0.00738	0.6098(70)	0.6041(102)	0.67271(22)
469(24)	4.0100	$6.77(10)\cdot10^{-2}$	243	6.39	0.53	210	0.157933	0.00718	0.6086(54)	0.6093(73)	0.67322(12)
469(24)	4.0200	$6.67(10)\cdot10^{-2}$	247	6.48	0.54	250	0.157696	0.00708	0.5947(54)	0.5927(77)	0.67147(14)
469(24)	4.0300	$6.57(10)\cdot10^{-2}$	250	6.58	0.55	256	0.157463	0.00699	0.6013(72)	0.6017(101)	0.67388(14)
469(24)	4.0400	$6.47(10)\cdot10^{-2}$	254	6.68	0.56	152	0.157235	0.00689	0.6033(80)	0.6028(121)	0.67353(16)
469(24)	4.0500	$6.38(10)\cdot10^{-2}$	258	6.78	0.56	150	0.157010	0.00680	0.5971(62)	0.6072(91)	0.67485(17)
469(24)	4.0700	$6.19(12)\cdot10^{-2}$	266	6.98	0.58	200	0.156573	0.00662	0.5972(143)	0.6119(195)	0.67829(32)

TABLE 6.1: The pion masses, the values of the inverse bare coupling β, the lattice spacing a in fm, the temperature T in MeV, the chirally extrapolated Sommer scale r_0 [147] in lattice units and $r_0\ T$, and the number n_{conf} of configurations are shown for the ensembles. The spatial $N_\sigma = 32$ and temporal $N_\tau = 12$ extents are the same for all ensembles. The number n_{copy} of gauge copies is fixed to 1. In the middle subtable the critical hopping parameter κ_c and the bare twisted mass $a\mu_0$ (in units of the lattice spacing) are also shown. The renormalization factors for the transverse and longitudinal gluon as well as for the ghost dressing function obtained for the renormalization scale $\mu = 2.5$ GeV are given in the rightmost subtable, denoted as $\tilde{Z}_T$, $\tilde{Z}_L$ and $\tilde{Z}_J$, respectively.

Label	A12	B12	C12
m_π[MeV]	316(16)	398(20)	469(24)
β_c from $\sigma^2_{\bar{\psi}\psi}$	3.89(3)	3.93(2)	3.97(3)
T_χ[MeV]	202(7)	217(5)	229(5)
β_c from $\langle \mathfrak{Re}(L) \rangle_R$	-	4.027(14)	4.050(15)
T_{deconf}[MeV]	-	249(5)	258(5)

TABLE 6.2: Extracted (pseudo-) critical couplings β_c and corresponding temperatures for the ensembles A12, B12, and C12 (see revised version of [123]) corresponding to three different pion mass values m_π and a time-like lattice extent $N_\tau = 12$.

Investigations for the case $N_F = 2$ using improved WILSON fermions [157] are also supporting a coincidence of both temperatures within errorbars.

Moreover, the value of transition temperature is also another problematic issue. For example, the BROOKHAVEN/BIELEFELD collaboration [158] using staggered fermions gets for transition temperature $T_c = 196(3)$ MeV, which is much higher than the transition temperatures found by the WUPPERTAL group [155] for the deconfining and chiral transitions - $T_{\text{deconf}} = 170(7)$ MeV, and $T_\chi = 146(5)$ MeV, respectively. This discrepancy might be resolved thanks to the use of finer lattices [155]. Thereby, one understand the importance to check the consistency of these results preferably using different lattice discretizations, and to compare between them. Therefore, many efforts are devoted to investigate different discretizations to understand the nature of the finite temperature phase transition as in [156] (domain wall), [154] (twisted mass) and [159] (improved WILSON fermions).

We provide hereafter gluon and ghost propagator data using the twisted-mass discretization which might be confronted for example to [50] using improved WILSON fermions. Quite recently, in [160] quarks flavors effects on the ghost and gluon propagators have been studied for the cases $N_F = 2$ and $N_F = 2+1$ and for mass range of 270 to 510 MeV using twisted mass fermions. In this last reference no dependence on the temperature for the gluon and ghost propagators was found. Moreover, the authors observed a decrease of the gluon propagator with increasing the number of flavors while the ghost propagator is slightly enhanced.

We present in Fig. 6.1 first results for the bare, i.e. unrenormalized dressing functions for a few β (or equivalently temperatures) for the pion masses $m_\pi = 469,\ 398$ and 316 MeV. The unrenormalized transverse Z_T and longitudinal Z_L gluon dressing functions together with the unrenormalized ghost dressing function J as a function of the physical momentum q for a few temperatures indicated in the legends by their β-values. We agreed to take the renormalization point for this fermionic study $\mu = 2.5$ GeV. In order to find the renormalized dressing function one needs to apply the following relation

$$\begin{aligned} Z^{ren}_{T,L}(q,\mu) &\equiv \tilde{Z}_{T,L}(\mu) Z_{T,L}(q) \\ J^{ren}(q,\mu) &\equiv \tilde{Z}_J(\mu) J(q) \end{aligned} \tag{6.1}$$

with the $\tilde{Z}$-factors defined such that $Z^{ren}_{T,L}(\mu,\mu) = J^{ren}(\mu,\mu) = 1$ and are shown in Table 6.1.

A further observation is that the values of $\tilde{Z}_T$ and $\tilde{Z}_L$ are quite close to each other independent of the temperatures considered. This difference in values does not exceed 5% for all pion masses. Therefore, we conclude that the ultraviolet part of our gluon propagator is not affected with crossing any pseudo-critical temperature, and remains not phase sensitive. The aim is to present data set to be used as an input for *DS* or *FRG* equations within the momentum region 0.4 GeV $\geq$ $q \geq$ 3.0 GeV. We present these data in terms of fitting formulas for the bare gluon and ghost dressing functions.

At a first glance one observes from Fig. 6.1 that the the behavior of Z_L to be quite different from the behavior of Z_T, whatever m_π values are considered. The transverse dressing function Z_T shows less response to the temperature while the curves describing $Z_L(q)$ fan out for momenta below the renormalization scale $\mu = 2.5$ GeV according to the β values (or temperatures). This observation was already made us previously in the case of pure gauge theory [49]. Still in this latter case the strong temperature response of D_L in comparison to the present fermion case is due to the existence of a confirmed first order phase transition in the pure gauge sector of *QCD*.

As we did before for the case of pure gauge theory (see [49]) we fit here again the gluon dressing function with the GRIBOV-STINGL formula [26, 150] used in Refs. [151, 149] and derived in the so-called "Refined GRIBOV-ZWANZIGER" approach [161, 162]. We remind the reader that this fit function looks like

$$Z_{fit}(q) = q^2 \frac{c\,(1+d\,q^{2n})}{(q^2+r^2)^2+b^2}\,. \tag{6.2}$$

Our fit results (with excellent χ^2_{dof} values within the fitting range $[0.4\text{ GeV}, 3.0\text{ GeV}]$) for all available temperature values are displayed in Table 6.3. We have made many tests, and found out that this formula works nicely in the given range already without the b^2 term and for a fixed exponent $n = 1$. However, it might happen that moving to the infrared (smaller momenta) this formula would generate a non-zero b^2-term. Therefore, in this case a pair of complex-conjugate (complex masses) would arise. For the ultraviolet region, and especially above 3 GeV, we had also encountered problems to describe the data with this fit formula as logarithmic corrections (important at this regime) are not taken into account.

We have also tried to parametrize the ghost dressing function J using another type of fit function, namely

$$J_{fit}(q) = \left(\frac{f^2}{q^2}\right)^k + \frac{h\,q^2}{q^2+m^2_{gh}}\,. \tag{6.3}$$

Here, the fit parameter m_{gh} plays a mass-like role. We examined different situations keeping this parameter as a free parameter. However, we got results consistent with $m_{gh} = 0$. Therefore, we dropped this infrared mass parameter from our fit procedure. Our fit results are provided for the range $[0.4\text{ GeV}, 4.0\text{ GeV}]$ and shown in Table 6.4. Because of small statistical errors on

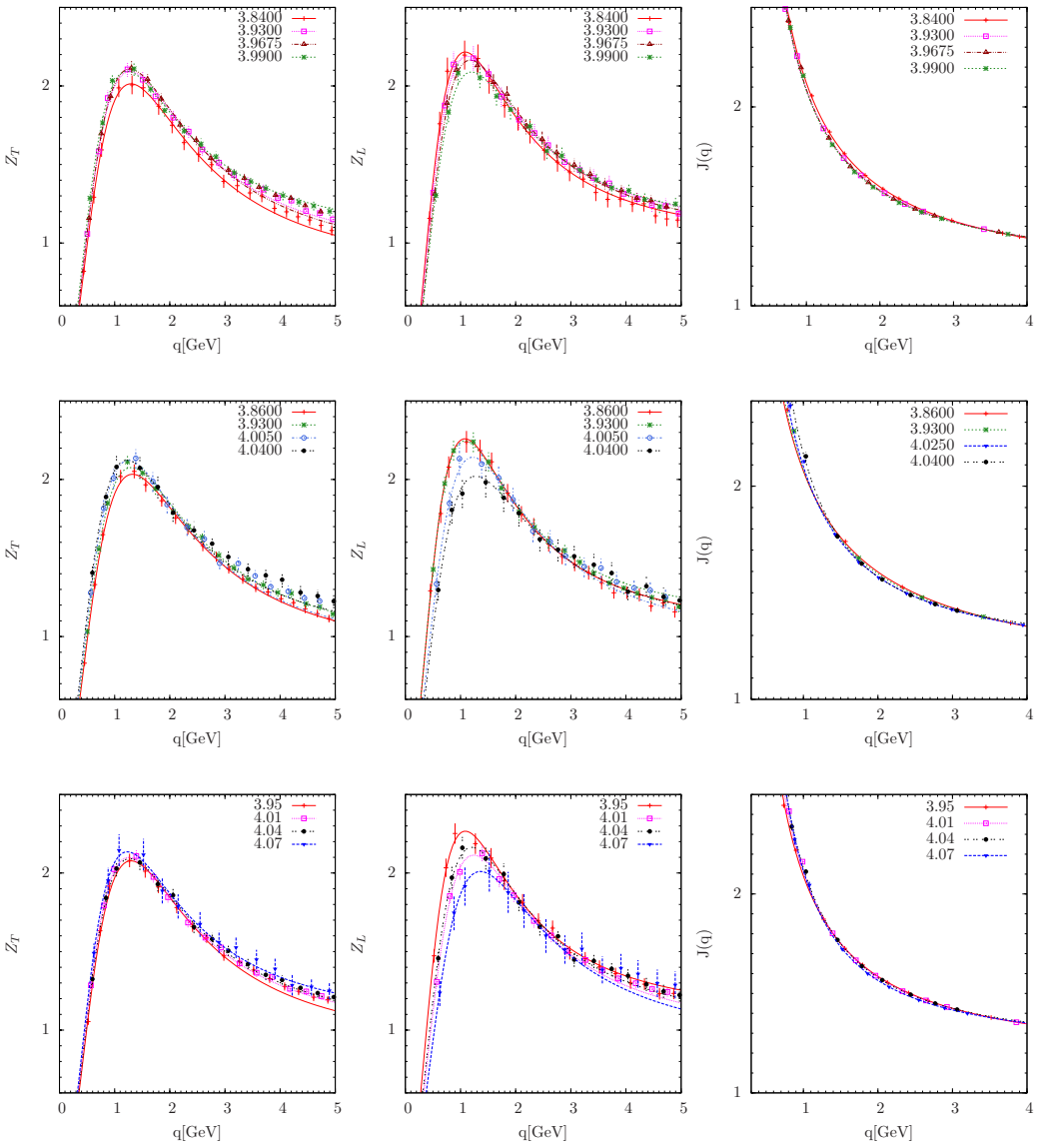

FIGURE 6.1: The unrenormalized transverse gluon Z_T (left panel), longitudinal gluon Z_L (middle panel) dressing functions and the unrenormalized ghost dressing function J (right panel) as functions of the momentum q [GeV] for different (inverse) coupling values β (or temperatures) as given in the legend. The corresponding pion mass values (from top to bottom panels) are $m_\pi \simeq 316,\ 398$ and 469 MeV.

Parameters	D_L fits				D_T fits			
T [MeV]	c/a^2	d/a^2	$a\,r$	χ^2_{dof}	c/a^2	d/a^2	$a\,r$	χ^2_{dof}
187	1.334(132)	0.744(138)	0.415(14)	0.19	1.868(142)	0.420(78)	0.510(12)	0.13
199	1.183(59)	0.872(79)	0.390(7)	0.16	1.729(60)	0.463(40)	0.486(5)	0.66
215	1.032(101)	1.013(188)	0.370(13)	0.12	1.371(104)	0.647(111)	0.431(10)	0.36
222	1.049(93)	0.941(159)	0.370(11)	0.16	1.218(76)	0.757(96)	0.411(8)	0.22
225	0.932(103)	1.148(233)	0.355(14)	0.13	1.208(88)	0.744(122)	0.405(10)	0.05
228	1.023(108)	0.979(206)	0.369(13)	0.27	1.256(83)	0.682(107)	0.410(9)	0.10
230	0.938(119)	1.165(277)	0.359(15)	0.09	1.099(93)	0.852(156)	0.387(11)	0.07
235	0.914(98)	1.143(224)	0.358(13)	0.38	0.982(70)	1.026(143)	0.369(9)	0.38
Parameters	D_L fits				D_T fits			
T [MeV]	c/a^2	d/a^2	$a\,r$	χ^2_{dof}	c/a^2	d/a^2	$a\,r$	χ^2_{dof}
193	1.271(116)	0.799(143)	0.401(13)	0.19	1.811(109)	0.459(66)	0.501(9)	0.32
199	1.218(83)	0.808(107)	0.391(9)	0.11	1.637(88)	0.523(63)	0.477(8)	0.66
215	0.982(91)	1.092(177)	0.356(12)	0.11	1.389(84)	0.651(86)	0.437(8)	0.37
228	1.034(86)	0.928(160)	0.366(10)	0.67	1.151(71)	0.819(110)	0.397(8)	0.48
236	1.171(265)	0.699(430)	0.383(42)	0.21	1.035(171)	0.965(310)	0.383(21)	0.25
241	1.006(145)	0.924(281)	0.366(19)	0.15	1.092(104)	0.784(162)	0.381(12)	0.25
246	0.922(133)	1.087(297)	0.356(18)	0.12	1.035(87)	0.891(164)	0.373(10)	0.44
248	0.845(94)	1.278(270)	0.346(13)	0.11	1.020(78)	0.904(144)	0.368(9)	0.21
254	0.824(173)	1.252(502)	0.348(24)	0.08	0.837(111)	1.237(329)	0.340(15)	0.12
Parameters	D_L fits				D_T fits			
T [MeV]	c/a^2	d/a^2	$a\,r$	χ^2_{dof}	c/a^2	d/a^2	$a\,r$	χ^2_{dof}
222	0.952(78)	1.127(169)	0.348(10)	0.35	1.338(80)	0.645(89)	0.427(8)	0.63
228	0.993(100)	1.003(199)	0.351(12)	0.32	1.290(104)	0.648(127)	0.416(11)	0.14
235	0.883(96)	1.203(236)	0.343(13)	0.19	1.126(91)	0.797(139)	0.389(10)	0.28
243	0.998(82)	0.945(157)	0.368(10)	0.23	1.009(61)	0.937(115)	0.371(7)	0.32
247	1.010(80)	0.918(156)	0.356(9)	1.08	1.027(67)	0.946(124)	0.375(8)	0.07
250	0.900(87)	1.108(223)	0.349(11)	0.67	1.096(79)	0.775(135)	0.380(9)	0.48
254	0.870(103)	1.131(275)	0.340(14)	0.25	0.941(84)	1.018(191)	0.359(11)	0.22
258	0.826(89)	1.251(260)	0.344(13)	0.25	1.053(69)	0.781(126)	0.367(8)	0.67
266	0.971(250)	0.894(559)	0.371(32)	0.01	0.792(130)	1.291(405)	0.328(34)	0.15

TABLE 6.3: Results from fits with the Gribov-Stingl formula Eq. (6.2) for the unrenormalized Z_T (right table) and Z_L (left table) dressing functions. The fit range is $[0.4 : 3.0]$ GeV. The values in parentheses indicate the fit errors estimated with the bootstrap method. The parameters b and n were fixed to $b = 0$ and $n = 1$, respectively. The pion mass values are $m_\pi = 316(16)$ MeV (upper), $m_\pi = 398(20)$ MeV (middle) and $m_\pi = 469(24)$ MeV (bottom subtables), respectively.

m_π(MeV)	β	a^2f^2	h/a^2	k	χ^2_{dof}
316(16)	3.8400	0.4580(17)	1.0916(61)	0.5111(78)	0.69
316(16)	3.8800	0.41822(7)	1.0904(19)	0.4950(23)	8.59
316(16)	3.9300	0.37046(9)	1.1355(39)	0.5438(55)	2.29
316(16)	3.9525	0.35672(9)	1.1387(36)	0.5462(52)	2.40
316(16)	3.9675	0.34636(7)	1.1501(33)	0.5642(54)	5.20
316(16)	3.9900	0.33093(8)	1.1571(30)	0.5736(56)	7.01
398(16)	3.8600	0.4464(21)	1.0419(40)	0.4444(35)	31.1
398(16)	3.9300	0.3802(19)	1.0962(53)	0.4945(58)	21.4
398(20)	3.9900	0.3380(07)	1.1466(25)	0.5612(39)	24.0
398(20)	4.0050	0.441(84)	0.90(14)	0.41(06)	0.21
398(20)	4.0175	0.3189(09)	1.1623(31)	0.5834(60)	6.4
398(20)	4.0250	0.3155(08)	1.1630(25)	0.5853(52)	17.4
398(20)	4.0400	0.3135(21)	1.2200(90)	0.696(21)	0.93
469(24)	3.9500	0.3621(09)	1.1325(38)	0.5397(53)	2.3
469(24)	3.9700	0.3519(07)	1.1426(31)	0.5554(48)	4.2
469(24)	3.9900	0.3405(12)	1.1555(45)	0.5787(81)	2.3
469(24)	4.0100	0.3295(07)	1.1607(24)	0.5873(48)	13.1
469(24)	4.0200	0.3270(08)	1.1557(27)	0.5778(51)	7.0
469(24)	4.0300	0.3130(08)	1.1538(26)	0.5660(48)	7.9
469(24)	4.0400	0.3100(11)	1.2015(55)	0.648(12)	2.3
469(24)	4.0500	0.3082(11)	1.2109(51)	0.677(12)	0.94
469(24)	4.0700	0.2913(20)	1.2156(79)	0.682(19)	0.39

TABLE 6.4: Fit results for the unrenormalized ghost dressing function with the fitting function according to Eq. (6.3). The momentum fitting ranges are $[0.4 : 4.0]$ GeV.

our ghost data our χ^2_{dof} values are not optimal. Moving to lower temperatures even makes these values worser, and even including the mass-like term would not improve the situation. Still, the fitting curves do not deviate too much from the data points reaching a maximum deviation of 5%.

6.2.2 The T dependence of the gluon and ghost propagators

In order to identify the dependency of the gluon and ghost data as a function of the temperature, we present in Fig. 6.2 the ratios of the renormalized dressing functions or propagators

$$R_{T,L}(q,T) = D^{ren}_{T,L}(q,T)/D^{ren}_{T,L}(q,T_{\min}), \tag{6.4}$$

$$R_G(q,T) = G^{ren}(q,T)/G^{ren}(q,T_{\min}). \tag{6.5}$$

Within Fig. 6.2 we show ratios as functions of the temperature T for 6 fixed (interpolated) momentum values $q \neq 0$. To make the temperature effects more visible we normalized them with respect to the lowest temperature values T_{min} available for the given pion masses as described in Eq. (6.4).

We observe a monotonous decrease for the values of $R_L(q,T)$ with the temperature. The gradient of this decrease is stronger for smaller momenta. This behavior is also seen through the crossover region. On the other hand, $R_T(q,T)$ shows a slight increase within the same range. Regarding the ghost ratio $R_G(q,T)$ shows a small rise at small momenta, specially at at $T \simeq T_{\text{deconf}}$. This might be explained as an artifact of the fit function, which does not work for this momenta range.

Furthermore, we show the ratio of the renormalized transverse gluon propagator R_T at zero momentum as a function of the temperature at the three pion mass values in the upper row of Fig. 6.3. We see a clear rise towards T_{deconf} for the middle mass, whereas for the other mass values there are only weak indications for such a behavior. We have drawn in the lower row the data obtained for the inverse renormalized longitudinal propagator D_L at zero momentum versus temperature. This quantity can be identified as a quantity proportional to the square of infrared gluon screening mass. This quantity rises as expected for all the three sets of masses having an inflexion temperature point within the crossover region. Therefore, $D_L^{-1}(0)$ might play an important role to indicate some temperature reaction in the crossover region. Yet, the zero momentum data we are providing here are certainly subject to different factors as finite size effects and Gribov effects. Moreover, we think that increasing our statistics is necessary to precise our conclusions.

We summarize our results saying that in all these three pion mass cases, D_L react stronger than D_T especially for momenta below 1.5 MeV. In fact, we presented a computation of Landau gauge gluon and ghost propagators in the range 0.4 GeV to 3.0 GeV within lattice QCD with $N_f = 2$ flavors, see also our paper [52]. We were able to cover the whole crossover temperature range for our three charged pion masses in the range from 300 MeV up to 500 MeV thanks to configurations provided by the tmfT collaboration. We provide fit results which turned out optimal for the longitudinal as well as transversal gluon dressing function but somewhat suboptimal for the ghost dressing function. Our goal is to provide helpful input data to the DS and FRG equations to study the behavior of the hadronic matter. The longitudinal propagator seems to react stronger crossing the transition region as the transverse does for non-zero momenta. We have also presented separately the zero momenta data. We showed the zero momenta transverse propagator which reacts to the crossover region. Moreover, $D_L^{-1}(0)$ ($\propto$(square) electric screening mass) was also computed. We observed typical behavior for this latter giving indications where the crossover happens for the three pion masses. Still, our results need to be sharpened using higher statistics.

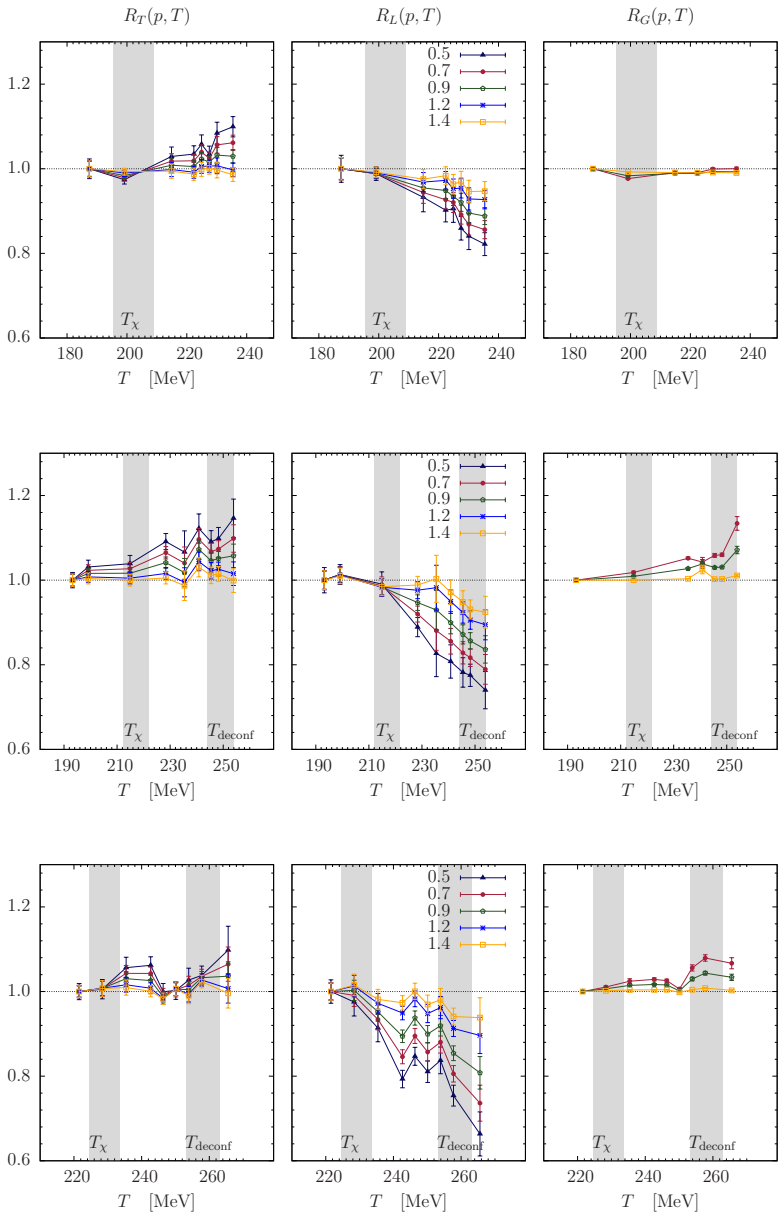

FIGURE 6.2: Ratios R_T, R_L and R_G for the renormalized transverse D_T^{ren} (left panel), longitudinal D_L^{ren} (middle panel) and ghost G^{ren} (right panel) propagators, respectively, as functions of the temperature T at a few non-zero momentum values p (indicated in units of [GeV]. The corresponding pion masses (from top to bottom) are $m_\pi \simeq 316,\ 398$ and 469 MeV. The vertical bands indicate the chiral and deconfinement pseudo-critical temperatures with their uncertainties (see Table 6.2).

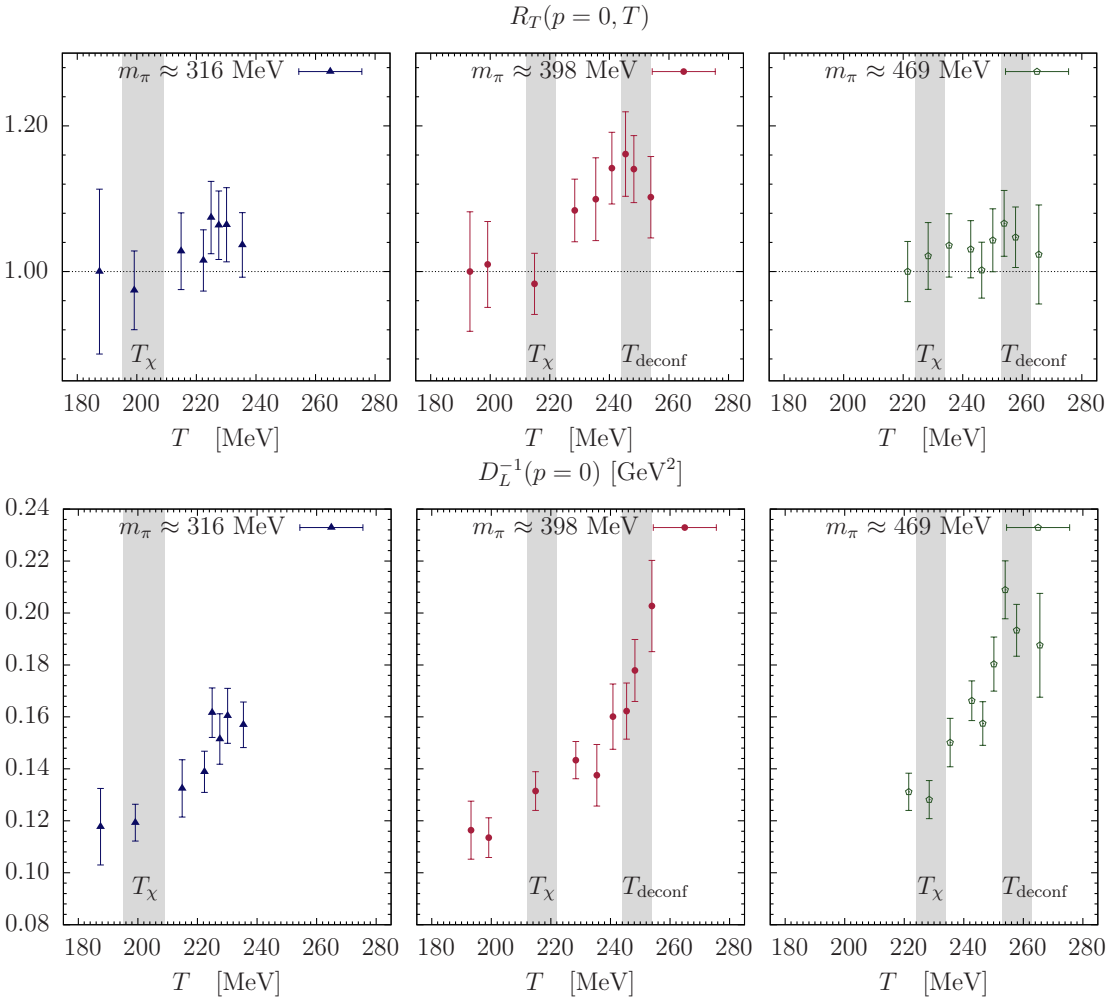

FIGURE 6.3: The upper row shows the ratio R_T at zero momentum for the three pion mass values indicated. The lower panels show the inverse renormalized longitudinal gluon propagator $D_L^{-1}(0)$.

CHAPTER 7

Alternative study for the LANDAU gauge fixing

DURING this chapter we present an original study of the gluon propagator $D(q)$ at zero temperature for the gauge group $SU(3)$. In fact, we explore here the influence of the GRIBOV problem on $D(q)$, and especially around the 1 GeV region as well as the zero-momentum values $D(0)$. As discussed before in Section 3.4.2 the gauge fixing to the LANDAU gauge traditionally practiced by maximizing the gauge functional leaves the GRIBOV copies problem open. We believe that such problem might be the origin to the fact that lattice results so far are supporting a decoupling behavior of the propagators contradicting the KUGO-OJIMA confinement criteria, see Section 2.1.4. On the other hand, we know that the *DSE* is providing both the decoupling solution and the scaling one which are quite different solutions around the momentum sensible region of $1\,GeV$ (and also below) [89]. These two types of *DSE* solutions arise due to different boundary conditions on the ghost propagator at zero momentum. We believe that such boundary conditions might suppress the optimal influence of the GRIBOV effects. That is, in order to judge with *DSE* might happen one needs somehow to get rid of the GRIBOV ambiguity, and try to define the gauge uniquely. In this respect *LQCD* might judge which solution happens in an effective way. In fact, our new ingredient here is to avoid the GRIBOV problem using a new criteria, namely considering gauge copies with minimal FADDEEV-POPOV operator eigenvalues λ_{min}. That is, this choice condition defines uniquely the gauge. We expect that a free-GRIBOV copies gauge condition should be the key to compare lattice propagators to the *DSE* solutions. We concentrate here on the gluon rather on the ghost propagator as we already know that ghost propagator gets more singular for small λ_{min} thanks to its spectral representation [137, 138].

7.1 Correlation between gauge functional and λ_{min}

In order to study the $SU(3)$ gluon propagator $D(q)$ in pure gauge theory we hoped to understand the correlation between gauge functional and λ_{min} values. That is, we wanted first to understand how moving to smaller λ_{min} would effect in some sense the gauge functional values. Therefore, the maximum gauge functional value mostly used to fix the gauge might be here seen to not correspond to a gauge copy with the smallest λ_{min}. In [137, 138] it has been already observed that gauge copies with smallest λ_{min} are not in general the best copies *bc* with the highest gauge functional. However, it has also been observed that moving to larger volumes would shift the FADDEEV-POPOV eigenvalues to zero. This latter observation is in agreement with ZWANZIGER conjecture [28].

We consider in the present $SU(3)$ exploratory study a lattice volume of 16^4 with the inverse coupling of $\beta = 6.0$. Here, we generate a number of configuration and gauge copies equal respectively to $N_{\text{conf}} = 34$ and $N_{\text{copy}} = 50$. We study in Fig. 7.1 the variations of the normalized gauge functional F, namely $(F_{\max} - F)/F_{\max}$, with the smallest FP eigenvalues λ_{min} (for fixed configuration). The tendency is that moving to smaller λ_{min} one finds only a few number of gauge copies with higher $(F_{\max} - F)/F_{\max}$ values. This means that moving to the (unknown) absolute minima of F (being part of the fundamental modular region (FMR)) one shifts away from the GRIBOV horizon (characterized by $\lambda = 0$). In general, one concludes from Fig. 7.1 that no correlation is observed. This is in agreement with results from [137, 138] where best copies (in the gauge functional sense) do not correspond necessarily to the lowest λ. In fact, this is a fortunate situation since results regarding the gluon propagator might in principle provide independent results according to the criteria: highest F and λ_{min}.

In the next section let us compare the gluon propagator results measured according to different criteria, namely: highest F vs. smallest λ_{min} gauge copies. This study makes it apparent whether the GRIBOV would effect $D(q)$ especially for the low-lying λ_{min} regime. Note, that a typical solution of the gluon and ghost propagator have been mainly supported by the lattice namely called the decoupling solution [59, 60, 61]. These solutions show for $D(q)$ the realization of a plateau in the deep infrared. These solutions are not in agreement with the KOGU-OJIMA confinement criterion, but still considered as one of the mathematical solutions of *DSE* besides the scaling solutions, see Section 2.1.4 for more discussion.

7.2 The gluon propagator and its zero-momentum value $D(0)$

As said in the former section, in order to perform our previous study one needs to generate a couple of gauge copies for a fixed configuration. Next, one measures on each gauge copy its corresponding FP eigenvalues. Our new criteria is to choose the gauge copy with the smallest eigenvalue, namely λ_{min}. Therefore, one may compute the gluon propagator on such gauge copies, and even compare the same propagator to other different criteria as maximizing the gauge functional adopted so far. More interesting for us is the comparison between the lowest λ_{min} and

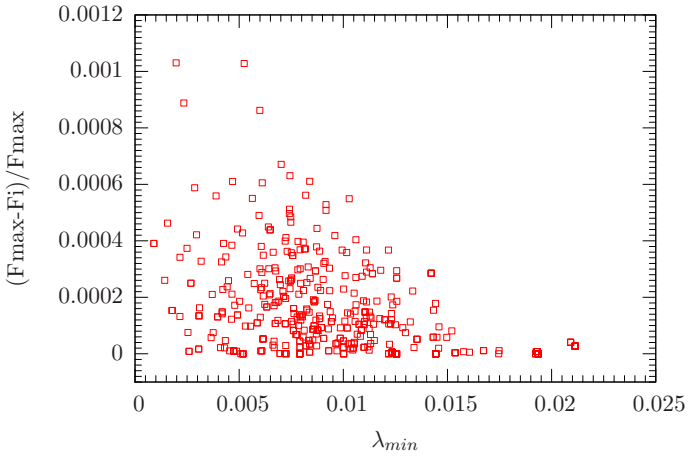

FIGURE 7.1: Correlation study between the normalized gauge functional F and the λ_{min}. $F_{\max}$ corresponds to the gauge copies with the highest F for a fixed configuration. Here we produce $N_{\text{conf}} = 34$ and $N_{\text{copy}} = 50$ for a lattice volume of 16^4 and $\beta = 6.0$.

the highest F. Let us recall that maximizing the gauge functional is a standard way to fix the gauge. This standard procedure was also used by us in order to fix the gauge copies to the LANDAU gauge thanks to iterative methods as *simulated annealing* for example. In the upcoming results we focus exclusively on the $SU(3)$ gluon propagator in the pure gauge theory. To perform the present study we increase the number of gauge copies up to $N_{copy} = 100$ in order to maximize the probability to find gauge copies with small FP eigenvalues. We observe from Fig. 7.2 the situation is not trivial for producing gauge copies with smaller λ_{min}. Moreover, one sees that the first gauge copies generated for a fixed configuration is nearly never the copy holding the lowest λ_{min}, and therefore a lot of gauge copies need to be produced in order to have a chance to minimize λ_{min}. Here, we study unfortunately only $N_{copy} = 100$ which might be not sufficient for such study. Moreover, in principle, we need to reach the momentum plateau (in the infrared) to observe the influence of FP eigenvalues. That is, moving to higher volumes and therefore even more smaller λ_{min}. Here we fix the volume only to 16^4 and the (inverse) coupling β is fixed to 6.00. Therefore our gluon propagator results might be afflicted by finite volume effects obviously, and not really reach the deep infrared where the GRIBOV effects dominate. Actually, we observe in Fig. 7.3 that comparing the (bare) gluon propagator measured on different type of gauge copies, namely gauge copies with the lowest λ_{min} vs. the ones with highest gauge functional F, show only small differences for our momentum range. Therefore, we conclude that the GRIBOV effects are absent. This is due in fact to the small volume we used which does not enable to reach small momenta where GRIBOV effects manifest. In parallel, following the strategy as us, the authors in [163] did the same study with the gauge group $SU(2)$. This investigation is less expensive than our $SU(3)$ study, and hence the volume of 56^4 is reached using $\beta = 2.3$. There

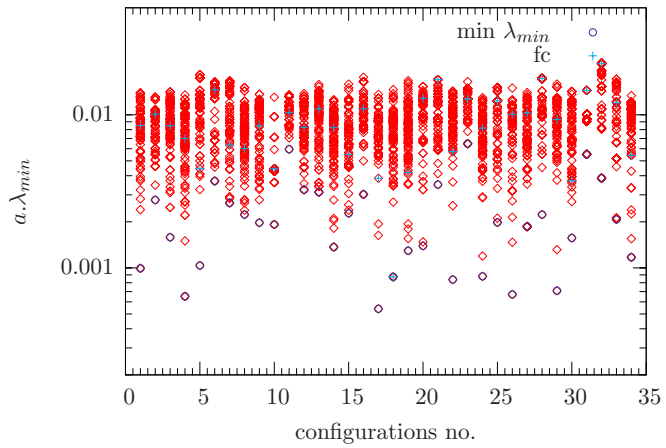

FIGURE 7.2: The lowest FP eigenvalues λ_{min} as a function of the number of configurations. The lattice volume and β correspond to 16^4 and 6.00 respectively. The number of configurations $N_{\text{conf}} = 34$, and the number of gauge copies $N_{\text{copy}} = 100$.

it is observed that the $D(q)$ takes different values according to the different criteria (minimal FP vs. maximum gauge functional) around the region of $1\,GeV$. Moreover, to get such effects the authors generated at least 210 gauge copies and 60 thermalized configurations to access very small λ_{min}. Back to our $SU(3)$ results we conclude that due small volume and not sufficient statistics one does not see real effects for the considered momenta range. Moreover, we see also in Fig. 7.4 that zero-momentum gluon propagator values $D(0)$ show no correlation with λ_{min}. This means that $D(0)$ might be not affected when moving to smaller λ_{min}, and no conclusion might be drawn at least for the present lattice parameters.

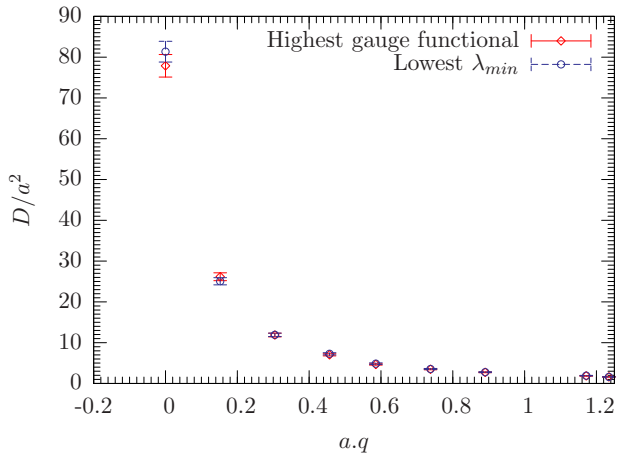

FIGURE 7.3: The bare gluon propagator D/a^2 as a function of the momenta $a \cdot q$ in units of the lattice spacing. The parameters are the same as in Fig. 7.2.

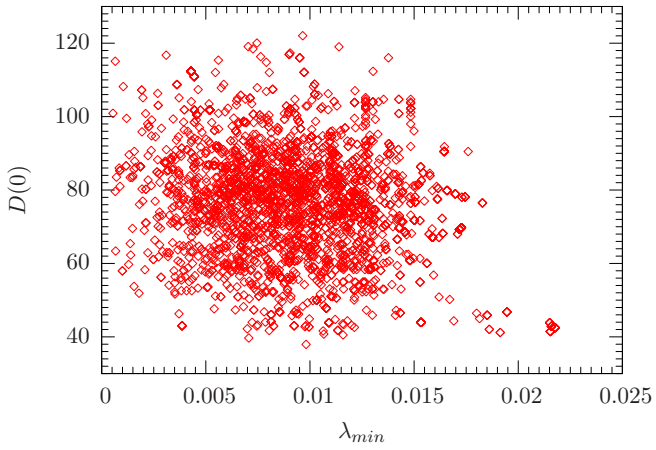

FIGURE 7.4: A scatter plot showing the zero-momentum gluon propagator value $D(0)$ as a function of λ_{min}. The lattice parameters are the same as in Fig. 7.2.

CHAPTER 8

Conclusion

In this thesis we dealt with different aspects of the $SU(3)$ LANDAU gauge gluon and ghost propagators within lattice *QCD* at finite temperature. Our present work was threefold: First of all, we investigate the pure gauge sector of *QCD*, also called the quenched approximation of *QCD*, see also our paper [49]. Within this sector we computed the gluon and ghost propagators for different temperatures covering the first order phase transition (from 0.5 T_c to 3 T_c). Our critical (inverse) coupling in this case was fixed to $\beta_c = 6.337$ corresponding to $N_\tau = 12$. We got clear signal for a temperature phase order transition thanks to the POLYAKOV loop (and its susceptibility) and the longitudinal part of the gluon propagator D_L. The transverse part D_T of the gluon propagator shows a weak temperature dependence. We improved the sensitivity around T_c even for higher momenta thanks to functional combinations of D_L. These latter new constructs might play the role of 'order parameters' at least for quenched *QCD*. Our pure gauge study concentrate on the momenta range [0.6,8.0] GeV, and not intend the reach the infrared region. In fact, our goal is to provide data as input for the *DS* equations for momenta around the sensible range of 1 GeV. For that, we extracted the continuum limit of our data after investigating finite size and GRIBOV effects. We show that these latter are small at least for our limited momentum range. We believe that choosing a higher critical beta (corresponding to $a = 0.055\,\mathrm{fm}$) and a moderate 3d volume ($(2.64\,\mathrm{fm})^3$) favored us to get close the continuum limit. On the other hand the ghost propagator shows weak temperature dependence as expected.

A second important part of our work was to study full *QCD* with $N_F = 2$ maximally twisted fermions, see [52]. Thanks to the tmfT collaboration we had access to configurations corresponding to three values of (charged) pion masses, namely: 316, 398 and 469 MeV. These configurations were generated using the twisted mass action providing an automatic O(a) improvement. For this study we concentrate on the momenta range [0.4,3.0] GeV. We computed the gluon and ghost propagators, and show their temperature dependence. The strong temperature response to the crossover region belongs to the (electric sector) D_L rather than (magnetic sector) D_T. We show indications for a crosover reaction thanks to D_L (for non zero momentum) and D_T at zero momentum. Still, one needs to be careful and considers more statistics in order to draw

a definitive conclusion. To interpolate we fitted successfully our gluon data with the STINGL-GRIBOV formula. Regarding the ghost propagator the fitting results were not optimal. We have also considered $D_L^{-1}(0)$ (proportional to the electric screening mass) for our pion mass sets. This observable is an interesting order parameter showing where the crossover might happen. In our case, this observable shows indications for transition for our masses at different temperatures scales as expected. However, higher statistics are wished to sharpen the region where theory undergoes a crossover. Our goal from this fermionic study is to provide valuable data to the continuum functional methods, and also to give some indications for a crossover around the critical temperature region.

Finally, we experimented a new method to study the influence of the GRIBOV problem especially on the gluon propagator for the gauge group $SU(3)$. In fact, we tried to understand how strong is the influence of the choice of the gauge copies on the behavior of the gluon propagator. Below the sensible region of 1 GeV it is already known that *DSE* provides two different solutions corresponding to different boundary conditions. It is the role of *LQCD* to support or to reject one of these solution. We believe that GRIBOV ambiguity is an obstacle to clarify the support of *LQCD* to some well defined solution of *DSE*. Therefore, we adopted here a new criteria, to fix the gauge uniquely, and therefore avoid the GRIBOV problem. Namely, we take only gauge copies as close as possible to the GRIBOV horizon, i. e. gauge copies with the smallest FADDEEV-POPOV (FP) operator eigenvalues. In principle, the gluon propagator computed on these latter gauge copies might show deviations to the one obtained from standard maximal gauge functional procedure. However, we observe small deviations (within errorbars) because of the moderate lattice volume used, and eventually the reduced number of gauge copies and configurations.

Appendix

1 A note on the over-relaxation method

The method known as over-relaxation (OR) is an algorithm aiming to accelerate convergence of the gauge-fixing process. This method might be explained as an iterative process where the update on the gauge transformation matrices g_x is expressed as:

$$g_{\text{new}} = g_{\text{ch}}\, g_{\text{old}}, \tag{1}$$

where g_{ch} is the change in the update step.

Therefore, in principle choosing $g_{\text{old}} = g_x$, $g_{\text{old}} = g_x^{\text{solution}}$ and starting from a cold start for example, i. e. $g_{\text{old}} = \mathbb{I}$, one finds

$$g_{\text{ch}} = g_{\text{new}} = g_x^{\text{solution}}. \tag{2}$$

Thus, over-relaxation is implemented by applying iteratively g_{ch}, or equivalently to make the following replacement

$$g_x^{\text{solution}} \to (g_x^{\text{solution}})^{\alpha},\ 1 < \alpha < 2. \tag{3}$$

In fact, the relaxation method corresponds to setting $\alpha = 1$. During our gauge fixing process we have used OR after the so-called simulated annealing method[126, 127, 128, 31, 32]. The combination of these two methods improves the gauge-fixing significantly getting then gauge transformations close to the global maxima of the gauge functional in the LANDAU gauge. We fixed the maximum number of OR iterations to $N_{\text{it}}^{\max} = 80000$. This number was never reached but still as expected the number of iterations took higher values around the critical temperature T_c.

2 The GELL-MANN matrices

The generators for the group $SU(3)$ in the standard representation are given by

$$T_a = \frac{1}{2}\lambda_a, \tag{4}$$

where the eight GELL-MANN λ_a Matrices are 3×3 generalizations of the PAULI matrices, namely

$$\begin{aligned}
\lambda_1 &= \begin{bmatrix} 0 & 1 & 0 \\ 1 & 0 & 0 \\ 0 & 0 & 0 \end{bmatrix}, \lambda_2 = \begin{bmatrix} 0 & -i & 0 \\ i & 0 & 0 \\ 0 & 0 & 0 \end{bmatrix}, \lambda_3 = \begin{bmatrix} 1 & 0 & 0 \\ 0 & -1 & 0 \\ 0 & 0 & 0 \end{bmatrix}, \\
\lambda_4 &= \begin{bmatrix} 0 & 0 & 1 \\ 0 & 0 & 0 \\ 1 & 0 & 0 \end{bmatrix}, \lambda_5 = \begin{bmatrix} 0 & 0 & -i \\ 0 & 0 & 0 \\ i & 0 & 0 \end{bmatrix}, \lambda_6 = \begin{bmatrix} 0 & 0 & 0 \\ 0 & 0 & 1 \\ 0 & 1 & 0 \end{bmatrix}, \\
\lambda_7 &= \begin{bmatrix} 0 & 0 & 0 \\ 0 & 0 & -i \\ 0 & i & 0 \end{bmatrix}, \lambda_8 = \frac{1}{\sqrt{3}} \begin{bmatrix} 1 & 0 & 0 \\ 0 & 1 & 0 \\ 0 & 0 & -2 \end{bmatrix}.
\end{aligned} \tag{5}$$

3 The gamma matrices

On the lattice, one mostly uses the Euclidean gamma matrices γ_μ, with $\mu = 1,2,3,4$. This latters matrices may be related to the MINKOWSKI matrices γ_μ^M with $\mu = 0,1,2,3$. The latter matrices satisfy

$$\{\gamma_\mu^M, \gamma_\nu^M\} = 2\, g_{\mu,\nu}\, \mathbb{I}, \tag{6}$$

where $g_{\mu,\nu}$ denotes the metric defined as $g_{\mu,\nu} = \mathrm{diag}(1,-1,-1,-1)$ and $\mathbb{I}$ is the 4×4 unit matrix. Following these conventions one defines the Euclidean gamma matrices γ_μ as

$$\gamma_1 = -i\gamma_1^M,\ \gamma_2 = -i\gamma_2^M,\ \gamma_3 = -i\gamma_3^M,\ \gamma_4 = \gamma_0^M. \tag{7}$$

These γ_μ satify the anti-commutation relations

$$\{\gamma_\mu, \gamma_\nu\} = 2\, \delta_{\mu,\nu}\, \mathbb{I}. \tag{8}$$

One defines also γ_5 which commutes with all other γ_μ as

$$\gamma_5 = \gamma_1\gamma_2\gamma_3\gamma_4, \tag{9}$$

satisfying $\gamma_5^2 = \mathbb{I}$. An explicit form might be given to the Euclidean γ_ν matrices from a certain representation of the γ_ν^M. If one considers the chiral representation, namely where γ_5 is diagonal, then γ_ν take the form

$$\gamma_1 = \begin{bmatrix} 0 & 0 & 0 & -i \\ 0 & 0 & -i & 0 \\ 0 & i & 0 & 0 \\ i & 0 & 0 & 0 \end{bmatrix}, \gamma_2 = \begin{bmatrix} 0 & 0 & 0 & -1 \\ 0 & 0 & 1 & 0 \\ 0 & 1 & 0 & 0 \\ -1 & 0 & 0 & 0 \end{bmatrix}, \gamma_3 = \begin{bmatrix} 0 & 0 & -i & 0 \\ 0 & 0 & 0 & i \\ i & 0 & 0 & 0 \\ 0 & -i & 0 & 0 \end{bmatrix}, \tag{10}$$

$$\gamma_4 = \begin{bmatrix} 0 & 0 & 1 & 0 \\ 0 & 0 & 0 & 1 \\ 1 & 0 & 0 & 0 \\ 0 & 1 & 0 & 0 \end{bmatrix}, \gamma_5 = \begin{bmatrix} 1 & 0 & 0 & 0 \\ 0 & 1 & 0 & 0 \\ 0 & 0 & -1 & 0 \\ 0 & 0 & 0 & -1 \end{bmatrix}.$$

BIBLIOGRAPHY

[1] **CTEQ** Collaboration, R. Brock *et al.*, "Handbook of perturbative QCD; Version 1.1: September 1994", *Rev. Mod. Phys.* (1994) .

[2] S. Bethke and J. Pilcher, "Tests of perturbative QCD at LEP", *Ann.Rev.Nucl.Part.Sci.* **42** (1992) 251–289.

[3] J. Engelen and P. Kooijman, "Deep inelastic scattering at HERA: A review of experimental results in the light of quantum chromodynamics", *Prog.Part.Nucl.Phys.* **41** (1998) 1–47.

[4] D. Gross and F. Wilczek, "Ultraviolet Behavior of Nonabelian Gauge Theories", *Phys.Rev.Lett.* **30** (1973) 1343–1346.

[5] H. Politzer, "Reliable Perturbative Results for Strong Interactions?", *Phys.Rev.Lett.* **30** (1973) 1346–1349.

[6] G. 't Hooft and M. Veltman, "Regularization and Renormalization of Gauge Fields", *Nucl.Phys.* **B44** (1972) 189–213.

[7] T. Renk, *QCD matter under extreme conditions : heavy ion collisions*. PhD thesis, München, Techn. Univ., 2002. `http://d-nb.info/966327764/34`.

[8] A. Linde, "Infrared Problem in Thermodynamics of the Yang-Mills Gas", *Phys. Lett.* **B96** (1980) 289.

[9] J.-P. Blaizot and E. Iancu, "The quark-gluon plasma: Collective dynamics and hard thermal loops", *Phys. Rept.* **359** (2002) 355–528, `arXiv:hep-ph/0101103`.

[10] J. Blaizot, E. Iancu, and A. Rebhan, "Selfconsistent hard thermal loop thermodynamics for the quark gluon plasma", *Phys.Lett.* **B470** (1999) 181–188, `arXiv:hep-ph/9910309 [hep-ph]`.

[11] J. Blaizot, E. Iancu, and A. Rebhan, "The Entropy of the QCD plasma", *Phys.Rev.Lett.* **83** (1999) 2906–2909, `arXiv:hep-ph/9906340 [hep-ph]`.

[12] E. B. J.O. Andersen and M. Strickland, "Screened perturbation theory to three loops", *Phys.Rev.* **D63** (2001) 105008, arXiv:hep-ph/0007159 [hep-ph].

[13] S. Scherer, "Introduction to chiral perturbation theory", *Adv.Nucl.Phys.* **27** (2003) 277, arXiv:hep-ph/0210398 [hep-ph].

[14] M. Creutz, *Quarks, gluons and lattices*. 1984.

[15] I. Montvay and G. Muenster, *Quantum fields on a lattice*. Cambridge, UK: Univ. Pr. (1994) 491 p. (Cambridge monographs on mathematical physics).

[16] H. Rothe, "Lattice gauge theories: An Introduction", *World Sci. Lect. Notes Phys.* **59** (1997) 1–512.

[17] J. Smit, "Introduction to quantum fields on a lattice: A robust mate", *Cambridge Lect.Notes Phys.* **15** (2002) 1–271.

[18] B. Svetitsky and L. Yaffe, "Critical Behavior at Finite Temperature Confinement Transitions", *Nucl.Phys.* **B210** (1982) 423.

[19] R. Pisarski, "Notes on the deconfining phase transition", arXiv:hep-ph/0203271 [hep-ph].

[20] L. von Smekal, A. Hauck, and R. Alkofer, "A solution to coupled Dyson-Schwinger equations for gluons and ghosts in Landau gauge", *Ann. Phys.* **267** (1998) 1, arXiv:hep-ph/9707327.

[21] A. Hauck, L. von Smekal, and R. Alkofer, "Solving a coupled set of truncated QCD Dyson-Schwinger equations", *Comput.Phys.Commun.* **112** (1998) 166, arXiv:hep-ph/9804376 [hep-ph].

[22] C. Roberts and S. Schmidt, "Dyson-Schwinger equations: Density, temperature and continuum strong QCD", *Prog.Part.Nucl.Phys.* **45** (2000) S1–S103, arXiv:nucl-th/0005064 [nucl-th].

[23] P. Maris and C. Roberts, "Dyson-Schwinger equations: A Tool for hadron physics", *Int.J.Mod.Phys.* **E12** (2003) 297–365, arXiv:nucl-th/0301049 [nucl-th].

[24] H. Gies, "Running coupling in Yang-Mills theory: A flow equation study", *Phys.Rev.* **D66** (2002) 025006, arXiv:hep-th/0202207 [hep-th].

[25] J. Pawlowski, D. Litim, S. Nedelko, and L. von Smekal, "Infrared behaviour and fixed points in Landau gauge QCD", *Phys. Rev. Lett.* **93** (2004) 152002, arXiv:hep-th/0312324.

[26] V. Gribov, "Quantization of non-Abelian gauge theories", *Nucl. Phys.* **B139** (1978) 1.

[27] D. Zwanziger, "Non-perturbative Landau gauge and infrared critical exponents in QCD", *Phys. Rev.* **D65** (2002) 094039, arXiv:hep-th/0109224.

[28] D. Zwanziger, "Non-perturbative Faddeev-Popov formula and infrared limit of QCD", *Phys. Rev.* **D69** (2004) 016002, hep-ph/0303028.

[29] T. Kugo and I. Ojima, "Local covariant operator formalism of nonabelian gauge theories and quark confinement problem", *Prog. Theor. Phys. Suppl.* **66** (1979) 1.

[30] T. Kugo, "The universal renormalization factors z(1) / z(3) and color confinement condition in non-abelian gauge theory", (1995) , hep-th/9511033.

[31] V. Bornyakov, V. Mitrjushkin, and M. Müller-Preußker, "SU(2) lattice gluon propagator: continuum limit, finite- volume effects and infrared mass scale m_IR", *Phys. Rev.* **D81** (2010) 054503, arXiv:0912.4475 [hep-lat].

[32] I. Bogolubsky, E.-M. Ilgenfritz, M. Müller-Preußker, and A. Sternbeck, "Lattice gluodynamics computation of Landau gauge Green's functions in the deep infrared", *Phys. Lett.* **B676** (2009) 69–73, arXiv:0901.0736 [hep-lat].

[33] T. Bakeev, E.-M. Ilgenfritz, V. Mitrjushkin, and M. Müller-Preußker, "On practical problems to compute the ghost propagator in SU(2) lattice gauge theory", *Phys. Rev.* **D69** (2004) 074507, hep-lat/0311041.

[34] I. Bogolubsky, G. Burgio, V. Mitrjushkin, and M. Müller-Preußker, "Landau gauge ghost and gluon propagators in SU(2) lattice gauge theory: Gribov ambiguity revisited", *Phys. Rev.* **D74** (2006) 034503, hep-lat/0511056.

[35] A. Sternbeck, E.-M. Ilgenfritz, M. Müller-Preußker, and A. Schiller, "Towards the infrared limit in SU(3) Landau gauge lattice gluodynamics", *Phys. Rev.* **D72** (2005) 014507, hep-lat/0506007.

[36] I. Bogolubsky, V. Bornyakov, G. Burgio, E.-M. Ilgenfritz, V. Mitrjushkin, and M. Müller-Preußker, "Improved Landau gauge fixing and the suppression of finite-volume effects of the lattice gluon propagator", *Phys. Rev.* **D77** (2008) 014504, arXiv:0707.3611 [hep-lat].

[37] V. Bornyakov, V. Mitrjushkin, and M. Müller-Preußker, "Infrared behavior and Gribov ambiguity in SU(2) lattice gauge theory", *Phys. Rev.* **D79** (2009) 074504, arXiv:0812.2761 [hep-lat].

[38] U. Heller, F. Karsch, and J. Rank, "The gluon propagator at high temperature", *Phys. Lett.* **B355** (1995) 511–517, arXiv:hep-lat/9505016.

[39] U. Heller, F. Karsch, and J. Rank, "Gluon propagator at high temperature: Screening, improvement and nonzero momenta", *Phys. Rev.* **D57** (1998) 1438–1448, arXiv:hep-lat/9710033.

[40] A. Cucchieri, F. Karsch, and P. Petreczky, "Propagators and dimensional reduction of hot SU(2) gauge theory", *Phys. Rev.* **D64** (2001) 036001, arXiv:hep-lat/0103009.

[41] A. Cucchieri and T. Mendes, "What's up with IR gluon and ghost propagators in Landau gauge? A puzzling answer from huge lattices", *PoS* **LAT2007** (2007) 297, arXiv:0710.0412 [hep-lat].

[42] A. Cucchieri, A. Maas, and T. Mendes, "Infrared properties of propagators in Landau-gauge pure Yang-Mills theory at finite temperature", *Phys. Rev.* **D75** (2007) 076003, arXiv:hep-lat/0702022.

[43] C. Fischer, A. Maas, and J. Müller, "Chiral and deconfinement transition from correlation functions: SU(2) vs. SU(3)", *Eur. Phys. J.* **C68** (2010) 165–181, arXiv:1003.1960 [hep-ph].

[44] V. Bornyakov and V. Mitrjushkin, "SU(2) lattice gluon propagators at finite temperatures in the deep infrared region and Gribov copy effects", arXiv:1011.4790 [hep-lat].

[45] A. Cucchieri and T. Mendes, "Further Investigation of Massive Landau-Gauge Propagators in the Infrared Limit", *PoS* **LATTICE2010** (2010) 280, arXiv:1101.4537 [hep-lat].

[46] J. Mandula and M. Ogilvie, "The gluon propagator at finite temperature", *Phys. Lett.* **B201** (1988) 117.

[47] T. S. A. Nakamura, I. Pushkina and S. Sakai, "Screening of hot gluon", *Phys.Lett.* **B549** (2002) 133–138, arXiv:hep-lat/0208075 [hep-lat].

[48] T. S. A. Nakamura and S. Sakai, "Lattice calculation of gluon screening masses", *Phys.Rev.* **D69** (2004) 014506, arXiv:hep-lat/0311024 [hep-lat].

[49] R. Aouane, V. Bornyakov, E. Ilgenfritz, V. Mitrjushkin, M. Müller-Preußker, *et al.*, "Landau gauge gluon and ghost propagators at finite temperature from quenched lattice QCD", *Phys.Rev.* **D85** (2012) 034501, arXiv:1108.1735 [hep-lat].

[50] V. Bornyakov and V. Mitrjushkin, "Lattice QCD gluon propagators near transition temperature", arXiv:1103.0442 [hep-lat].

[51] S. Furui and H. Nakajima, "Infrared features of unquenched finite temperature lattice Landau gauge QCD", *Phys. Rev.* **D76** (2007) 054509, arXiv:hep-lat/0612009.

[52] R. Aouane, F. Burger, E.-M. Ilgenfritz, M. Müller-Preußker, and A. Sternbeck, "Landau gauge gluon and ghost propagators from lattice QCD with Nf=2 twisted mass fermions at finite temperature", arXiv:1212.1102 [hep-lat].

[53] B. Gruter, R. Alkofer, A. Maas, and J. Wambach, "Temperature dependence of gluon and ghost propagators in Landau gauge Yang-Mills theory below the phase transition", *Eur.Phys.J.* **C42** (2005) 109–118, arXiv:hep-ph/0408282 [hep-ph].

[54] A. Maas, J. Wambach, and R. Alkofer, "The high-temperature phase of Landau gauge Yang-Mills theory", *Eur.Phys.J.* **C42** (2005) 93–107, arXiv:hep-ph/0504019 [hep-ph].

[55] J. Braun, H. Gies, and J. Pawlowski, "Quark confinement from color confinement", *Phys. Lett.* **B684** (2010) 262–267, arXiv:0708.2413 [hep-th].

[56] C. Fischer, "Deconfinement phase transition and the quark condensate", *Phys.Rev.Lett.* **103** (2009) 052003, arXiv:0904.2700 [hep-ph].

[57] G. Boyd, J. Engels, F. Karsch, E. Laermann, C. Legeland, *et al.*, "Thermodynamics of SU(3) lattice gauge theory", *Nucl.Phys.* **B469** (1996) 419–444, arXiv:hep-lat/9602007 [hep-lat].

[58] K. Fukushima and K. Kashiwa, "Polyakov loop and QCD thermodynamics from the gluon and ghost propagators", arXiv:1206.0685 [hep-ph].

[59] A. Cucchieri and T. Mendes, "Constraints on the IR behavior of the ghost propagator in Yang-Mills theories", *Phys. Rev.* **D78** (2008) 094503, arXiv:0804.2371 [hep-lat].

[60] A. Cucchieri and T. Mendes, "Constraints on the IR behavior of the gluon propagator in Yang-Mills theories", *Phys. Rev. Lett.* **100** (2008) 241601, arXiv:0712.3517 [hep-lat].

[61] I. Bogolubsky, E.-M. Ilgenfritz, M. Müller-Preußker, and A. Sternbeck, "The Landau gauge gluon and ghost propagators in 4D SU(3) gluodynamics in large lattice volumes", *PoS* **LAT2007** (2007) 290, arXiv:0710.1968 [hep-lat].

[62] J. Collins, *Renormalization. An introduction to renormalization, the renormalization group, and the operator product expansion*. 1984.

[63] M. Srednicki, *Quantum field theory*. 2007.

[64] L. Faddeev and V. Popov, "Feynman diagrams for the Yang-Mills field", *Phys. Lett.* **B25** (1967) 29.

[65] A. G. Williams, "Nonperturbative QCD, gauge fixing, Gribov copies, and the lattice", *Prog.Theor.Phys.Suppl.* **151** (2003) 154–160, arXiv:hep-lat/0304003 [hep-lat].

[66] C. Becchi, A. Rouet, and R. Stora, "Renormalization of the Abelian Higgs-Kibble Model", *Commun.Math.Phys.* **42** (1975) 127–162.

[67] C. Becchi, A. Rouet, and R. Stora, "Renormalization of Gauge Theories", *Annals Phys.* **98** (1976) 287–321.

[68] I. Tyutin, "Gauge Invariance in Field Theory and Statistical Physics in Operator Formalism", arXiv:0812.0580 [hep-th].

[69] A. Slavnov, "Ward Identities in Gauge Theories", *Theor.Math.Phys.* **10** (1972) 99–107.

[70] J. Taylor, "Ward identities and charge renormalization of the Yang- Mills field", *Nucl. Phys.* **B33** (1971) 436.

[71] R. Alkofer and L. von Smekal, "The infrared behavior of QCD Green's functions: Confinement, dynamical symmetry breaking, and hadrons as relativistic bound states", *Phys. Rept.* **353** (2001) 281, hep-ph/0007355.

[72] C. Itzykson and J. Zuber, *Quantum field theory*. 1980.

[73] R. Rivers, *Path integral methods in quantum field theory*. 1987.

[74] C. Roberts and A. Williams, "Dyson-Schwinger equations and their application to hadronic physics", *Prog.Part.Nucl.Phys.* **33** (1994) 477–575, arXiv:hep-ph/9403224 [hep-ph].

[75] C. Fischer, "Infrared properties of QCD from Dyson-Schwinger equations", *J. Phys.* **G32** (2006) R253–R291, arXiv:hep-ph/0605173.

[76] A. Cucchieri, T. Mendes, and A. Mihara, "Numerical study of the ghost-gluon vertex in Landau gauge", *JHEP* **12** (2004) 012, arXiv:hep-lat/0408034.

[77] A. Sternbeck, E.-M. Ilgenfritz, M. Müller-Preußker, and A. Schiller, "Studying the infrared region in landau gauge qcd", *PoS* **LATTICE 2005** (2005) 333, hep-lat/0509090.

[78] W. Schleifenbaum, A. Maas, J. Wambach, and R. Alkofer, "Infrared behaviour of the ghost gluon vertex in Landau gauge Yang-Mills theory", *Phys. Rev.* **D72** (2005) 014017, arXiv:hep-ph/0411052.

[79] L. von Smekal, R. Alkofer, and A. Hauck, "The infrared behavior of gluon and ghost propagators in Landau gauge QCD", *Phys. Rev. Lett.* **79** (1997) 3591, arXiv:hep-ph/9705242.

[80] P. Watson and R. Alkofer, "Verifying the Kugo-Ojima confinement criterion in Landau gauge QCD", *Phys. Rev. Lett.* **86** (2001) 5239, arXiv:hep-ph/0102332.

[81] C. Lerche and L. von Smekal, "On the infrared exponent for gluon and ghost propagation in Landau gauge QCD", *Phys. Rev.* **D65** (2002) 125006, arXiv:hep-ph/0202194.

[82] C. Fischer and H. Gies, "Renormalization flow of Yang-Mills propagators", *JHEP* **10** (2004) 048, arXiv:hep-ph/0408089.

[83] C. S. Fischer and J. M. Pawlowski, "Uniqueness of infrared asymptotics in Landau gauge Yang-Mills theory. II.", *Phys. Rev. D* **80** (Jul, 2009) 025023. http://link.aps.org/doi/10.1103/PhysRevD.80.025023.

[84] C. Fischer and J. Pawlowski, "Uniqueness of infrared asymptotics in Landau gauge Yang- Mills theory II", arXiv:0903.2193 [hep-th].

[85] D. Atkinson and J. Bloch, "QCD in the infrared with exact angular integrations", *Mod.Phys.Lett.* **A13** (1998) 1055–1062, arXiv:hep-ph/9802239 [hep-ph].

[86] V. Bornyakov, V. Mitrjushkin, and R. Rogalyov, "Gluon Propagators in 3D SU(2) Theory and Effects of Gribov Copies", arXiv:1112.4975 [hep-lat].

[87] A. Sternbeck and L. von Smekal, "Infrared exponents and the strong-coupling limit in lattice Landau gauge", *Eur. Phys. J.* **C68** (2010) 487–503, arXiv:0811.4300 [hep-lat].

[88] L. von Smekal, "Landau gauge QCD: Functional methods versus lattice simulations", arXiv:0812.0654 [hep-th].

[89] C. Fischer, A. Maas, and J. Pawlowski, "On the infrared behavior of Landau gauge Yang-Mills theory", *Annals Phys.* **324** (2009) 2408–2437, arXiv:0810.1987 [hep-ph].

[90] T. Muta, "Foundations of quantum chromodynamics. Second edition", *World Sci.Lect.Notes Phys.* **57** (1998) 1–409.

[91] W. Marciano and H. Pagels, "Quantum Chromodynamics: A Review", *Phys.Rept.* **36** (1978) 137.

[92] S. Weinberg, *The quantum theory of fields. Vol. 2: Modern applications*. 1996.

[93] C. Fischer and J. Pawlowski, "Uniqueness of infrared asymptotics in Landau gauge Yang- Mills theory", *Phys. Rev.* **D75** (2007) 025012, arXiv:hep-th/0609009.

[94] Y. Fujimoto and H. Yamada, "Finite temperature renormalization group equations via Wilson loop", *Phys.Lett.* **B212** (1988) 77.

[95] M. Chaichian and M. Hayashi, "QCD coupling constant at finite temperature", *Acta Phys.Polon.* **27** (1996) 1703–1718, arXiv:hep-ph/9605205 [hep-ph].

[96] L. Gendenshtein, "Renormalization group at finite temperatures and the liberation of quarks.", *Yad.Fiz.* **29** (1979) 1639–1645.

[97] K. Kajantie and J. Kapusta, "Behavior of Gluons at High Temperature", *Annals Phys.* **160** (1985) 477.

[98] K. Enqvist and K. Kajantie, "Effects of temperature dependent coupling constant evolution on the unification scale", *Mod.Phys.Lett.* **A2** (1987) 479.

[99] H. Nakkagawa, A. Niegawa, and H. Yokota, "Nonabelian gauge couplings at finite temperatures in the general covariant gauge", *Phys.Rev.* **D38** (1988) 2566.

[100] C. Gattringer and C. B. Lang, "Quantum chromodynamics on the lattice", *Lect.Notes Phys.* **788** (2010) 1–211.

[101] J. A. Müller, *A Dyson-Schwinger Approach to Finite Temperature QCD*. PhD thesis, TU Darmstadt, January, 2011. http://tuprints.ulb.tu-darmstadt.de/2395/.

[102] C. DeTar and U. Heller, "QCD Thermodynamics from the Lattice", *Eur.Phys.J.* **A41** (2009) 405–437, arXiv:0905.2949 [hep-lat].

[103] R. Pisarski and F. Wilczek, "Remarks on the chiral phase transition in chromodynamics", *Phys. Rev. D* **29** (Jan, 1984) 338–341. http://link.aps.org/doi/10.1103/PhysRevD.29.338.

[104] F. Karsch, E. Laermann and C. Schmidt, "The Chiral critical point in three-flavor QCD", *Phys.Lett.* **B520** (2001) 41–49, arXiv:hep-lat/0107020 [hep-lat].

[105] C. Bonati, G. Cossu, M. D'Elia, A. Di Giacomo and C. Pica, "The order of the QCD transition with two light flavors", *Nucl.Phys.* **A820** (2009) 243C–246C.

[106] S. Ejiri, F. Karsch, E. Laermann, C. Miao, S. Mukherjee, *et al.*, "On the magnetic equation of state in (2+1)-flavor QCD", *Phys.Rev.* **D80** (2009) 094505, arXiv:0909.5122 [hep-lat].

[107] A. Ukawa, "QCD phase transitions at finite temperatures", *Nucl.Phys.Proc.Suppl.* **17** (1990) 118–136.

[108] **Wuppertal-Budapest** Collaboration, S. Borsanyi *et al.*, "Is there still any T_c mystery in lattice QCD? Results with physical masses in the continuum limit III", *JHEP* **1009** (2010) 073, arXiv:1005.3508 [hep-lat].

[109] J. Kapusta, *Finite temperature field theory*. 1989.

[110] K. Kajantie, M. Laine, K. Rummukainen, and Y. Schröder, "The Pressure of hot QCD up to g6 ln(1/g)", *Phys.Rev.* **D67** (2003) 105008, arXiv:hep-ph/0211321 [hep-ph].

[111] K. Kajantie, M. Laine, K. Rummukainen, and Y. Schröder, "How to resum long distance contributions to the QCD pressure?", *Phys.Rev.Lett.* **86** (2001) 10–13, arXiv:hep-ph/0007109 [hep-ph].

[112] P. Bowman, U. Heller, D. Leinweber, A. Williams, and J. Zhang, "Quark propagator from LQCD and its physical implications", *Lect.Notes Phys.* **663** (2005) 17–63.

[113] **UKQCD** Collaboration, D. Leinweber, J. Skullerud, A. Williams, and C. Parrinello, "Asymptotic scaling and infrared behavior of the gluon propagator", *Phys. Rev.* **D60** (1999) 094507, hep-lat/9811027.

[114] K. Wilson, "Confinement of quarks", *Phys.Rev.* **D10** (1974) 2445–2459.

[115] P. Hasenfratz and F. Niedermayer, "Perfect lattice action for asymptotically free theories", *Nucl.Phys.* **B414** (1994) 785–814, arXiv:hep-lat/9308004 [hep-lat].

[116] K. Symanzik, "Continuum Limit and Improved Action in Lattice Theories. 1. Principles and phi**4 Theory", *Nucl.Phys.* **B226** (1983) 187.

[117] K. Symanzik, "Continuum Limit and Improved Action in Lattice Theories. 2. O(N) Nonlinear Sigma Model in Perturbation Theory", *Nucl.Phys.* **B226** (1983) 205.

[118] M. Lüscher, S. Sint, R. Sommer, and P. Weisz, "Chiral symmetry and O(a) improvement in lattice QCD", *Nucl.Phys.* **B478** (1996) 365–400, arXiv:hep-lat/9605038 [hep-lat].

[119] G. P. Lepage, "Redesigning lattice QCD", arXiv:hep-lat/9607076 [hep-lat].

[120] M. Lüscher and P. Weisz, "Computation of the Action for On-Shell Improved Lattice Gauge Theories at Weak Coupling", *Phys.Lett.* **B158** (1985) 250.

[121] A. Shindler, "Twisted mass lattice QCD", *Phys. Rept.* **461** (2008) 37, arXiv:0707.4093 [hep-lat].

[122] **ETM** Collaboration, R. Baron *et al.*, "Light Meson Physics from Maximally Twisted Mass Lattice QCD", *JHEP* **08** (2010) 097, arXiv:0911.5061 [hep-lat].

[123] F. Burger, E.-M. Ilgenfritz, M. Kirchner, M. Lombardo, M. Müller-Preußker, *et al.*, "The thermal QCD transition with two flavours of twisted mass fermions", arXiv:1102.4530 [hep-lat].

[124] F. Burger, M. Kirchner, M. Müller-Preußker, E.-M. Ilgenfritz, M.-P. Lombardo, *et al.*, "Pseudo-Critical Temperature and Thermal Equation of State from $N_f = 2$ Twisted Mass Lattice QCD", arXiv:1212.0982 [hep-lat].

[125] S. Necco and R. Sommer, "The N(f) = 0 heavy quark potential from short to intermediate distances", *Nucl. Phys.* **B622** (2002) 328, hep-lat/0108008.

[126] G. Bali, V. Bornyakov, M. Müller-Preußker, and F. Pahl, "New algorithm for gauge fixing in SU(2) lattice gauge theory", *Nucl. Phys. Proc. Suppl.* **42** (1995) 852–854, arXiv:hep-lat/9412027.

[127] G. Bali, V. Bornyakov, M. Müller-Preußker, and K. Schilling, "Dual superconductor scenario of confinement: A systematic study of gribov copy effects", *Phys. Rev.* **D54** (1996) 2863–2875, hep-lat/9603012.

[128] I. Bogolubsky, V. Bornyakov, G. Burgio, E.-M. Ilgenfritz, V. Mitrjushkin, M. Müller-Preußker, and P. Schemel, "The Landau gauge gluon propagator: Gribov problem and finite-size effects", *PoS* **LAT2007** (2007) 318, arXiv:0710.3234 [hep-lat].

[129] C. Parrinello and G. Jona-Lasinio, "A modified Faddeev-Popov formula and the Gribov ambiguity", *Phys. Lett.* **B251** (1990) 175.

[130] D. Zwanziger, "Quantization of gauge fields, classical gauge invariance and gluon confinement", *Nucl. Phys.* **B345** (1990) 461.

[131] A. Nakamura and M. Plewnia, "Gauge fixing ambiguity and photon propagators in compact U(1) lattice gauge theory", *Phys. Lett.* **B255** (1991) 274.

[132] V. Bornyakov, V. Mitrjushkin, M. Müller-Preußker, and F. Pahl, "Dirac sheets and gauge fixing in U(1) lattice gauge theory", *Phys. Lett.* **B317** (1993) 596–603, arXiv:hep-lat/9307010.

[133] I. Bogolubsky, V. Mitrjushkin, M. Müller-Preußker, and P. Peter, "Lorentz gauge and Gribov ambiguity in the compact lattice U(1) theory", *Phys. Lett.* **B458** (1999) 102–108, arXiv:hep-lat/9904001.

[134] I. Bogolubsky, V. Mitrjushkin, M. Müller-Preußker, P. Peter, and N. Zverev, "Fermionic correlators and zero-momentum modes in quenched lattice QED", *Phys. Lett.* **B476** (2000) 448–454, arXiv:hep-lat/9912017.

[135] D. Zwanziger, "Vanishing color magnetization in lattice Landau and Coulomb gauges", *Phys. Lett.* **B257** (1991) 168–172.

[136] D. Zwanziger, "Fundamental modular region, Boltzmann factor and area law in lattice gauge theory", *Nucl. Phys.* **B412** (1994) 657.

[137] A. Sternbeck, E.-M. Ilgenfritz, M. Müller-Preußker, and A. Schiller, "Landau gauge ghost and gluon propagators and the Faddeev-Popov operator spectrum", *Nucl.Phys.Proc.Suppl.* **153** (2006) 185–190, arXiv:hep-lat/0511053 [hep-lat].

[138] A. Sternbeck, E. M. Ilgenfritz, and M. Müller-Preußker, "Spectral properties of the Landau gauge Faddeev-Popov operator in lattice gluodynamics", *Phys. Rev.* **D73** (2006) 014502, arXiv:hep-lat/0510109.

[139] L. von Smekal, M. Ghiotti, and A. Williams, "Decontracted double BRST on the lattice", *Phys. Rev.* **D78** (2008) 085016, arXiv:0807.0480 [hep-th].

[140] F. Llanes-Estrada and R. Williams, "Two infrared Yang-Mills solutions in stochastic quantization and in an effective action formalism", *Phys.Rev.* **D86** (2012) 065034, arXiv:1207.5950 [hep-th].

[141] L. McLerran and B. Svetitsky, "A Monte Carlo study of SU(2) Yang-Mills theory at finite temperature", *Phys.Lett.* **B98** (1981) 195.

[142] A. Sternbeck, E.-M. Ilgenfritz, M. Müller-Preußker, A. Schiller, and I. Bogolubsky, "Lattice study of the infrared behavior of QCD Green's functions in Landau gauge", *PoS* **LAT2006** (2006) 076, hep-lat/0610053.

[143] A. Sternbeck, *The infrared behavior of lattice QCD Green's functions*. PhD thesis, Humboldt-University Berlin, 2006. hep-lat/0609016.

[144] N. Cabibbo and E. Marinari, "A new method for updating $SU(N)$ matrices in computer simulations of gauge theories", *Phys. Lett.* **B119** (1982) 387.

[145] A. Maas, "Gluons at finite temperature in Landau gauge Yang-Mills theory", *Mod. Phys. Lett.* **A20** (2005) 1797–1811, arXiv:hep-ph/0506066.

[146] J. Mandula and M. Ogilvie, "Efficient gauge fixing via overrelaxation", *Phys. Lett.* **B248** (1990) 156.

[147] R. Sommer, "A new way to set the energy scale in lattice gauge theories and its applications to the static force and alpha-s in SU(2) Yang-Mills theory", *Nucl. Phys.* **B411** (1994) 839, hep-lat/9310022.

[148] G. Damm, W. Kerler, and V. Mitrjushkin, "Gluon propagator and zero-momentum modes in SU(2) lattice gauge theory", *Phys. Lett.* **B433** (1998) 88, arXiv:hep-lat/9802028.

[149] A. Cucchieri and T. Mendes, "Electric and magnetic Landau-gauge gluon propagators in finite-temperature SU(2) gauge theory", arXiv:1105.0176 [hep-lat].

[150] M. Stingl, "A Systematic extended iterative solution for quantum chromodynamics", *Z.Phys.* **A353** (1996) 423, arXiv:hep-th/9502157 [hep-th].

[151] A. Cucchieri, T. Mendes, and A. Taurines, "SU(2) Landau gluon propagator on a 140**3 lattice", *Phys.Rev.* **D67** (2003) 091502, arXiv:hep-lat/0302022 [hep-lat].

[152] A. Maas, "Describing gluons at zero and finite temperature", *Chin. J. Phys.* **34** (2010) 1328–1330, arXiv:0911.0348 [hep-lat].

[153] E.-M. Ilgenfritz, K. Jansen, M. Lombardo, M. Müller-Preußker, M. Petschlies, *et al.*, "Phase structure of thermal lattice QCD with N(f) = 2 twisted mass Wilson fermions", *Phys.Rev.* **D80** (2009) 094502, arXiv:0905.3112 [hep-lat].

[154] **tmfT** Collaboration, F. Burger *et al.*, "Thermal transition temperature from twisted mass QCD", *PoS* **LATTICE2010** (2010) 220, arXiv:1009.3758 [hep-lat].

[155] Y. Aoki, Z. Fodor, S. Katz, and K. Szabo, "The QCD transition temperature: Results with physical masses in the continuum limit", *Phys. Lett.* **B643** (2006) 46–54, arXiv:hep-lat/0609068.

[156] M. Cheng, N. H. Christ, M. Li, R. Mawhinney, D. Renfrew, *et al.*, "The finite temperature QCD using 2 + 1 flavors of domain wall fermions at N (t) = 8", *Phys.Rev.* **D81** (2010) 054510, arXiv:0911.3450 [hep-lat].

[157] V. Bornyakov, R. Horsley, Y. Nakamura, M. Polikarpov, P. Rakow, *et al.*, "Finite temperature phase transition with two flavors of improved Wilson fermions", arXiv:1102.4461 [hep-lat].

[158] M. Cheng *et al.*, "The QCD equation of state with almost physical quark masses", *Phys. Rev.* **D77** (2008) 014511, arXiv:0710.0354 [hep-lat].

[159] B. Brandt, H. Wittig, O. Philipsen, and L. Zeidlewicz, "Towards the $N_f = 2$ deconfinement transition temperature with $O(a)$ improved Wilson fermions", *PoS* **LATTICE2010** (2010) 172, arXiv:1008.2143 [hep-lat].

[160] A. Ayala, A. Bashir, D. Binosi, M. Cristoforetti, and J. Rodriguez-Quintero, "Quark flavour effects on gluon and ghost propagators", *Phys.Rev.* **D86** (2012) 074512, arXiv:1208.0795 [hep-ph].

[161] D. Dudal, J. Gracey, S. Sorella, N. Vandersickel, and H. Verschelde, "A refinement of the Gribov-Zwanziger approach in the Landau gauge: infrared propagators in harmony with the lattice results", *Phys. Rev.* **D78** (2008) 065047, arXiv:0806.4348 [hep-th].

[162] D. Dudal, N. Vandersickel, H. Verschelde, and S. Sorella, "The dynamical origin of the refinement of the Gribov-Zwanziger theory", *Phys.Rev.* **D84** (2011) 065039, arXiv:1105.3371 [hep-th].

[163] A. Sternbeck and M. Müller-Preußker, "Lattice evidence for the family of decoupling solutions of Landau gauge Yang-Mills theory", arXiv:1211.3057 [hep-lat].

LIST OF FIGURES

LIST OF TABLES

Selbständigkeitserklärung

Ich erkläre, dass ich die vorliegende Arbeit selbständig und nur unter Verwendung der angegebenen Literatur und Hilfsmittel angefertigt habe.

Rafik Aouane
Berlin, den 20.12.2012